Surrogate models and automated CAD of passive microwave components

Adam Lamęcki

Ph.D. Thesis

Gdansk University of Technology
Department of Electronics, Telecommunications and Computer Science

Supervisor: Prof. Michał Mrozowski

Gdańsk 2007

Rodzicom

Contents

Symbol conventions and abbreviations

Symbol conventions

$\mathbf{A}$	-	matrix
$\mathbf{A}(\cdot)$	-	matrix valuated function
$\mathbf{I}$	-	unit matrix
$(\cdot)^{-1}$	-	matrix inverse
$(\cdot)^{T}$	-	matrix/vector transposition
$(\cdot)^{H}$	-	matrix/vector hermite transposition
$\sigma(\cdot)$	-	singular values of matrix
$\mathbf{a}$	-	vector
a	-	scalar
i	-	imaginary unit
$Re(\cdot)$	-	real part
$Im(\cdot)$	-	imaginary part
$\hat{\cdot}$	-	reference data
$(\cdot)_{max}$	-	maximum value
$(\cdot)_{mean}$	-	mean value

General symbols

f	-	frequency
ω	-	angular frequency
s	-	complex frequency
$\mathbf{A}, \mathbf{B}, \mathbf{C}, \mathbf{D}$	-	state-space representation matrices
$\mathbf{Y}, \mathbf{Z}$	-	admittance, impedance matrix
$\mathbf{S}$	-	scattering matrix
Δ	-	real absolute error
E_{RMS}	-	root mean square error
E_{RSE}	-	relative square error
E_{MSE}	-	mean square error
ε	-	absolute error between two approximations
ξ	-	acceptable distortion of frequency domain response

Selected abbreviations

ADS	-	Advanced Design Studio
ANN	-	Artificial Neural Networks
BCF	-	Branched-Continued Fraction
CAD	-	Computer-Aided Design
FD	-	Frequency domain
LTI	-	Linear time-invariant
MCM − D	-	Multi Chip Module - Deposited
MoM	-	Method of Moments
MOR	-	Model Order Reduction
PE	-	Passivity enforcement
QP	-	Quadratic programming
RBF	-	Radial Basis Functions
SI	-	Signal integrity
SoC	-	System-On-Chip
SoP	-	System-On-Package
TD	-	Time domain
TLS	-	Total Least Squares
VF	-	Vector fitting

Chapter 1

Introduction

1.1 Background and motivation

Since the first application of electromagnetic waves for wireless communication demonstrated by Guglielmo Marconi in 1896, an enormous progress in application of radio frequency, micro- and milimeter-waves has been observed [112]. Marconi's experiment of Moorse code transmission over the distance of two miles (3.2 kilometers) started a revolution in the electronics and telecommunications that changed lives of billions of people. Marconi's first radio operated at the frequency of about 1000MHz, which is in microwave range, but later scientists concentrated on development of long-distance devices that worked at low frequencies. A next milestone of microwave radio development was the invention of diode vacuum tube by J. Ambrose Fleming in 1904 and triode vacuum tube by Lee DeForest in 1907. Those devices allowed one to construct receivers and sources of microwave signals and started a revolution in commercial applications of microwaves. Today, over 100 years since those first attempts, the revolution of high-frequency personal communications evolves. New wireless technologies, like Wi-Fi, Bluetooth or third-generation cellular phones (UMTS) became wide-spread and popular. Recently, the digital computing applications also enter the gigahertz range. A success of those technologies and rapid increase of customers' demands and system requirements make the manufacturers to search for a new solutions in wireless technology. The progress is observed both in active devices (high speed InP HBT and GaN HEMT transistors) and passive components (high quality passives for integrated applications, interconnects and packages). Briefly, the most important trends in the development of high-frequency systems can be pointed as follows:

- Increase in the operational frequency for high speed data transfer applications. High frequency devices allow one to transmit data at high rates (10Gb/s and above) and miniaturize the device dimensions. As shown in [96] a rapid growth of market of microwave and millimeter wave integrated circuits (MMIC) that operate in 20GHz-100GHz frequency is expected. High variation of attenuation of radio signals in this frequency band makes it attractive for use it in both near and far communication systems. Systems operating above 70GHz should provide a data rates about 10Gb/s.
- Integration of digital and analog, passive and active parts of circuits into a single chip (SoC) [34, 86]. The integration includes analog parts, like RF transcivers, and digital

parts, such as memory blocks and logic circuits. For example, a silicon-germanium SiGe BiCMOS technology that allows one to integrate both analog and digital circuits into a single chip was developed [62]. A current progress of miniaturization allows a designer to integrate a full wireless Bluetooth transceiver into a single CMOS chip [103] (figure 1.1).

- Development of multi-chip-module (MCM) devices technology for system on package (SoP) applications. SoP provides a complete package solution for RF module with integration of various elements, including antennas, filters, baluns and RF transceivers into a single package [119, 120]. MCM philosophy is based on three dimensional, multilayered, high density architectures, where several independent elements are connected together by interconnect network.
- Increasing demands on interconnect networks used in high-frequency devices [87, 105]. The interconnects distribute the analog or high data rate digital signals over the system (chip-to-chip and module-to-module connections). The application of three-dimensional (3D) circuit architecture in modern designs is observed. The quality of the interconnect network limits the overall speed of the device.
- Increasing applications of multilayered low temperature co-fired ceramic (LTCC) components for applications in SoP [77]. LTCC allows one to miniaturize passive elements (resonators, filters, couplers) with high reliability and low-cost. The problem of shrinking of ceramics during firing can be controlled with improving accuracy. Additionally the producers started to work on zero-shrink processes,
- Development of ultra-wideband (UWB) communication devices that operate in 3,6-10,1GHz frequency range. UWB transceivers operate on the noise floor along with other RF systems [131],
- Increasing market of automotive anti-collision radars operating at 76-77GHz. This enforces an evolution of low cost high-frequency integrated solutions,
- Several attempts have been made to define the standards of next generation of cellular networks (4G). The initial requirements are extremely high, future devices should integrate several interfaces, e.g. Bluetooth, Wi-Fi, GPS and cellular phone into a single chip [53].

1.1.1 Design strategies for high frequency circuits

The increase in the operational frequency along with a growing integration of high frequency devices makes a system design an enormous challenge for engineers. Currently, one of the hot topics is the development of fast and versatile modelling and simulation tools for high-complexity and/or highly-integrated devices. Three main features required from modern CAD software tools are the abilities to:

- handle distributed components (like interconnects),
- analyze mixed analog-digital devices,
- perform a signal-integrity (SI) analysis of a design,

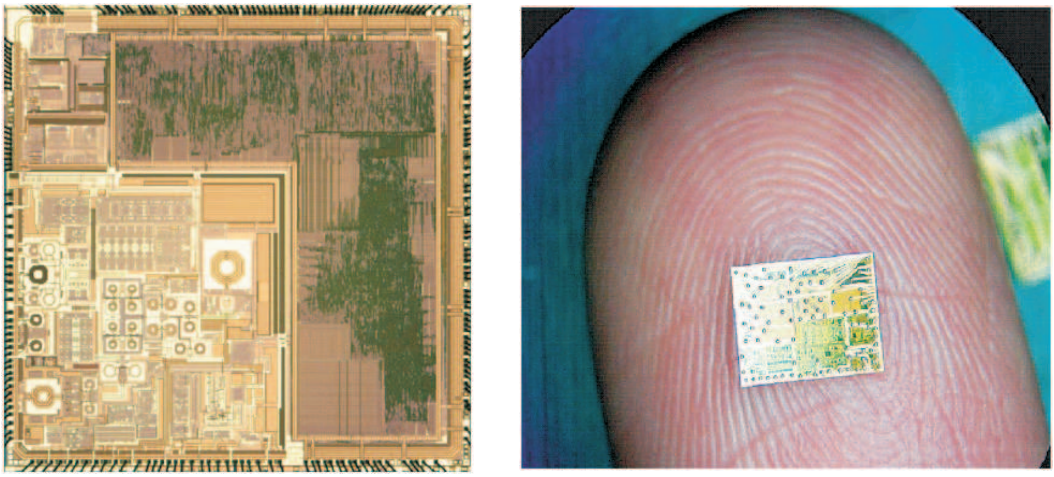

Figure 1.1: Die photo of a fully integrated miniature CMOS Bluetooth chip [103]

Additionally, tightening time-to-market constraints enforce the adaptation of new design methodologies. In general, the system design design is a hierarchic process, with the major steps as follow:

- System concept
- System specification
- Architectural design
- Pre-layout design
- Post-layout design
- System assembly

The first stage is a general concept of the system, which gives the basic information about the functions of the final product and estimated cost. Based on this information the engineers can prepare general specifications of the system, that incudes not only electric parameters (such as power supply, BER, range of transmission), but also mechanical requirements (such as size, weight, type of support). The next step is to design the architecture of the system, i.e. decompose the system into separate blocks and define their specifications (both electrical and mechanical). Pre-layout and post-layout design of the basic building blocks are the main steps that involve RF/microwave engineering.

Pre-layout design The result of the pre-layout stage is an electric scheme of the circuit composed of lumped elements that represent passive and active (linear and non-linear) components. On this stage several of the parasitic effects are not taken into account. Traditional pre-layout design of analog microwave components and systems is carried out using circuit simulators. The simulator uses lumped elements, transmission lines and relies on S,Y, or Z

parameters of individual components making up the circuit. The advantage of such approach is a speed of the simulation which allows optimization.

There are few circuit simulators on the market that are dedicated to microwave components design, the two most popular ones being the Advanced Design Studio (ADS) from Agilent [127] and Microwave Office from AWR [130]. The software, besides lumped elements and ideal transmission lines, has a built-in library of surrogate models of simple discontinuities made in the most popular microwave technologies. For example, the ADS has the following libraries:

- Microstrip elements: line, various types of line bend, gap, step, tee-junction, cross-junction, coupled lines, via, open-circuited and short-circuited line, butterfly stub, planar inductors and capacitors.
- Stripline elements: line, various types of line bend, step, open-circuited and short-circuited line, tee-junction, cross-junction, coupled lines.
- Coplanar waveguide elements: line, open-circuited and short-circuited stubs, gap, coupled lines.
- Finline: unilateral, bilateral and insulated finline and termination
- Rectangular waveguide: waveguide, bifurcated waveguide and termination.

The library consists of the most popular elements, however the problem is the accuracy and versatility of the models. For example, the ADS to represent the 90-degree microstrip bend uses the Kirchning, Jansen and Koster model that has the following limitations [57]:

- $0.2 \leq \frac{w}{H} < 6$
- $2.36 \leq \varepsilon_r \leq 10.4$
- $f_{max} \leq \frac{12GHz}{H[mm]}$

where w is the width of the strip, H is the height of the substrate and f_{max} is maximum model frequency. The versatility of the model is then a strongly restricted. If one compares the contents of the libraries with current and emerging technologies, it is obvious that there is a common need for novel libraries of surrogate models. For example, the analysis of multilayer structures like those made on silicon substrate in SiGe CMOS process is not possible using the standard models.

Post-layout design Post-layout simulation is a much longer process. In microwave frequencies the passive electronic circuits are distributed, so the response depends on the structure dimensions and topology. Several parasitic effects, that could be neglected at lower frequencies, must be included in simulation on microwave frequencies due to their influence on device's operation. For example, the effects that should not be neglected at high frequencies include:

- For digital circuits:

  - signal delays,
  - signal distortion,
  - ringing,
  - crosstalk,
  - losses.

- For analog circuits:
  - cross-couplings,
  - dispersion,
  - skin effect,
  - frequency dependent losses,
  - parasitic radiation.

The parasitic effects of passive components and new technologies can be accounted for in high-accuracy electromagnetic simulators. There are several full-wave solvers capable of analysis of microwave devices, using different simulation techniques such as finite differences in time domain (FD-TD) [20, 115, 132], finite elements (FEM) [55, 111], method of moments (MoM) [91, 122] or mode-matching [24]. Each technique is better or worse suited for a given technology, but a common factor of electromagnetic approach is a high numeric cost of problem solution which leads to very long time of computation, especially in the case of complex structures. Additionally, an effort to provide the input data (like geometry) and to ensure the correct conditions of simulation can be substantial.

To overcome the aforementioned issues the following tools are needed:

- Techniques of construction of libraries of high accuracy models of basic building blocks, especially dedicated to passive components made in emerging technologies,
- Versatile techniques that could bind the circuit simulators with parameterized models of passive components or electromagnetic simulators.

1.1.2 Automated design

Due to advancement in algorithm and increase in CPU's processing speed it has recently become possible to perform a design with automated design procedure, that consists of three major steps:

- Selection of the best circuit topology,
- Preliminary synthesis of circuit elements,
- Optimization of the design to fulfill the requirements.

The first step of the design can be realized as an expert system [94] that gives an engineer some advice about the circuit topology that fits best to the design requirements. Then a synthesis of initial circuit is performed, for example using surrogate models. Finally the design is optimized to fit the requested specification.

The most effort in the topic of automated design is made in the area of circuit optimization. Using the optimization approach on initial, coarse parameters (geometry, media, etc.) of device an engineer constructs a goal function, the minimization of which gives input parameters that makes the design to fulfill the requested specification. Several strategies were proposed for circuit optimization [10, 27, 51, 54, 56]. What is important, the optimization approach is efficient when the evaluation of the goal function is fast, but becomes a burden when an electromagnetic solver is involved. Therefore, the application of the parameterized surrogate models based on the results of electromagnetic simulations, can significantly improve the performance of the optimization approach.

1.2 Scope, claims and goals of this work

The main goal of this thesis is to develop a set of new tools for automated design by optimization of complex microwave and millimeter-wave structures. The automated design strategy is a very wide issue itself, it is not a goal of this thesis to present its possible realizations. This thesis is mostly concentrated on applications of the surrogate models and equivalent circuits for the fast, automated design of microwave components and equivalent circuits. The following claims are made:

- **It is possible to create automatically high accuracy multi-parametric surrogate models of microwave components based on results of EM-simulations;**
- **An equivalent circuit with guaranteed passivity can be driven directly from EM simulations, measurements or surrogate models response.**
- **The application of surrogate models makes it possible to speed-up the automated design schemes based on optimization techniques.**

In order to prove the claims the following steps are undertaken:

- **A new technique of construction of the surrogate models of microwave components in a form of multivariate rational function is introduced;**
- **The device response is represented in the frequency domain as a rational model;**
- **A new technique of a passivity enforcement of the rational model is introduced;**
- **Directly from the rational model an equivalent circuit of a device is constructed;**
- **Examples of applications of surrogate models in automated design of microwave components are given.**

1.3 Chapter outline

In Chapter 2 a general overview and the surrogate models and techniques of equivalent circuits construction along with measures of the model accuracy are presented. In Chapter 3 the proposed technique of multivariate surrogate models is presented and discussed in detail. Several issues are covered: multivariate rational interpolation scheme, automated selection of support points, automated selection of model order, automated division of parameter space.

General techniques of extraction of the frequency independent equivalent circuits of distributed elements from scattering/admittance parameters are presented in Chapter 4. The equivalent circuit may be derived in a form of RLC circuits or more generally as realizations of transfer functions which besides RLC elements involve controlled sources.

In Chapter 5 the techniques of passivity enforcement of non-passive models are shown. Passivity enforcement assures that the created equivalent circuit is passive for all frequencies while preserving its frequency response. Several applications are presented. Resulting circuits are well suited for time-domain analysis, by means of the popular SPICE simulator.

To show the applications of the technique some advanced examples are presented in Chapter 6. In the same chapter it is demonstrated that the passivity enforcement technique can also be applied for response of surrogate models. As a result a new type of parameterized equivalent circuit of a device is obtained, that can be used both in time and frequency analysis. Parameterized SPICE circuit enables an optimization of geometry of a distributed circuit within SPICE.

Chapter 2

Models and model metrics

In this chapter different types of models used in microwave circuit design are introduced and metrics required for their quality assessment are presented.

2.1 Surrogate/behavioral models

The basic idea behind surrogate/behavioral modelling is a construction of a ”black-box” representation of the circuit that closely approximates the response of the original structure within the range of its input parameters (Fig. 2.1). In most cases the inputs of the model $x_1, x_2, \ldots, x_N$ are the frequency and/or structure dimensions, while the outputs describe the device's response. The advantage of surrogate models is that once the model is created it can be used in many different designs, thus the gain of its construction is high.

Surrogates are used in many aspects of a microwave circuit design: from initial design to final optimization and yield analysis. Currently the accuracy and speed of analysis of commercial simulators dedicated to RF-designs rely on fast and accurate surrogate models of microwave discontinuities. For a microwave designer one of the most important requirements regarding the circuit simulator is the quality and diversity of models library. Several CAD-tools for microwave design are available on the market, but most of them are applicable for design on pre-layout stage (lumped networks). Some of them, like Agilent's Advanced Design System or AWR's Microwave Office are well suited for well-known, standard technologies (microstrip or coplanar) on standard substrates. To handle more complex structures the built-in electromagnetic solver based on method of moments (MoM) can be used. However, the limitation of current CAD-tools is connected to limited library of surrogate/behavioral models that would include the parasitic effects present in microwave frequency band and could handle complex and/or multi-layer structures present in emerging technologies, such as LTCC, LCP or MCM-D. As a consequence, approximate formulas must be used that are often too inaccurate for design of system components and one has to perform time consuming electromagnetic simulation. This could be avoided if one was able to generate new set of surrogate models whenever new technologies emerges.

The simplest form of a surrogate models are closed-form formulae. This approach has been used by microwave engineers for over six decades, and it is still popular today. The main drawback of closed-form expressions is that they are hard to derive and also their

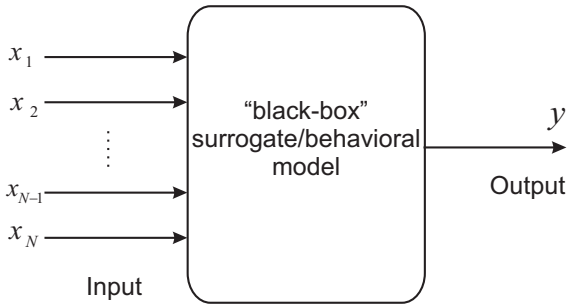

Figure 2.1: Basic idea of surrogate/behavioral modelling

Table 2.1: Comparison of the surrogate models

Feature	Mathematical	Non-evident
Parameters	Few	Few
Easy to implement	Yes	No
Versatile	No	Yes

accuracy is limited. In recent years several research groups have been investigating techniques of automated and systematic construction of complex models involving several design variables. The idea is to use an electromagnetic simulation to provide the data for model construction. This way a new technology emerges, a new library of basic building blocks can be constructed and used in simulator. The most common approach is to model admittance/impedance characteristics or scattering parameters of the device. Other circuit's characteristics can be modelled as well, as shown in [64, 65]. The main requirement from a designer point of view is the quality and diversity of models library. The mostly required are models based on the results of electromagnetic simulations, which assure the best accuracy of circuit analysis. The surrogate models can be categorized on two basic classes:

- Mathematical models: the response of a device is approximated as a mathematical function involving various types of basis functions: polynomial, rational or radial basis functions.

- Non-evident models: artificial neural networks (ANN)

The basic features of each category are shown in table 2.1.

The problem of multidimensional modelling is formulated as follows: for an N-variate unknown function $\widehat{F}(\boldsymbol{x}) = \widehat{F}(x_1, x_2, \ldots, x_N)$ find a function/relation $F(\boldsymbol{x})$ that approximates well its value for an arbitrary point $\boldsymbol{x_s} = [(x_{s1}, x_{s2}, \ldots, x_{sN}]$ inside of parameter range Γ:

$$F(\boldsymbol{x_s}) \approx \widehat{F}(\boldsymbol{x_s}) \qquad \boldsymbol{x_s} \in \Gamma \tag{2.1}$$

In general $\widehat{F}(\boldsymbol{x_s})$ represents a response of the electronic device (in the form of scattering, admittance, impedance functions or any other circuit parameters) and vector $\boldsymbol{x}$ consists of device parameters: frequency of operation, geometric dimensions and material properties.

It is assumed that Γ is an N-dimensional rectangular box. A distinctive feature of the microwave engineering is high cost of evaluation of values of reference function F. Therefore, an efficient technique of surrogate model construction should minimize the set of interpolation nodes $\boldsymbol{X} = [\boldsymbol{x}_1, \boldsymbol{x}_2, \ldots, \boldsymbol{x}_{\boldsymbol{M}}]^T$, which would significantly reduce the time of the model construction.

2.1.1 Model metrics

In every model construction method the main question is how to assess the accuracy of the created model, because in most cases the accuracy of the model limits the range of its applications. There are several techniques of verification of the model accuracy and error definitions which are commonly used for different modeling techniques.

Let us assume that $\widehat{F}(\boldsymbol{x}_{\boldsymbol{k}})$ denotes the value of the modelled (reference) function $\widehat{F}$ evaluated at an arbitrary point $\boldsymbol{x}_{\boldsymbol{k}} = [x_{k1}, x_{k2}, \ldots, x_{kN}]$. Additionally, $F(\boldsymbol{x}_{\boldsymbol{k}})$ represents the approximated value of $\widehat{F}(\boldsymbol{x}_{\boldsymbol{k}})$. The model parameters $\boldsymbol{x}_{\boldsymbol{k}}$ form a test set of support points $\boldsymbol{X} = [\boldsymbol{x}_{\boldsymbol{1}}, \boldsymbol{x}_{\boldsymbol{2}}, \ldots, \boldsymbol{x}_{\boldsymbol{K}}]^T$. With such notation, one can define various measures of approximation error.

2.1.1.1 Absolute error

An absolute error is defined as a difference between the reference data and the model (approximation), computed for arbitrary point $\boldsymbol{x}_k$:

$$\Delta = |\widehat{F}(\boldsymbol{x}_{\boldsymbol{k}}) - F(\boldsymbol{x}_{\boldsymbol{k}})| \tag{2.2}$$

When a set of K support points is investigated, one can define a mean and maximum absolute errors:

$$\Delta_{max} = \max_k \left(\Delta(\boldsymbol{x}_{\boldsymbol{k}})\right) \tag{2.3}$$

$$\Delta_{mean} = \frac{1}{K} \sum_{k=1}^{K} |\widehat{F}(\boldsymbol{x}_{\boldsymbol{k}}) - F(\boldsymbol{x}_{\boldsymbol{k}})| \tag{2.4}$$

Both errors have a statistical meaning when K is large and both can be represented in decibels as Δ[dB] = $20\log(\Delta)$. The above error measures are basic indicators of accuracy of the model.

Additionally, if adaptive sampling of support points is considered (described in details in section 3.3.3), two approximations are constructed: $F_1(\boldsymbol{x}_{\boldsymbol{k}})$ and $F_2(\boldsymbol{x}_{\boldsymbol{k}})$. In this case it is important to evaluate a maximum absolute error between those models in model domain Γ, which is defined as:

$$\varepsilon = \max_{\boldsymbol{x} \in \Gamma} |F_1(\boldsymbol{x}) - F_2(\boldsymbol{x})| \tag{2.5}$$

2.1.1.2 Root mean square error

A root mean square error E_{RMS} is an estimation of standard deviation and is defined as:

$$E_{RMS} = \frac{1}{K} \sqrt{\sum_{k=1}^{K} (|\widehat{F}(\boldsymbol{x}_{\boldsymbol{k}}) - F(\boldsymbol{x}_{\boldsymbol{k}})|)^2} \tag{2.6}$$

This measure is commonly used for verification of artificial neural networks models [133].

2.1.1.3 Relative square error

The other error measure, used in [26, 79, 81], is a relative squared error E_{RSE} defined for an arbitrary point $\boldsymbol{x_k}$ as:

$$E_{RSE} = \frac{|\widehat{F}(\boldsymbol{x_k}) - F(\boldsymbol{x_k})|^2}{(1+|\widehat{F}(\boldsymbol{x_k})|)^2} \tag{2.7}$$

For a set of K points, it is convenient to define a mean and a maximum relative square errors:

$$E_{RSEmax} = \max_k \left(E_{RSE}(\boldsymbol{x_k})\right) \tag{2.8}$$

$$E_{RSEmean} = \frac{1}{K}\sum_{k=1}^{K} |E_{RSE}(\boldsymbol{x_k})| \tag{2.9}$$

The relative square error can be computed in decibels:

$$E_{RSE}[dB] = 20\log\left(\frac{|\widehat{F}(\boldsymbol{x_k}) - F(\boldsymbol{x_k})|}{(1+|\widehat{F}(\boldsymbol{x_k})|)}\right) \tag{2.10}$$

Since $(1+|\widehat{F}(\boldsymbol{x_k})|)^2 \geq 1$, the following statements are always true:

$$E_{RSEmax} \leq \Delta_{max} \tag{2.11}$$

$$E_{RSEmean} \leq \Delta_{mean} \tag{2.12}$$

Additionally, when the scattering parameters of passive device are modelled, then $|\widehat{F}(\boldsymbol{x_k})| \leq 1$. Therefore:

$$\frac{\Delta_{max}}{2} \leq E_{RSEmax} \leq \Delta_{max} \tag{2.13}$$

$$\frac{\Delta_{mean}}{2} \leq E_{RSEmean} \leq \Delta_{mean} \tag{2.14}$$

which is important for comparison of various techniques.

2.1.2 Techniques of parameterized models construction.

There have been several attempts to create a versatile technique of surrogate model construction: form the simplest approach involving a look-up tables (low accuracy and huge number of support points) to more advanced technique involving artificial neural networks [25, 30, 133]. ANN models have been successfully deployed in several RF and microwave applications, such as passive components, transmission lines, CPW components, inductors, FETs, amplifiers and filters [78, 100, 121]. However the drawbacks of ANNs, which are an unknown network topology and long training process, significantly limit their usage in automated model construction.

Several techniques were proposed that involve different interpolation schemes. Most popular ones use polynomial and rational representation [38]. In the considered algorithm,

frequency is handled separately from the physical parameters. The procedure has two stages. At first, multidimensional models are created at the selected frequency points by expanding the multivariate functions into series of orthogonal multinomials. The expansion coefficients are found by solving a system of interpolation conditions. In this stage the support points are added in an entirely adaptive way. Next the frequency dependence is added by one-dimensional rational interpolation of the models response. The procedure creates models with good accuracy, but it is obvious that excluding frequency from the adaptive sampling procedure may result in non-optimal number of support points. Results presented so far also show that the technique is efficient for up to three parameters. It is noteworthy that the technique is integrated into ADS Momentum electromagnetic simulator as the *Model Composer* module, which proves the importance of new model libraries for microwave circuit design.

Lehmensiek and Meyer [79–81] developed a technique based on Thiele-type branched continued fraction representation of a rational function. The algorithms operate on basis of univariate adaptive sampling along a selected dimension. Thus, while the support points do not fill the grid completely, they are being added along straight lines passing through multidimensional space. The efficiency of the algorithms was illustrated on two- and three-dimensional models.

The surrogates can also be created with application of radial basis functions (RBF) [33, 71]. However, tests carried out by our research group show that the RBFs are inefficient in the case of complex devices. The selection of the best value of the unknown shape-parameter of radial functions [101] is the main issue. On the other hand usage of the RBFs significantly reduce the problems with ill-conditioning.

There are approaches that use statistical tools for model construction like Kriging [110] and Design of Experiment (DOE) [113] techniques. Kriging is a special form of interpolation function that employs the correlation between neighboring points to determine the overall function at an arbitrary point. DOE makes a series of tests in which a set of input variables is changed and the experimenter can identify the reasons for changes in the outputted response. Based on this knowledge one can construct a statistical model of the test structure. Both techniques can be applied to create of simple models with low accuracy and are dedicated to coarse tuning of the design.

Even low accuracy surrogate models can be useful in design. A space-mapping technique proposed by Bandler [11, 60, 61, 125] allows one to link a low accuracy, coarse model with a high accuracy model of different complexities.

2.2 Equivalent circuits for time-domain analysis

Surrogate models are useful in the design of linear part of high frequency circuit. If the circuit involves non-linear devices, then the results of linear analysis have to be incorporated in the non-linear simulation. Since its introduction, the SPICE (Simulation Program with Integrated Circuit Emphasis) circuit simulator, has became an industry standard for design of low-frequency analog and mixed analog-digital circuits. SPICE is a time-domain oriented circuit simulator and has several advantages, namely:

- versatile library of models of active/nonlinear elements provided directly from com-

ponent manufacturers,

- ability to perform a transient simulation of the non-linear circuits,
- ability to mix both analog and digital circuits, like RF-blocks and memory/logic(control) blocks with time-domain approach,
- ability to preform a signal integrity (SI) analysis of the component or the system as a whole.

Despite of its advantages, the application of SPICE to high frequency networks suffers from lack of built-in models for accurate simulation of high frequency, distributed passive circuits, like these needed for analysis of distributed interconnect networks [87, 105]. The basic elements incorporated in SPICE are lumped elements such as resistors, capacitors, inductors, and various types of current and voltage sources. Extending the application area of SPICE to higher frequencies requires SPICE-compatible equivalent circuits of distributed multiport passive elements, e.g. interconnects.

The parameterized mathematical models can not be directly incorporated into SPICE since existing modelling techniques are mostly focused on construction of surrogate models in frequency domain. Most of the electromagnetic simulators and measurements also give the data in frequency domain. The evaluation of the model response usually involves evaluation of closed-form formulas, which is not possible within SPICE. As a result, if one wants to take advantage of the speed offered by surrogate models in nonlinear simulations, techniques that allow one to incorporate frequency domain data into the time-domain analysis in SPICE are needed.

To extract a SPICE model of a distributed passive device without explicitly performing frequency domain simulation the full wave partial element equivalent circuit (PEEC) technique can be used [117]. However, PEEC has several limitations: it is time-expensive, the resulting circuit has a large number of nodes which grows rapidly with the increase of structure complexity. It also suffers from stability issues. What is even more important PEEC is applicable only to homogeneous media.

2.2.1 Existing solutions employing FD data in TD simulations.

Several techniques of binding SPICE with frequency domain data exist that can be useful if the frequency domain data is strictly passive. One solution is to utilize a convolution technique which allows one to incorporate the tabulated data directly into time-domain simulation [13]. This approach is computationally inefficient due to many time steps in simulation. A faster recursive convolution technique [84] uses a rational representation of the data. Both techniques can be used when the input data (and corresponding rational model) is passive. Lack of passivity may lead to convergence problems.

The most versatile solution would be to transform the data from frequency domain to the lumped equivalent circuit that can be used in both frequency and time-domain analysis. The techniques presented in [8, 9, 92, 118] show how to realize a stable rational representation of the transfer function as a SPICE-compatible equivalent circuit. Since a passive rational model results in a passive equivalent circuit, the issue is to create a passive rational function.

To ensure passivity of the model, one can introduce additional constraints directly on a stage of construction of rational representation of admittance parameters, like in [106] or [35]. However, these constraints are not sufficient to ensure passivity in broad band. Another approach proposed in [88] is derived from the pole-residue form of rational function and can generate a passive macromodel over infinite frequency range, but the enforcement problems might appear when real poles occur. A different solution, presented in [49], enforces passivity condition at discrete frequencies, therefore resulting macromodel can be non-passive at frequencies that were not taken into account during passivity enforcement. It is possible to try to select the distribution of frequency points in such manner that the constructed rational model is passive [28], however this approach does not guarantee success.

To generate a passive macromodel from passive, frequency tabulated data, one can use a model order reduction techniques (MOR) that use Krylov-subspace methods, like in [1, 93, 107]. An equivalent circuit can be constructed directly from the macromodel, as shown in [2] or [99].

The aforementioned techniques can be directly applied if the data is passive. However, very often this condition is not fulfilled, as in the case of parameterized mathematical surrogate models or measurement data. Additionally, most of the techniques do not guarantee the passivity of the model for all frequencies.

In such a case the passivity has to be enforced, i.e. the model has to be corrected to restore the passivity. Guaranteed passivity can be achieved by applying either the method based on convex optimization [22] or an iterative procedure that enforces passivity while minimizing the distortion of the time domain response [43, 45, 108]. However, in several practical applications (like filter or other resonant circuits), one may be interested in controlling of the accuracy of the frequency response in a specific frequency band. The convex optimization approach can handle only problems with a low number of states [22]. In both techniques residues of the rational function are perturbed which implies that for a multiport circuits the number of variables to be adjusted is large.

Chapter 3

Parameterized surrogate models

3.1 Introduction

This chapter presents basics of advanced techniques of parameterized surrogate models construction. A new technique is introduced that allows one to create a mathematical surrogate model of scattering parameters of an arbitrary structure. The main idea is to represent the transfer function of the device being modelled with a multivariate complex-valued rational function [66, 68, 75]. The technique is an extension of the technique presented in [3] to the multivariate case. Several improvements were introduced to automate the procedure, namely the adaptive sampling over the whole parameter space for efficient selection and minimizing the number of support points. The models have the accuracy comparable to full wave simulations but at the same time the computational speed similar to the closed form formulas. As a result it is possible to achieve fast optimization of microwave circuits manufactured in emerging and new technologies, for which accurate models have not been developed yet. Specifically the following issues are addressed in this chapter:

- Formulation of the problem as a multivariate rational interpolation scheme,
- Improvement of stability of the interpolation solvers by replacing multinomials with better conditioned orthogonal polynomials,
- Support points selection using adaptive sampling,
- Automated selection of the model order,
- Automated division of the parameter space that allows one to create different low order models in each subspace,
- Merging sub-models into a single model covering a wider parameters range.

3.2 Closer look on alternative techniques

In order to be able to compare the new technique with the existing ones, main alternative approaches are discussed first.

Table 3.1: The number of support points needed for N-dimensional fully filled rectangular grid with resolution D (points per dimension)

Variables	Resolution D					
	1	2	3	4	5	6
1	1	2	3	4	5	6
2	2	4	9	16	25	36
3	3	8	27	64	125	216
4	4	16	81	256	725	2196
5	5	32	243	1024	3125	7776
6	6	64	729	4049	15625	46656
7	7	128	2187	16384	78125	279936

3.2.1 Lookup tables

The simplest method of multivariate modelling is a *lookup table*. The model parameter space Γ is covered with a dense multidimensional rectangular grid and at the nodes of the grid the values of the modelled function are evaluated. The model response at the points between the nodes of the grid is evaluated using interpolation techniques, like spline interpolation. Such an approach is far from optimal, due to fast growth of the number of samples with the increasing grid resolution and the number of model parameters (see table 3.1). Moreover it suffers from non-linearities of model response. Lookup tables are used in LINMIC simulator [128].

3.2.2 Artificial neural networks

An artificial neural network (ANN) has recently become one of the most popular technique for surrogate models construction [25, 30, 32, 78, 100, 121, 133, 134]. An artificial neural network is a mathematical model of a biological neural network. In practice, neural networks can be used as non-linear statistical data modeling tools, to model complex relationships between inputs and outputs or to find patterns in data.

3.2.2.1 Network structure

The most commonly used structure of the ANN is a multilayer perceptron network (MLP). The structure is built as L neuron layers and network of feed-forward neuron connections (Fig. 3.1). Layers one and L are called the input/output layers, respectively, and layers $2 \ldots L-1$ are hidden layers. From a mathematical point of view, a neural network can be described as a mapping of a set of N-dimensional input vectors $\boldsymbol{X}$ to M-dimensional output vectors $\boldsymbol{Y}$:

$$\boldsymbol{Y} = F(\boldsymbol{X}) \tag{3.1}$$

$$\boldsymbol{x_k} = (x_{1k}, x_{2k}, \ldots, x_{Nk}) \tag{3.2}$$

$$\boldsymbol{y_k} = (y_{1k}, y_{2k}, \ldots, y_{Mk}) \tag{3.3}$$

The mapping is described by a set of factors $w^l_{i,j}$, each one representing weight of the connection between i-th neuron of $l-1$-th layer and j-th neuron of l-th layer.

The output of i-th neuron of l-th layer $y_{l,i}$ is defined as a nonlinear function (called activation function, usually sigmoidal), which takes as an argument a linear combination of its inputs (outputs of N_{l-1} neurons in previous layer $y_{l-1,j}$) taken with different weights:

$$y_{l,i} = f(\chi_{l,i}) = \frac{1}{1+e^{-\chi_{(l,i)}}} \tag{3.4}$$

where $i = 1 \ldots N_{l-1}$,$l = 2 \ldots N_L$ and $\chi_{l,i}$ is a weighted sum of neuron inputs:

$$\chi_{l,i} = \sum_{j=1}^{N_{l-1}} w^l_{(i,j)} \cdot y_{(l-1,j)} \tag{3.5}$$

An overall response of the network is usually computed in the feed-forward process [134]. The external inputs are first fed to the input neurons and the first layer outputs $\boldsymbol{x} = (x_1, x_2, \ldots, x_N)$ are fed to the second layer (hidden). The procedure continues a layer by layer, up to the layer L, computed with a constant set of weights W. Thus, the output of the network is $\boldsymbol{y} = (y_{L,1}, y_{L,2}, \ldots, y_{L,k})$.

3.2.2.2 Training

To find a relation F in (3.1) a process called "training" of the network is applied. It is an iterative procedure, during which the weights W are adjusted in order to minimize the error between the output of the network y_k and the training data b_k. The error is defined as a mean square error:

$$E_{Tr} = \frac{1}{Q} \sum_{q=1}^{Q} \left[\frac{1}{2} \sum_{m=1}^{M} (y_{q,m} - b_{q,m})^2 \right] \tag{3.6}$$

where Q is a number of data samples pairs $(\boldsymbol{x_k}, \boldsymbol{b_k}, (k = 1 \ldots Q)$ in training set. The most popular approach is to set initial values of $w^l_{i,j}$ to small random values from the range [-0.5,0.5]. Then a gradient based training technique, like conjugate gradient or quasi-Newton, can be applied to correct the weights. Gradient techniques require computation of error derivative $\partial E_{Tr} / \partial w^l_{i,j}$, and in the case of MLP network it is common to compute gradient using the error back-propagation (EBP) technique.

3.2.2.3 ANN validation

A validation error is computed using the measure (3.6) using a validation (test) data set (x_v, b_v). The validation error E_V is periodically evaluated during the training and is used as a stoping criterion for the training procedure.

3.2.2.4 Drawbacks of ANNs

Artificial neural network models have been found as a useful tool for microwave design. Sample applications involve models of passive components, transmission lines, CPW components, inductors, FET's, amplifiers and filters [78, 100, 121]. However, there are several issues that limit their applications for automated model construction, some of them are:

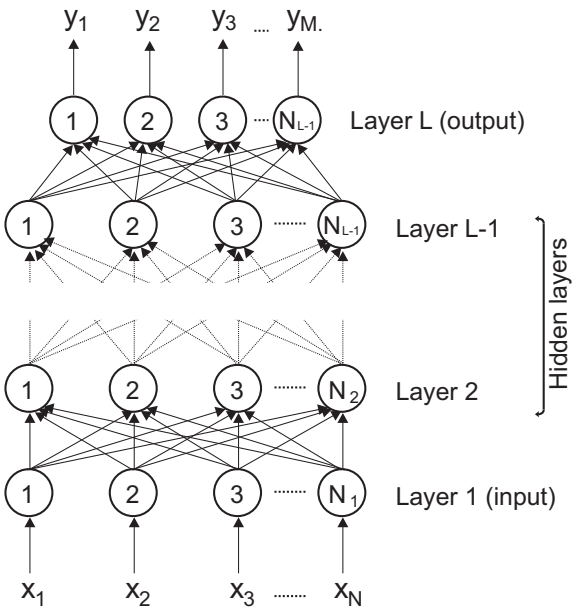

Figure 3.1: Structure overview of artificial neural network.

- **Network structure selection**. For an arbitrary modelled device with an unknown transfer function there is no rule how to set up the proper structure of the network (number of layers L and number of neurons of each layer N_l, $l = 1 \ldots L$). These parameters are key elements that determine the efficiency of the network training: the more neurons and layers the more complex responses can be modelled and the more difficult the training process is. Two phenomena are related to this issue:
  - Over-learning. When the network is too complex (consists of too many layers and/or neurons) comparing to complexity of modelled transfer function, the phenomenon of *over-learning* of the network can occur. In such a case the network only memorizes data, but does not generalize it well, resulting in over-complex response.
  - Under-learning. The opposite effect to over-learning can occur when the complexity of the network is insufficient to generalize the relation between the inputs and the outputs. It is called *under-learning* and as in the case of over-learning it leads to poor generalization.
- **Training set samples selection**. There is no general rule for selection of data that constitute the training set. Possible approaches are random data selection or regular patterns (uniform grids), but obviously, for such cases some areas in the parameter space may be under-sampled.

3.2.3 Interpolation based techniques

Several approaches exist that rely on different schemes of multivariate interpolation. The advantage of interpolation approach is that the model is completely described with interpo-

lation coefficients and moreover, it is fast to evaluate its response. Two types of interpolation techniques are the most common: polynomial and rational. The rational interpolation is far better suited for microwave engineering, because it can better approximate the functions that contain poles.

3.2.3.1 Burlisch-Stoer algorithm

One of the techniques of direct interpolation is the Burlisch-Stoer method. It involves Neville-type algorithm that allows one to interpolate tabulated data in a recurrence procedure. The algorithm is based on 1D Burlish-Stoer recursive rational interpolation technique [114]. For a set of points (x_i, S_i) (i=1... I), let us assume that R_k is a rational function of zero-degree (constant factor) that interpolates the point (x_k, S_k). Similarly, let us define $R_{k(k+1)}$ (k=1,...,I-1) which represents a rational function of order one that passes through points (x_k, S_k) and (x_{k+1}, S_{k+1}). In the same manner a higher order functions, up to $R_{(123...I)}$ are constructed. In general:

$$R_{k(k+1)...(k+m)} = R_{(k+1)...(k+m)} + \frac{R_{(k+1)...(k+m)} - R_{k(k+1)...(k+m-1)}}{\frac{x-x_k}{x-x_{k+m}}\left(1 - \frac{R_{(k+1)...(k+m)} - R_{k(k+1)...(k+m-1)}}{R_{(k+1)...(k+m)} - R_{(k+1)...(k+m)}}\right) - 1} \tag{3.7}$$

The univariate interpolation is exploited to higher dimension models with recursive procedure, as presented in [95]. It is assumed that the set of support points forms a fully filled non-equidistant rectangular grid. The set of support points forms a fully filled rectangular grid computed as a cartesian product:

$$\{(x_1^{(0)}, x_1^{(1)}, \ldots, x_1^{(N1)})\} \times \{(x_2^{(0)}, x_2^{(1)}, \ldots, x_2^{(N2)})\} \times \ldots \times \{(x_N^{(0)}, x_N^{(1)}, \ldots, x_1^{(NN)})\} \tag{3.8}$$

To find the model value at an arbitrary point $\boldsymbol{x_s}$ the algorithm starts with a 1D interpolation preformed along a single variable (for example x_1) with all other parameters $x_2, \ldots x_N$ set to fixed values $x_2 = x_{s2}, \ldots, x_N = x_{sN}$ - this is called a root process. If the values of the function at the interpolation nodes are known, the model is evaluated. If it is not the case, a new child process is started that perform a 1D interpolation along the next variable (x_2) with $x_1 = x_{s1}, x_3 = x_{s3}, \ldots, x_N = x_{sN}$. The procedure steps forward until a model for all unknown variables is evaluated.

3.2.3.2 Thiele-type BCF approach

In a similar manner an univariate Thiele-type branch-continued fraction (BCF) can be extended to a multivariate case [41]. With this approach univariate rational function $S(x)$ is represented as a convergent continued fraction computed at a set of points $(x^{(i)}, S_i)$, i=1... I:

$$\begin{aligned} R_k(x) \;=\; S_0 + \frac{x - x^{(0)}}{\phi_1(x^{(1)}, x^{(0)}) + \frac{x - x^{(1)}}{\phi_1(x^{(2)}, x^{(1)}, x^{(0)}) + \cdots}} \\ \cdots \frac{x - x^{(k-1)}}{\phi_k(x^{(k)}, x^{(k-1)}, \ldots, x^{(1)}, x^{(0)})} \end{aligned} \tag{3.9}$$

where:

$$\phi_1(x^{(i)},x^{(0)}) = \frac{x^{(i)}-x^{(0)}}{S_i - S_0} \quad i = 1,2,\ldots,I \tag{3.10}$$

$$\phi_k(x^{(i)},x^{(k-1)},\ldots,x^{(1)},x^{(0)}) = \frac{x^{(i)}-x^{(k-1)}}{\phi_{k-1}(x^{(i)},x^{(k-2)},\ldots,x^{(0)}) - \phi_{k-1}(x^{(k-1)},x^{(k-2)},\ldots,x^{(0)})}, \quad \begin{array}{c} i = k,k+1,\ldots I, \\ k = 2,3,\ldots,I \end{array} \tag{3.11}$$

This form can be generalized to the multivariate case: N-variate function $S(\boldsymbol{X}) = S(x_1,x_2,\ldots,x_N)$ is approximated as:

$$R(x_1,x_2,\ldots,x_N) = R_0(x_2,\ldots,x_N|x_1^{(0)}) + \cfrac{x_1 - x_1^{(0)}}{R_1(x_2,\ldots,x_N|x_1^{(1)}) + \cfrac{x_1 - x_1^{(1)}}{R_2(x_2,\ldots,x_N|x_1^{(2)}) + \ldots \cfrac{x_1 - x_1^{(N1)}}{R_{N1}(x_2,\ldots,x_N|x_1^{(N1)})}}} \tag{3.12}$$

Each of the $(N-1)$ variate functions $R_0,R_1,\ldots,R_{N1}$ can also be represented in a form of BCF function similar to (3.12) and described with functions of $N-2$ variables. The procedure is repeated and at the lowest level univariate functions are constructed using (3.9). A drawback of such a technique is that support points must form a full rectangular grid. A modification of multivariate BCF function was proposed in [79] to allow adaptive sampling. Instead of using direct values of modelled function at the nodes of the rectangular grid, the method uses approximated values are used obtained from previously computed interpolants. The adaptive scheme exploited in [79] improves the efficiency of the technique. However, the support points are still placed in the structured manner and their placement is far from optimal.

3.2.3.3 MAPS approach

A MAPS (multidimensional adaptive parameter sampling) technique, proposed in [31, 38], separates the frequency from other parameters of modelled device. The approach relies on the scattering parameters description of the device. With this approach the scattering parameter S_{ij} is represented in a form:

$$S(f,\boldsymbol{x}) \approx M(f,\boldsymbol{x}) = \sum_m C_m(f)P_m(\boldsymbol{x}) \tag{3.13}$$

where $P_m(\boldsymbol{x})$ is a set of basis functions in form of orthonormal multinomials, $\boldsymbol{x} = [x_1,x_2,\ldots,x_N]$ is a vector of geometric parameters and $C_m(f)$ represents weights that depend on frequency and has a polynomial or rational form. Model construction is completed in two steps. At first, at discrete frequency points $f_1, f_2, \ldots, f_k$, multinomial models are fitted to the scattering parameters. The frequencies are selected using the adaptive frequency sampling (AFS) technique [31]. The models are built with the same set of basis functions and share the same set of support points $\boldsymbol{X}_s$. The selection of the support points over geometric parameters exploits an adaptive sampling technique. Once the models have been developed discrete

values of the multinomial coeffcients are extracted and fitted on a set of discrete frequencies $f_1, f_2, \ldots, f_k$ as the frequency dependent functions $C_m(f)$. If the model is inaccurate, the set of frequencies is appended.

The separation of frequency from the other model parameters makes the technique of adaptive support point selection not optimal, especially in the case of frequency sampling. An addition of a single frequency point requires computing of a polynomial $P_m(\boldsymbol{x})$ at this particular frequency which, in turn, requires adding several data points for different geometries.

3.3 Fully-adaptive multivariate rational interpolation

3.3.1 Interpolation problem formulation

In this thesis a novel technique is proposed that creates an interpolant of an N-variate, real or complex valued smooth function $\widehat{S}(\underline{X}) = \widehat{S}(x_1, x_2, ..., x_N)$ as a rational function [68]:

$$S(x_1, x_2, ..., x_N) = \frac{A(\underline{X})}{B(\underline{X})} = \frac{A(x_1, x_2, ..., x_N)}{B(x_1, x_2, ..., x_N)} \tag{3.14}$$

where both numerator $A(\underline{X})$ and denominator $B(\underline{X})$ are multinomials (sum of monomials multiplied by scalar coefficients). The complete set of the monomials can be listed as elements of matrix [12]:

$$\begin{array}{l}
\text{Row 1 : } 1 \\
\text{Row 2 : } x_1 \;\; x_2 \;\; \ldots \;\; x_N \\
\text{Row 3 : } x_1^2 \;\; x_1x_2 \;\; \ldots \;\; x_1x_N \;\; x_2^2 \;\; x_2x_3 \;\; \ldots \;\; x_N^2 \\
\text{Row 4 : } x_1^3 \;\; x_1^2x_2 \;\; x_1^2x_3 \;\; \ldots \;\; x_1^2x_N \;\; x_2^3 \;\; x_2^2x_1 \;\; x_2^2x_3 \;\; \ldots \;\; x_N^3 \\
\ldots
\end{array}$$

The m-th row contains all monomials with sum of powers at each variable equal m-1. With such an assumption, the multinomials of numerator/denominator can be described by a vector $V = [v_1, v_2, \ldots, v_N]$, where v_i determines the maximum power allowed for the i-th variable. For example, in the case of a three-variate multinomial whose order is described by vector $V = [3\ 2\ 2]$, the following monomials are selected:

$$\begin{array}{l}
\text{Row 1 : } 1 \\
\text{Row 2 : } x_1 \;\; x_2 \;\; x_3 \\
\text{Row 3 : } x_1^2 \;\; x_1x_2 \;\; x_1x_3 \;\; x_2^2 \;\; x_2x_3 \;\; x_3^2 \\
\text{Row 4 : } x_1^3 \;\; x_1^2x_2 \;\; x_1^2x_3 \;\; x_1x_2^2 \;\; x_2^2x_3 \;\; x_1x_3^2 \;\; x_2x_3^2 \;\; x_1x_2x_3
\end{array}$$

In further investigations it is assumed that both the numerator A and the denominator B of (3.14) have the same orders, therefore $V_A = V_B = V$.

In general, the problem (3.14) is non-linear and the unknown coefficients a_i and b_i corresponding to the multinomials of numerator and denominator of 3.14 can be found enforcing its linearization and requiring that equation:

$$A(\underline{X}) - \widehat{S}(\underline{X})B(\underline{X}) = 0 \tag{3.15}$$

is fulfilled on at least $L \geq M_1 + M_2$ support points, where M_1 and M_2 are the numbers of unknown coefficients a_i and b_i. The fitting problem can be transformed to the matrix form:

$$[A \ -B] \begin{bmatrix} a \\ b \end{bmatrix} = 0 \tag{3.16}$$

where a and b are the vectors of unknown coefficients and $[A]_{L\times M_1}, [B]_{L\times M_2}$ are matrices involving the values of the monomials appearing in numerator and denominator of (3.14) as well as the values of the interpolated function at the support points. The linear problem is solved applying the total least squares technique (TLS), as described in Appendix B. [1]

3.3.2 Condition number improvement

The condition number in the least squares method measures the sensitivity of the solution of a system of linear equations to errors in the data. The condition number allows one to decide if the solution of the least squares is reliable and accurate. Specifically, the value of the condition number near to one indicates well-conditioned least squares problem. The condition number is computed as a ratio of the largest singular value of matrix that forms a least squares problem to the smallest one. A major issue of rational interpolation is poor conditioning of equation system. In order to cope with this problem two techniques are recommended:

- Mapping each of variables to a line segment <-1,1>
- Substitution of simple monomials with orthogonal Tchebychev polynomials

The first technique is a simple linear mapping of the model domain to the multidimensional box with side of line segment. The mapping strongly improves the conditioning due to a significant reduction of dynamics of elements of system matrix (bad-scaling). The mapping of a i-th variable x_i is expressed by the formula:

$$x_{i,m} = 2\frac{(x_i - x_{0,i})}{\Delta x_i} \tag{3.17}$$

where $x_{i,m}$ is the mapped variable, $x_{0,i}$ denotes center point of the parameter range and Δx_i denotes the width of the parameter range.

In order to improve the conditioning of the interpolation problem even further the regular elements of power series x_i^n which form the monomials are replaced with Tchebychev polynomials $T_n(x_i)$, that are orthogonal on line segment $< -1, 1 >$. The comparison of standard power series and orthogonal Tchebychev polynomials is shown in figures 3.2 and 3.3. It can be seen that Tchebychev polynomials offer more complex shape in the domain <-1,1> than

[1] Three years after the basics of the technique presented in this thesis were published, an alternative technique was proposed in [26] that has several common elements with the one described in this thesis. The authors use a low-displacement rank technique to solve the rational interpolation problem and show the advantages of the non-structured adaptive sampling.

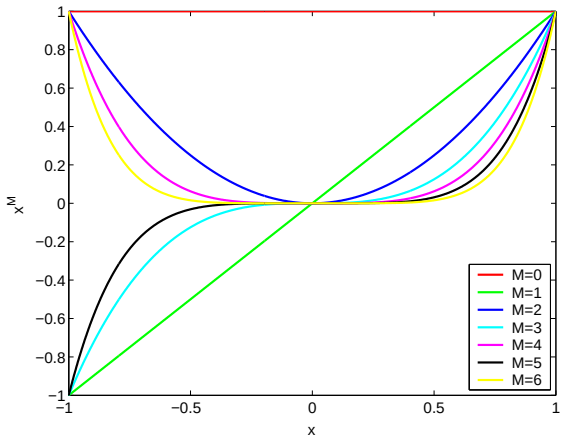

Figure 3.2: Power series

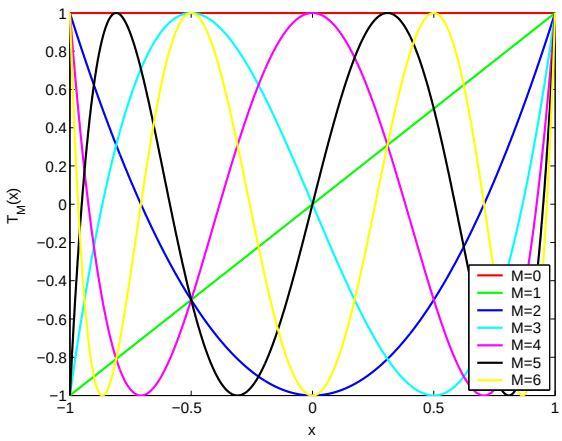

Figure 3.3: Tchebychev polynomials

simple power series and that improves the conditioning. Tchebychev polynomials can be computed using a recurrence formula:

$$\begin{aligned} T_1(x) &= 1 \\ T_2(x) &= x \\ T_3(x) &= 2x-1 \\ T_4(x) &= 4x^2-3x \\ &\vdots \quad\quad \vdots \\ T_{n+1}(x) &= 2x\cdot T_n(x) - T_{n-1}(x) \end{aligned}$$

As a result, the set of monomials is transformed into the form:

Row 1 : 1

Row 2 : $T_1(x_1)\ T_1(x_2)\ \ldots\ T_1(x_N)$

Row 3 : $T_2(x_1)\quad T_1(x_1)T_1(x_2)\quad \ldots\ T_1(x_1)T_1(x_N)\quad T_2(x_2)\quad T_1(x_2)T_1(x_3)\ \ldots T_2(x_N)$

Row 4 : $T_3(x_1)\quad T_2(x_1)T_1(x_2)\quad T_2(x_1)T_1(x_3)\quad \ldots\ T_2(x_1)T_1(x_N)\quad T_3(x_2)\ T_2(x_2)T_1(x_1)\ T_2(x_2)T_1(x_3)\ldots T_3(x_N)$

...

The construction and evaluation of such a system is more complex than in the case of simple power series, however it gives better accuracy of the resulting interpolation.

The advantages of application of orthogonal polynomials and domain mapping is illustrated using the example of interpolation of reflection coefficient S_{11} of rectangular iris in WR62 a waveguide. The electromagnetic simulation of the structure was carried out using the mode-matching technique. The iris structure is shown in Fig. 3.4. The model has four parameters: frequency f, iris width a, height b and thickness d. The range of input parameters is presented in table 3.2. The response of the iris, shown in Fig. 3.5, presents complex and resonant behavior.

The structure parameter range was covered with rectangular grid with density D=4 and D=6. The electromagnetic response of the structure at the nodes of the grid was computed and the resulting multidimensional dataset was interpolated with orthogonal and non-orthogonal functions, with and without mapping of model domain. The results are presented

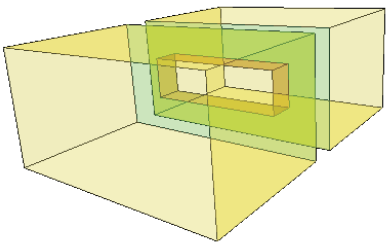

Figure 3.4: Iris in rectangular waveguide.

Table 3.2: Parameter range of resonant iris case

Parameter	Range
frequency f	11.855GHz - 18.02GHz
width a	6.32mm - 15.8mm
height b	4.74mm - 7.899mm
thickness d	0.2mm - 2mm

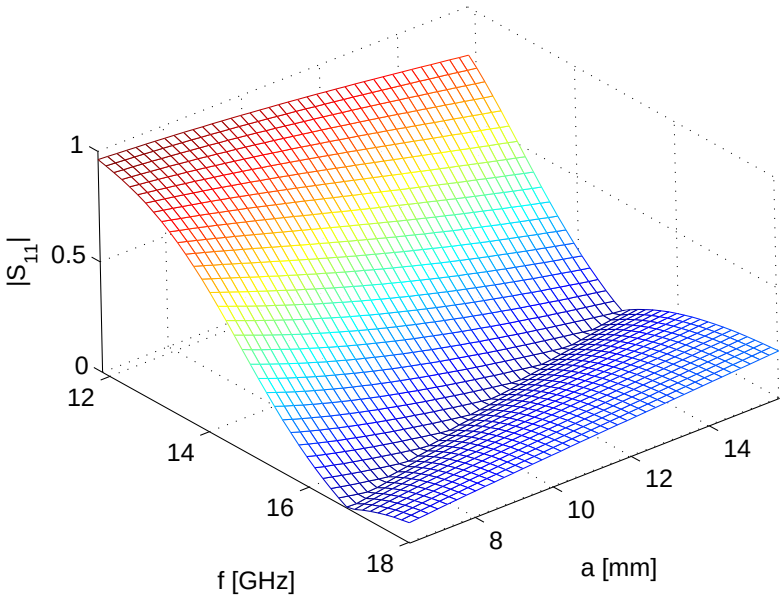

Figure 3.5: Sample S_{11}(f,a) response of iris in WR62 rectangular waveguide with iris height $b = 6.32$mm and iris thickness $d = 1.1$mm.

in Tab. 3.3 and 3.4, respectively. It is seen that both techniques provide a significant reduction of the condition number. The best results are obtained when both techniques are applied simultaneously. This results can be generalized to modelling of other structures.

3.3.3 Selection of support points

Optimal support point selection is an essential issue of every interpolation scheme. It is of significant importance in the case of modelling of multivariate functions where the number of support points can be enormous. Since each support point corresponds to one electromagnetic simulation of a device being modelled, it is obvious that minimization of the number of samples is critical. The basic techniques of support points selection involve rectangular grids or random locations. The more complex ones use adaptive point selection in the model domain, as presented in section 3.2.

Table 3.3: Condition number computed for a waveguide iris case for rectangular grid with divisions $D = 4$ and different polynomials

Model order V	Space, Polynomials		
	Non-mapped, Regular	Mapped, Regular	Mapped, Tchebychev
[2 2 2 2]	6692.3	186.3	136.5
[3 3 3 3]	508300	1489.5	1139.1

Table 3.4: Condition number computed for a waveguide iris case for rectangular grid with divisions $D = 6$ and different polynomials

Model order V	Space, Polynomials		
	Non-mapped, Regular	Mapped, Regular	Mapped, Tchebychev
[2 2 2 2]	7428	194.1	142.7
[3 3 3 3]	275350	1037	746.4

3.3.3.1 Adaptive sampling

The algorithm described in the thesis employs an adaptive sampling technique called also *reflective exploration* [38, 68]. In this technique two models $\hat{S}_1$ and $\hat{S}_2$ of different orders are created using the same set of data $\boldsymbol{X}$. It is convenient to introduce the inter-model error ε, which is the maximum difference between the models S_1 and S_2 over model domain Γ. Then, assuming the error ε corresponds to point $\boldsymbol{x_i} \in \Gamma$, the idea of adaptive sampling is to extend the data set $\boldsymbol{X}$ by adding the point $\boldsymbol{x_i}$ and develop the models again. Such a procedure, reiterated, leads to an improvement of model quality and assures the points are selected at optimal locations, which minimizes the total number of samples used. It is especially advisable if the models are based on results of computationally expensive calculations, such as electromagnetic simulations.

The difference between previous solutions and the one used in this work is that the adaptive search is performed over the whole model domain avoiding structured pattern. As a result the appended points are selected at arbitrary locations in the model domain, like presented in figure 3.6. The points are appended at the locations corresponding to maximum of error function:

$$\varepsilon = \varepsilon(\boldsymbol{x}) = \|\hat{S}_1(\boldsymbol{x}) - \hat{S}_2(\boldsymbol{x})\| \tag{3.18}$$

Finding such locations corresponds to a problem of search of maximum of a multivariate function over a multi-dimensional box:

$$\boldsymbol{x_i} \;:\; \min_{\boldsymbol{x}} \quad \varepsilon(\boldsymbol{x}) \tag{3.19}$$

which, especially in the case of high number of model parameters, has to be efficiently implemented. Genetic optimization procedure [39] was applied for this reason, as it allows one to find a global, not local, maximum of a function.

It has to be noted that although adaptive sampling minimizes the error ε, the real accuracy of resulting model can be worse than the achieved value ε_0. Such a situation is possible when both models converge to a similar solution which slightly differs from the electromagnetic response. Let Δ_{S1} and Δ_{S2} represent the absolute error of models $\hat{S}_1(\underline{X})$ and $\hat{S}_2(\underline{X})$ related

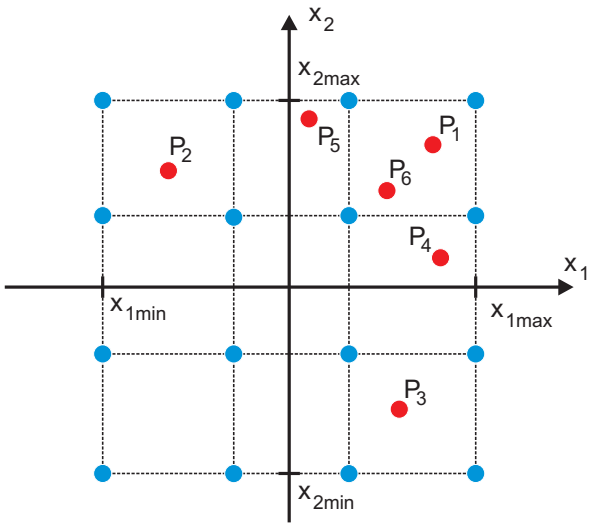

Figure 3.6: Two dimensional example of support points selection - added points (in red) are placed in a non-regular manner over the parameter space.

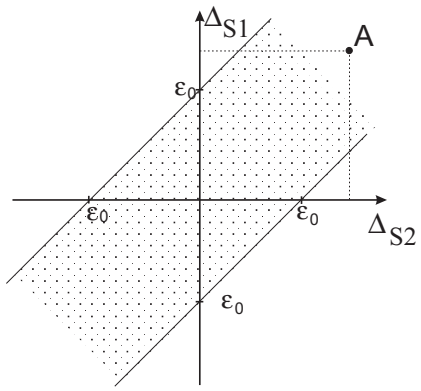

Figure 3.7: Range of model error for mismatch between models equal error ε.

to electromagnetic response and assume that the maximum acceptable error between both models is ε_0. The possible values of model error Δ_{S1} and Δ_{S2} are illustrated in figure 3.7 (dotted area). For example, for point A, the real error Δ_{S1}, Δ_{S2} of both models is higher than ε_0, however the relative error between both models is below ε because the real errors of both models have the same signs.

One-dimensional illustration. A general idea of adaptive sampling is illustrated on 1-dimensional example. For an unknown function $f(x)$ two polynomial models $S_1(x)$ and $S_2(x)$ are computed with orders $M_1 = 9$ and $M_2 = 10$, as presented in Fig.3.8a. At the point of the highest error an additional support point is selected, appended to the set of support points and the models are recomputed as shown in Fig. 3.8b. The accuracy of the models increased in region surrounding the added point (denoted in the figure with a circle). The procedure is repeated, as shown in Fig. 3.8c and once again a significant improvement of

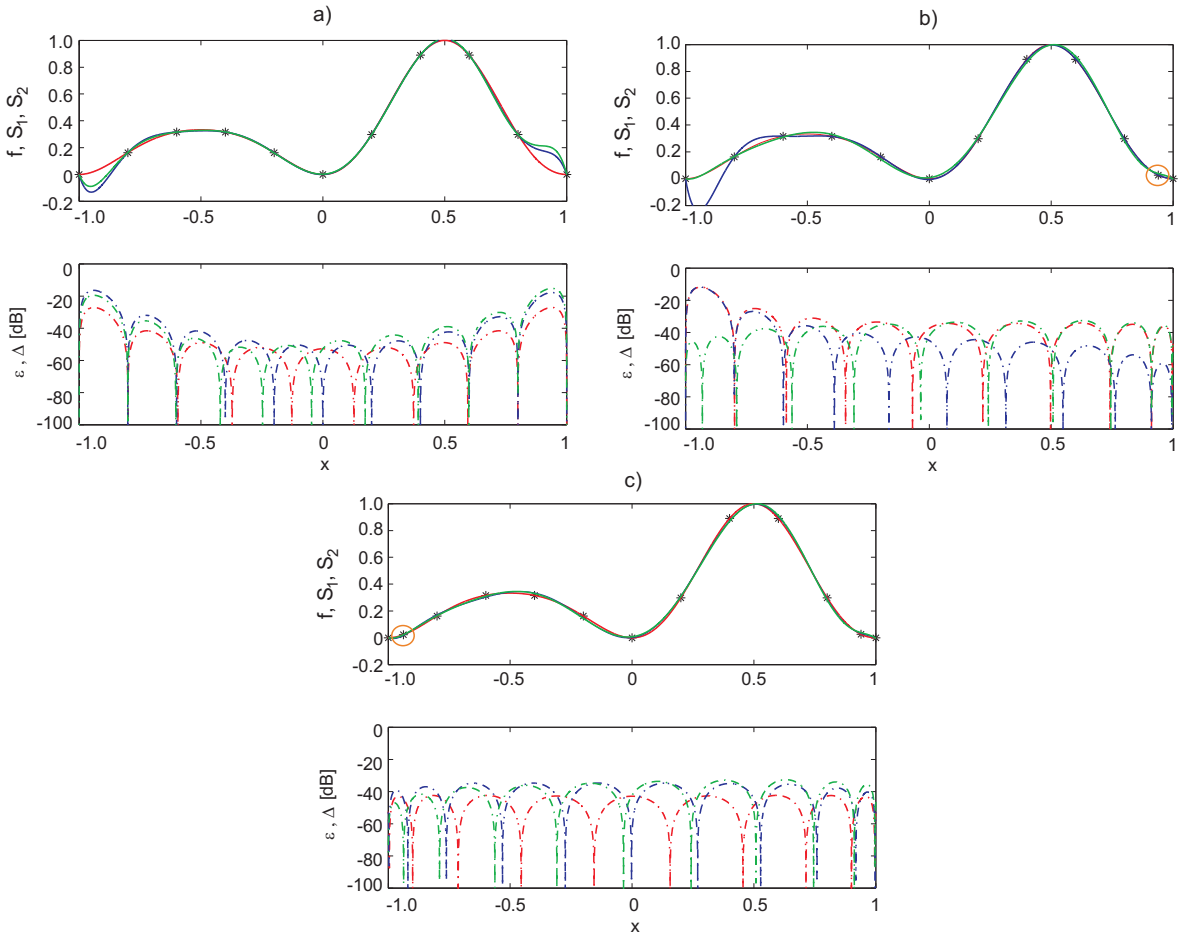

Figure 3.8: An 1-dimensional example of adaptive support point selection. (—) original (modelled) function, (—) model S_1 (M=9), (—) model S_2 (M=10), (-.-.-) error ε, (-.-.-)error Δ_{S1}, (-.-.-) error Δ_{S2}.

model accuracy can be seen.

3.3.3.2 Clustering and ill-conditioning detection

During the adaptive sampling process clustering of support points can occur, i.e. subsequent support points are added at the same location. The interpolation problem is then expanded with points which do not give any extra information about the device response, but make the problem bigger and more difficult to solve. Such a situation should be avoided, therefore if the algorithm detects such behavior, the parameter space is divided into 2^N smaller subspaces (each dimension is halved) and the locations of biggest mismatch between models in those 2^N subspaces are found. The set of points is appended to the data set and the adaptive sampling continues.

The proposed scheme of adaptive sampling makes it possible to detect if the interpolation problem is ill-conditioned. The models obtained as the solution of ill-conditioned system do not match each other and, in result, error between both models is large (namely $\varepsilon > 1$). If such situation occurs at the initial stage of model construction, when the number of support points is small, the best solution to improve the conditioning is to add more points to the

system. Another situation when the ill-conditioning of the system occurs is when the order of the models becomes too high. In this case the, scheme of parameter space division can be applied to construct the model, as described in section 3.3.6.

3.3.4 QR-update.

The adaptive sampling procedure requires updating both models each time a support point is added. It means, that one has to recompute the TLS solution of interpolation problem in every iteration. To reduce the numerical cost of this operation the *QR*-update procedure can be used [40]. Assuming that matrix C has a factorization $C = Q \cdot R$, where Q is orthogonal and R is upper triangular, addition of a single support point appends a vector w^T to the matrix C and, in result, one obtains the updated matrix:

$$\hat{C} = \begin{bmatrix} w^T \\ C \end{bmatrix} \tag{3.20}$$

Additionally, one can notice that:

$$diag(1, Q^T) \cdot \hat{C} = \begin{bmatrix} w^T \\ R \end{bmatrix} = H \tag{3.21}$$

where H is an upper Hessenberg matrix. It is possible to apply a set of n subsequent Givens rotations that transform H to upper triangular form:

$$R_1 = J_n^T \; J_{n-1}^T \; \ldots \; J_1 \tag{3.22}$$

Once the Givens rotations are known, the matrix Q_1 can be computed as:

$$Q_1 = diag(1, Q) \; J_1 \; J_2 \; \ldots \; J_n \tag{3.23}$$

Matrices R_1 and Q_1 form a *QR* factorization of matrix $\hat{C} = Q_1 \cdot R_1$.

The full *QR* factorization from scratch is an algorithm of complexity $O(N^3)$, while update of the existing Q and R matrices is $O(N^2)$ algorithm. However, the application of QR-update requires to store in computer memory the matrices Q, R and Q_1, R_1. Therefore, for updating big linear problems a large amount of computer memory is required.

3.3.5 Model order selection

A versatile modelling procedure should allow one to create models of devices of different complexity. Therefore, an important element of every model construction technique is a model order estimation. The optimum model order is defined as the order which assures the lowest model error prediction on test data for given training data. There are several statistical criteria for model order selection, like AIC or MDL criteria [4, 102]. However, they can be applied to autoregressive (AR) estimation models of an observed data sequence and are not applicable to the investigated multivariate rational interpolation scheme. In this work a new scheme of model order estimation is proposed that:

- Allows one to detect if the order of current model is too low,
- Provides a criterion for selection of higher model order.

Table 3.5: Initial grid density D vs. the number of model parameters

N	D	D^N	Unknows
2	4	16	12
3	3	27	20
4	3	81	30
5	3	243	42
6	2	64	56
7	2	128	72

3.3.5.1 Initial orders

The adaptive sampling procedure starts with a sparse rectangular grid of support points and two low order models. The initial models should be of a similar order and, in fact, the more both models differ each from the other, the more data points are needed by the algorithm to converge. On the other hand the choice of initial models has a marginal influence on the accuracy of final models, because it is the lower order model that limits the accuracy. In practice it is enough to set $V_{S1}(1:N) = 2$ and enforce the order of the second model to be lower/higher by one at first variable, i.e. $V_{S2}(2:N) = 2$, $V_{S2}(1) = V_{S1}(1) \pm 1$.

The density D of the initial rectangular grid is set so as to assure the interpolation problem is not under-determined, i.e. the number of grid nodes is equal or greater than the number of unknown coefficients of higher-order rational model. The minimal grid resolution vs. the number of model parameters is presented in table 3.5.

3.3.5.2 Adaptive order selection strategy

The proposed model order estimation technique is strongly related to adaptive sampling technique and is based on the analysis of behavior of the error ε, which is monitored during the adaptive sampling.

The behavior of the error is a basic indicator whether the model order should be increased. It was stated previously that subsequent addition of support points improves the model quality until the stagnation phase. Stagnation of the error ε, if detected, indicates that using the current orders the further addition of support points would improve the model accuracy only marginally. A simple method to detect this situation is to observe the number of iterations without accuracy improvement. The number from range 2^{N-1} up to 2^N iterations without improvement is a good indicator that the current order is too low and has to be increased.

To make the algorithm more efficient, several higher-order model pairs are computed and compared with each other. A new model pair is created by increasing the i-th elements of vectors V_{S1} and V_{S2} by one. From this set of models, a pair of models which assures the biggest reduction of error ε is selected.

Illustrative example. To make the procedure more clear, the order selection strategy is presented on an two-dimensional example of modelling scattering parameter $S_{21}(f,a)$ of an

inductive iris in a rectangular waveguide. The goal for the interpolation error was set to $\varepsilon_0 = 0.001$. Figure 3.9a shows a plot of error ε vs. number of added points using adaptive sampling. The procedure started with two models: S_1 with order $V_{S1} = [1 \;\; 2]$ and S_2 with order $V_{S2} = [2 \;\; 2]$, both computed on a rectangular grid with 16 nodes. After addition of 4 support points, next 4 points did not provide any further decrease of error ε. This was a signal to increase the model orders. At that stage three pairs of higher order models were computed with corresponding errors ε:

- Pair 1:$V_{S1} = [1 \;\; 3]$ and $V_{S2} = [2 \;\; 3]$, with $\varepsilon = 0.04473$
- Pair 2:$V_{S1} = [2 \;\; 2]$ and $V_{S2} = [3 \;\; 2]$, with $\varepsilon = 0.03066$
- Pair 3:$V_{S1} = [2 \;\; 3]$ and $V_{S2} = [3 \;\; 3]$, with $\varepsilon = 0.08126$

Comparing the errors ε, pair 2 resulted in the largest error drop. Therefore, the new orders of the models were changed to be equal to $V_{S1} = [2 \;\; 2]$ and $V_{S2} = [3 \;\; 2]$ (the orders of the selected pair). Once the orders have been changed, the adaptive sampling continues.

The orders were changed two more times (after addition of 23-th and 31-st point) until the orders were high enough and models reached the requested accuracy. In Fig. 3.9a the plots of the real absolute errors Δ_{S1} and Δ_{S2} are also shown. It is seen that the real error can be higher than error ε. However, decrease of the error ε also mean improvement of the actual accuracy of the models. Additionally, in Fig. 3.9b a distribution of support points selected with adaptive sampling is depicted. It proves that the points are selected without any regular pattern.

In some cases the procedure is not sufficient to construct a single model of device response due the ill-conditioning of the interpolation problem. It may happen if the model orders are too high and then the technique of parameter space division is applied, as discussed in next section.

3.3.6 Division of parameter space

Division of parameter space is important if the response of complex device is modelled (for example has resonances) and/or superb accuracy is requested. In such cases it might be impossible to construct a single rational model which covers whole parameter space and assures the desirable accuracy. To overcome the problem an automated technique of parameter space division was developed.

The important issue is to define a criteria for space division. In the proposed technique two situations that results in division of parameter space during the adaptive sampling procedure:

- The size of the problem becomes too big to be efficiently solved,
- Further increasing of model orders leads to ill-conditioned interpolation problem.

If any of these two situations occurs, the adaptive sampling stops and the variance analysis for each of the model parameters is performed. The smaller the variance of distribution of samples related to parameter x_i is, the more data points are concentrated around mean value

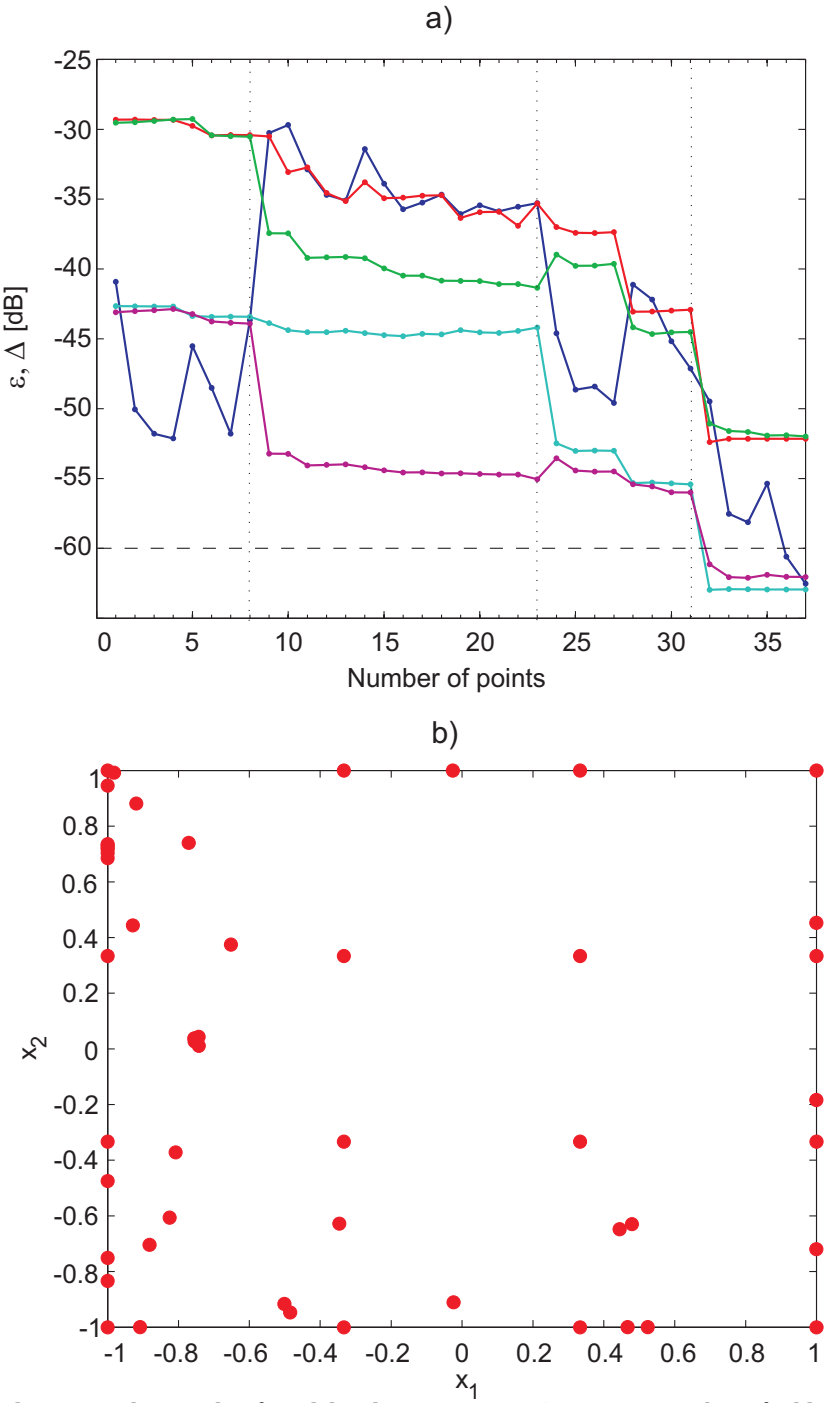

Figure 3.9: A 2-dimensional example of model order estimation: a) error vs. number of added support points, (—) error ε, (—)error Δ^{S1}_{max}, (—) error Δ^{S2}_{max} (—)error Δ^{S1}_{mean}, (—) error Δ^{S2}_{mean}
b) distribution of support points

of x_i. A high concentration of data points in an area suggests that in that place/dimension the model is poor, therefore that dimension is choosen to be divided. Algorithm creates two smaller subspaces with division of range of selected parameter into halves. The procedure is run recursively.

For an illustration purpose, the proposed technique of space division for a simple two-

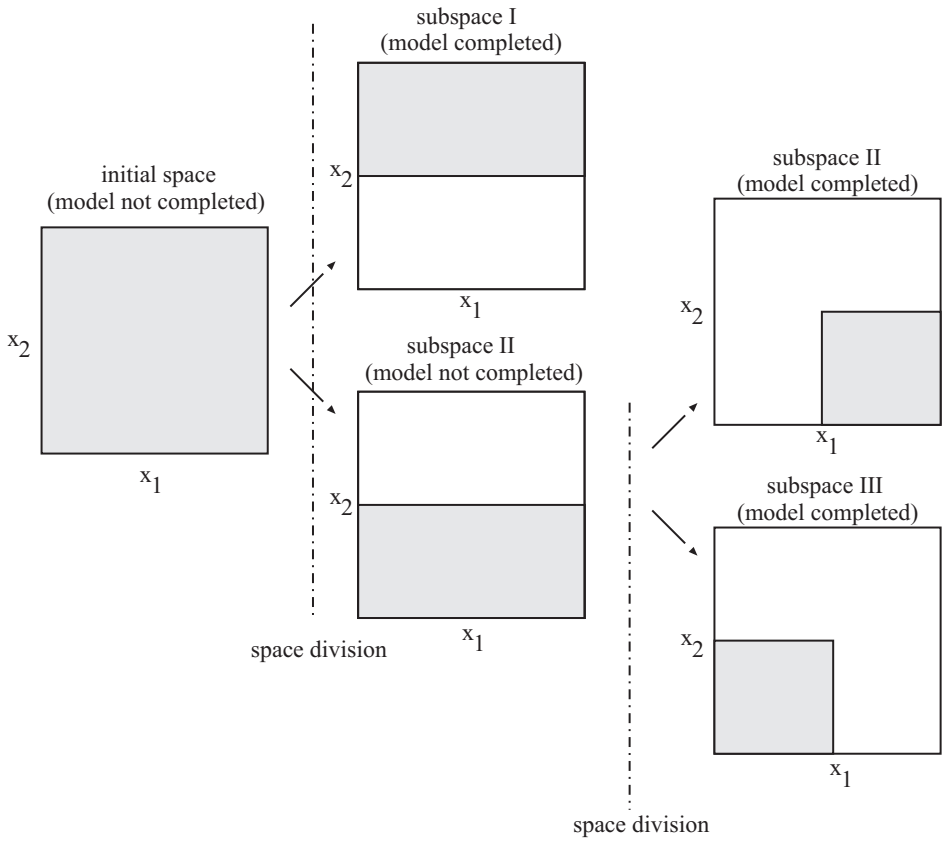

Figure 3.10: Sample space division in a two-dimensional case $S(x_1, x_2)$.

variate function $S(x_1, x_2)$ is presented in Fig. 3.10. The main loop of adaptive sampling was unable to create the single model of the structure. The figure depicts how the initial parameter space was divided into three non-overlaping smaller subspaces. The generalization of this approach to N-dimensional spaces is straightforward.

To show the robustness of the technique, a very accurate model of waveguide iris from section 3.3.2 was created. The required accuracy of model was established as $\varepsilon_0 = 0.001$ (-60dB). The procedure started with a sparse grid of 81 support points and adaptive sampling with order selection reduced the error level to value 0.002. Increasing of model orders resulted in ill-conditioning of the problem.

To achieve the requested accuracy the initial parameter space, shown in Table 3.2, was sequentially divided into three subspaces, presented in Table 3.6. At first, the range of width of iris was divided, then, in one of the subspaces, the frequency range was divided. For each subspace an independent model of the device response was created. The histogram and cumulative distribution function of the model error are presented on figure 3.11 and it shows that 90% of samples have accuracy better than -50dB. The mean error of model is -55.97dB and maximum error drops to -38.55dB. The total number of support points is M=460.

Table 3.6: Parameter ranges for three subspaces created with automated parameter division scheme

Param.	Model I	Model II	Model III
f [GHz]	11.855 - 18.02	11.855 - 14.9375	14.9375 - 18.02
a [mm]	6.32 - 11.06	11.06 - 15.8	11.06 - 15.8
b [mm]	4.74 - 7.899	4.74 - 7.899	4.74 - 7.899
d [mm]	0.2 - 2	0.2 - 2	0.2 - 2

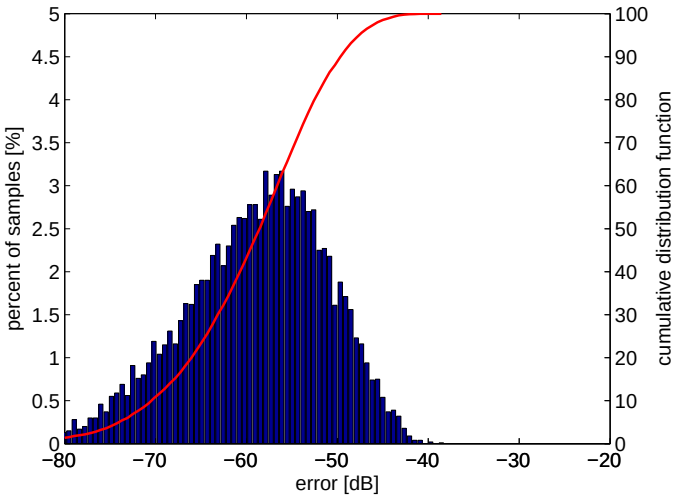

Figure 3.11: Histogram and cumulative distribution function of model error in the case of application of automated space division technique

3.3.6.1 Merging sub-models

One disadvantage of space division is a non-smooth response of the models at the point of connection of their domains. Since it is impossible to impose the continuity conditions directly into model computation algorithm, this problem has to be solved separately during computation of the model response. The problem is illustrated in Figure 3.12, that shows a plot of S_{11} parameter computed as the response of two models that cover this frequency range. The discontinuity of the response can be seen clearly at the point where the parameter space was divided.

In most of model applications the presence of response discontinuity is not an important issue. It is possible to perform a successful design using such a non-smooth model even when the gradient-based optimization of the structure is involved. However, if one needs a smooth response in the entire parameter space, it is possible to compensate for the discontinuity, for example by using a cubic spline interpolation procedures in the area of model connection, as presented in Figure 3.12. The a model response in the area of the models connection is computed from cubic spline interpolation using six points located near to the models connection (3 points from each model are taken into account). The application of cubic splines gives a smooth response with a continuous first derivative. Additionally, it is

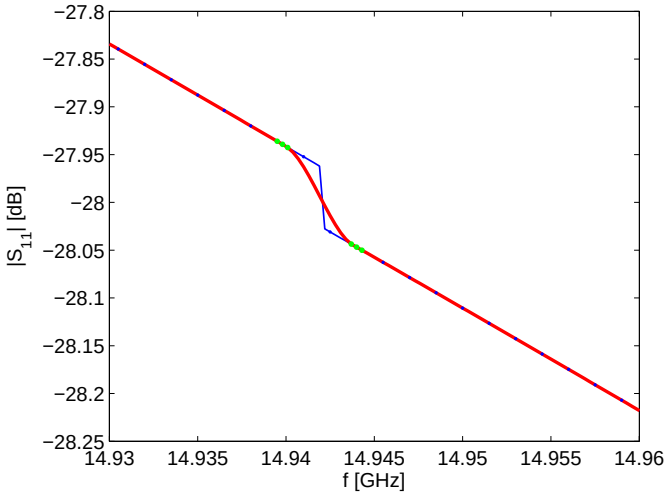

Figure 3.12: Results of the proposed technique of model's response discontinuity compensation: — Non-smooth model response, — spline compensated model response, ··· points used for spline computation

fast and easy to implement.

3.3.7 Models of multi-port components

The technique described in the previous paragraphs can only be used to construct models of a single scattering parameter versus frequency and structure dimensions. In practice, an engineer uses N-port components, which are described by scattering matrix that contains several scattering parameters:

$$\boldsymbol{S} = \begin{bmatrix} S_{11} & \cdots & S_{1N} \\ \vdots & \ddots & \vdots \\ S_{N1} & \cdots & S_{NN} \end{bmatrix} \tag{3.24}$$

To create a complete model of such a device, all S_{ij} elements of the scattering matrix should be modelled independently. To speed up this process, the successive models can utilize the results of electromagnetic simulations that were already performed. In such a case, at the beginning of model development, the sparse grid is used to create the model of first scattering parameter S_{11} with adaptive sampling and order selection. At this stage the results of the simulations of all scattering parameters are stored. Once the procedure has converged, all the stored data points can be used to start the generation of model of the subsequent scattering parameter. Each time the modelling of subsequent scattering parameter is started, a test for initial model orders can be performed. The test generates several models with increasing orders and evaluates the biggest mismatch between chosen pairs. The orders of the model pair with the smallest mismatch are used as the initial orders for adaptive model construction scheme. In the same manner the presented formulation of multi-port device model construction can also be used to create models of multi-mode devices, as discussed

in [75], where the generalized scattering matrix is used in which each considered mode represents a separate port.

3.3.8 Technique specific issues

3.3.8.1 Algorithm convergence

Since the technique uses adaptive sampling to select the support points and an adaptive scheme of model order selection, it can operate as an automated algorithm of surrogate model construction. However, the proposed multivariate modelling cannot guarantee that further increase of model order and addition of support points would provide more accurate model. This can be partly overcome by a procedure of automated space division, but nevertheless the construction of some sub-models can fail due ill-conditioning of interpolation problem, which can appear in smaller sub-domains. Therefore, in rare cases, when the requested accuracy ε is very high, the technique can fail to generate a surrogate model with prohibitively high accuracy. In such cases it would be needed to change the model properties in the area that such an unstable behavior appears, for example by widening or tightening of the range of model parameters.

3.3.8.2 Specific issues related to mesh based solvers

One of the most important issues of successful creation of rational model based on the electromagnetic simulation is smooth change of simulator response with changes of structure geometry. It is a common feature of mode-matching based simulators, but may cause problems if mesh-based solvers (like MoM or FDTD) are used. The problem is illustrated in Figure 3.13, where the S_{11} response of a microstrip stub on a MCM-D substrate versus the width of the stub is presented. The structure is simulated using ADS Momentum at the frequency 1GHz and re-meshed each time the structure dimensions change. The mesh frequency (a parameter used by ADS Momentum) is also set at 1GHz. It can be seen that the transfer function is not smooth in the entire domain, that indicates a non-physical response. A discontinuity of the response causes a huge problem for interpolation of data using rational functions, causing unjustifiable increase of the model order.

A way to circumvent this problem is to simulate the structure with a grid that is denser than the one resulting if considering the frequency alone. In the same figure the response of the same device is shown with mesh frequency set at 100GHz. In this case the response varies smoothly with the change of the geometry of the stub. A drawback of such a solution is an increased simulation time, due to a denser mesh.

3.3.9 A complete algorithm - flow chart

The flow chart of the proposed algorithm is presented in Figure 3.14. In the main loop an adaptive sampling of the parameter space is performed, the condition for increasing of model orders is checked and detection of ill-conditioning is done.

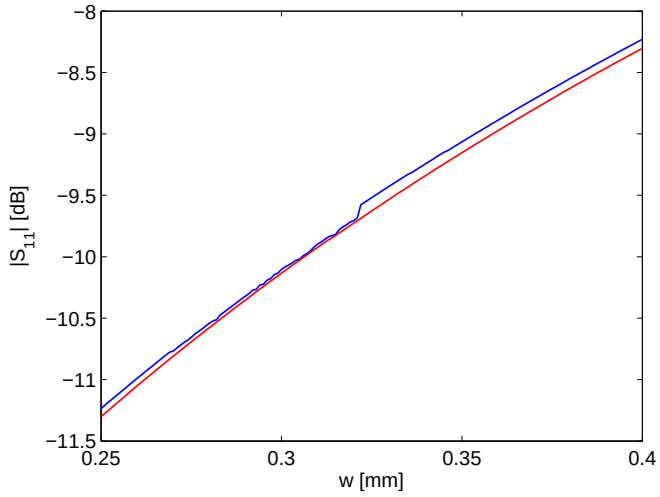

Figure 3.13: Response of the stub on the MCM-D substrate versus the stub width: — mesh computed at 1GHz, — mesh computed at 100GHz

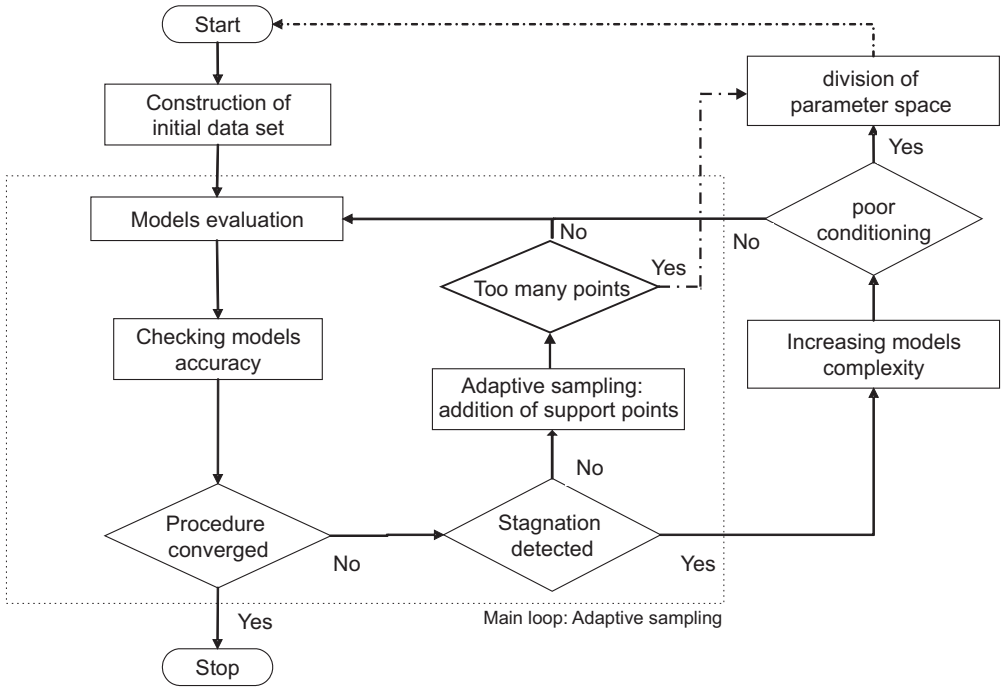

Figure 3.14: Flow chart of the complete algorithm

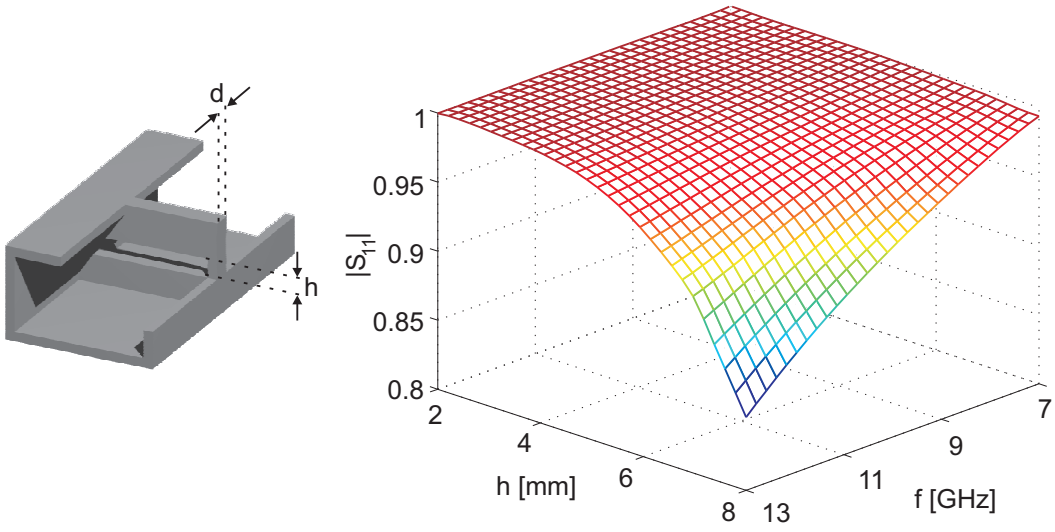

Figure 3.15: Capacitive iris geometry overview and sample iris response for fixed iris width $d = 0.5$mm.

3.4 Accuracy and efficiency comparison

In this section an application of proposed multivariate rational interpolation technique to responses of two waveguide structures is presented. In each case the model consists of three variables.

The same structures were already used in [79] as a test structures for validation of the BCF approach described in section 3.2.3.2, which allows us to compare the efficiency of the proposed and former technique. For the sake of comparison, the structures were also modelled using MLP artificial neural networks. In this case, two three-layer networks are used denoted as ANN I and ANN II. The former has 6 neurons in each layer and the latter has 9 neurons. Each network was trained on a uniform rectangular grid with increasing grid density.

The proposed technique was used two times with different initial orders. The first option, denoted as RAT I, has initial orders set as $V_{S1} = [1 \;\; 2 \;\; 2]$ and $V_{S2} = [2 \;\; 2 \;\; 2]$. In this case the density of base rectangular grid is $D = 3$. The second one, denoted as RAT II, has initial orders set as $V_{S1} = [2 \;\; 2 \;\; 2]$ and $V_{S2} = [3 \;\; 2 \;\; 2]$, which enforces $D = 4$.

3.4.1 Capacitive iris in WR90 waveguide

The first test structure is a capacitive iris in the WR90 waveguide. The iris structure, along with a sample iris response is shown in Fig. 3.15. The electromagnetic response of the iris was computed using the mode-matching technique.

A three-variate model of the transmission coefficient S_{21} was created using the proposed technique. The model consists of three parameters: frequency f, iris height h and iris thickness d. Table 3.7 shows the range of model parameters.

The accuracy of the created model (mean and maximum relative absolute errors) vs. the number of support points L for RAT I and RAT II schemes is presented in Tab. 3.8. In both cases the algorithm needed about 70 points to reach the relative error $E_{RSEmean}$ below -60dB.

Table 3.7: Range of parameters of capacitive iris model

Parameter	Range
frequency f	7GHz - 13GHz
height h	2mm - 8mm
thickness d	0.5mm - 5mm

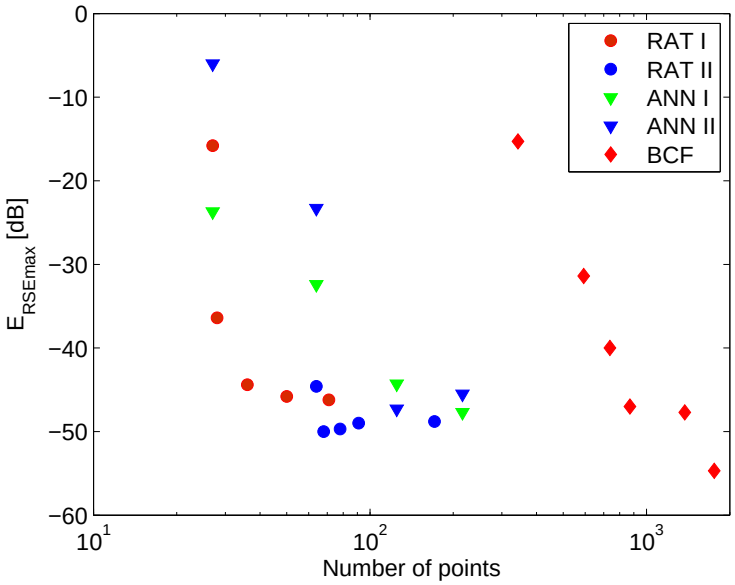

Figure 3.16: Capacitive iris example: Comparison of the error E_{RSEmax} vs. the number of points used to create model for different techniques.

It can be seen that the RAT II scheme gives better accuracy, but the cost is a higher number of support points.

The results of modelling with neural networks are presented in Tab. 3.9. The number of support points that gives comparable accuracy is much higher: the network ANN I needs 216 points and ANN II 125 points to achieve similar maximum error as RAT II with 64 points. Additionally, in both tables a mean square error E_{MSE} of the model computed on training set is shown. It is seen that there is no correlation between the E_{MSE} error and actual accuracy of the network.

Table 3.10 shows the results of BCF approach presented in [79]. In this case, the advantage of presented technique is obvious: the BCF technique needs about 871 points to have similar maximum error as RAT I with 71 points. However, these 871 points give -18dB lower mean error than RAT I.

The efficiency of various modelling techniques is compared in Fig. 3.16 that shows a graphic representation of error E_{RSEmax} vs. the number of support points used. It can be seen, that the proposed technique needs the smallest number of support points to achieve high accuracy and has the fastest convergence comparing to other approaches.

Table 3.8: Multivariate rational approach

RAT I			RAT II		
L	E_{RSEmax}	$E_{RSEmean}$	L	E_{RSEmax}	$E_{RSEmean}$
27	−15.8	−28.2	64	−44.6	−66.0
28	−36.4	−51.3	68	−50.0	−69.0
36	−44.4	−58.5	78	−49.7	−68.6
50	−45.8	−60.0	91	−49.0	−68.0
71	−46.2	−62.0	171	−48.8	−69.5

Table 3.9: ANN Results

	ANN I			ANN II		
L	E_{RSEmax}	$E_{RSEmean}$	E_{MSE}	E_{RSEmax}	$E_{RSEmean}$	E_{MSE}
27	−23.7	−41.9	$4.36 \cdot 10^{-25}$	−6.0	−34.6	$1.31 \cdot 10^{-29}$
64	−32.4	−60.9	$1.55 \cdot 10^{-9}$	−23.3	−43.9	$2.32 \cdot 10^{-10}$
125	−44.3	−67.0	$7.50 \cdot 10^{-8}$	−47.3	−75.1	$9.31 \cdot 10^{-10}$
216	−47.7	−73.8	$2.94 \cdot 10^{-8}$	−45.4	−77.9	$1.46 \cdot 10^{-9}$

Table 3.10: BCF approach results [79]

L	E_{RSEmax}	$E_{RSEmean}$
343	−15.3	−55.5
593	−31.4	−67.0
737	−40.0	−76.5
871	−47.0	−79.5
1375	−47.7	−91.7
1758	−54.7	−96.1

Table 3.11: Range of parameters of two-dimensional iris model

Parameter	Range
frequency f	8GHz - 12GHz
width a	8mm - 15mm
height b	1mm - 3mm

3.4.2 Two-dimensional iris in WR90 waveguide

The second test structure is a two-dimensional iris in the WR90 waveguide, shown along with a sample response in Fig. 3.17. The electromagnetic response of the iris was computed using the mode-matching technique. The model consists of three parameters: frequency f, iris width a and iris height b. Table 3.11 shows the range of model parameters. Since the response of the iris has a resonant character it is more difficult to model.

Table 3.12 shows the accuracy of created models for RAT I and RAT II schemes. Once again RAT II achieves higher accuracy, however the value of maximum relative error achieved in both cases is below -40dB.

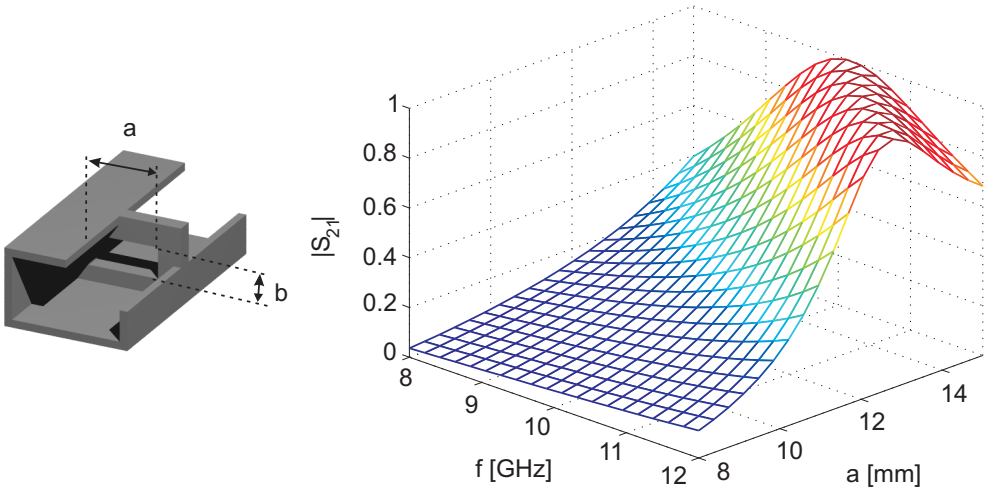

Figure 3.17: Two-dimensional iris geometry overview and sample iris response for fixed iris height $b = 1$mm.

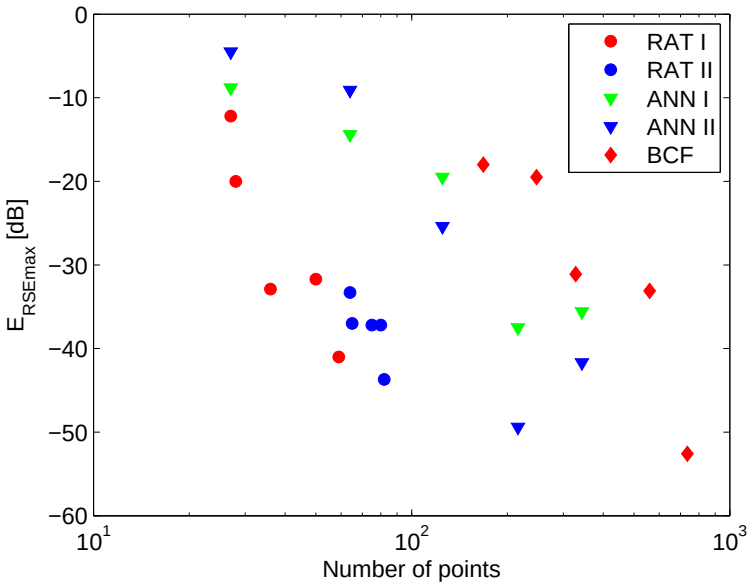

Figure 3.18: Resonant iris example: Comparison of the error E_{RSEmax} vs. the number of points used to create model for different techniques.

The results of modelling with neural networks are presented in Tab. 3.13. The resonant character of the modelled response caused lower efficiency of neural network scheme. The best result achieved with ANN II corresponds to 216 support points and maximum error at level -49.4dB. However, the increase of density of the grid caused over-training of the network and loss of accuracy.

Comparing the BCF modeling results presented in Tab. 3.14, the advantage of introduced adaptive rational interpolation scheme is apparent. With only 82 points one gets a model with better accuracy as the one that involves 328 samples with BCF. This example shows the benefits from use of the non-structured adaptive sampling in contrast to the structured or partly-structured ones. The results are illustrated in Fig. 3.18, that shows a graphic represen-

Table 3.12: Multivariate rational approach

RAT I			RAT II		
L	E_{RSEmax}	$E_{RSEmean}$	L	E_{RSEmax}	$E_{RSEmean}$
27	−12.2	−27.8	64	−33.1	−51.9
28	−20.0	−37.8	65	−37.0	−55.5
36	−32.9	−46.5	75	−37.2	−55.3
50	−31.7	−46.7	80	−37.2	−53.5
59	−41.0	−58.3	82	−43.7	−60.4

Table 3.13: ANN Results

	ANN I			ANN II		
L	E_{RSEmax}	$E_{RSEmean}$	E_{MSE}	E_{RSEmax}	$E_{RSEmean}$	E_{MSE}
27	−8.8	−20.6	$6.0\cdot10^{-10}$	−4.5	−21.8	$9.2\cdot10^{-23}$
64	−14.4	−37.2	$9.1\cdot10^{-6}$	−9.1	−27.5	$8.0\cdot10^{-10}$
125	−19.5	−56.0	$1.9\cdot10^{-6}$	−25.4	−60.0	$1.6\cdot10^{-7}$
216	−37.5	−61.8	$1.5\cdot10^{-6}$	−49.4	−68.7	$2.1\cdot10^{-7}$
343	−35.6	−60.4	$2.9\cdot10^{-6}$	−41.7	−68.7	$5.3\cdot10^{-7}$

Table 3.14: BCF approach results [79]

L	E_{RSEmax}	$E_{RSEmean}$
168	−18.0	−50.0
247	−19.5	−56.9
328	−31.1	−63.2
560	−33.1	−66.5
736	−52.6	−72.7

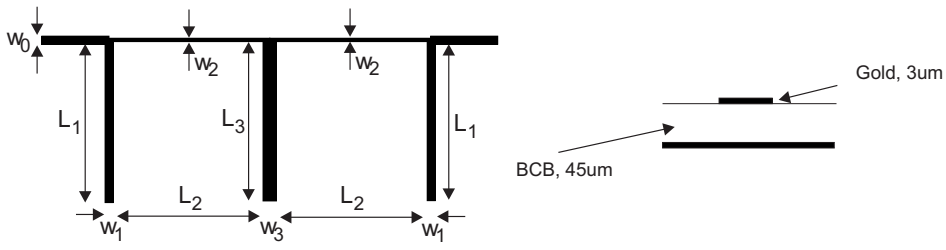

Figure 3.19: Structure layout with details of MCM-D substrate.

tation of maximum error E_{RSE} vs. number of support points used for different techniques. The figure confirms the best relation between the numeric cost needed to create model and model accuracy.

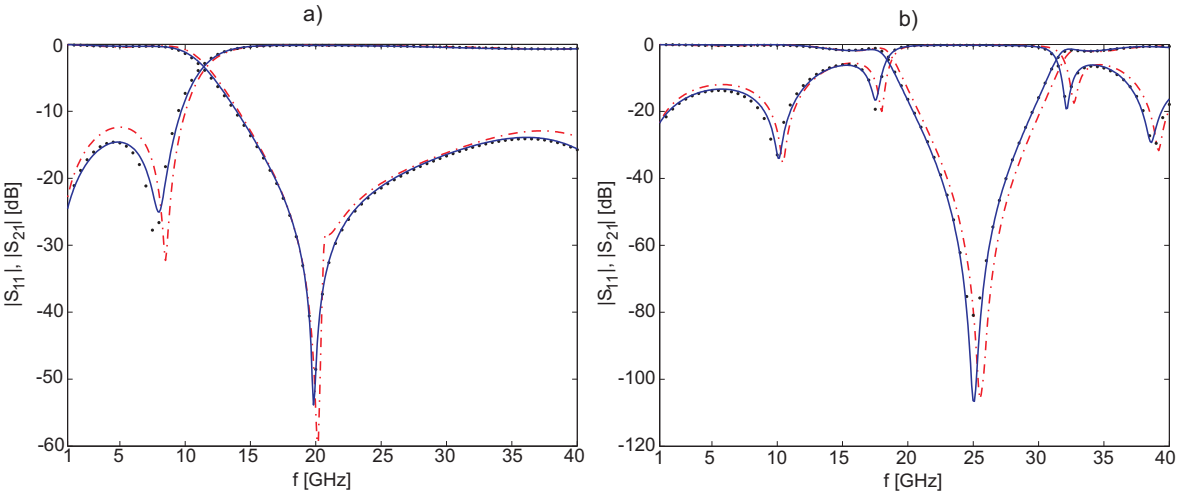

Figure 3.20: Accuracy comparison of structure response computed with the application of created rational models and built-in models from Agilent ADS circuit simulator: (···) electromagnetic response, (—) response obtained from created models, (-.-.-) response of models from Agilent ADS. Structure dimensions: a) $w_0 = 0.157$mm, $w_1 = 0.157$mm, $w_2 = 0.05$mm, $w_3 = 0.2$mm, $L_1 = 2.5$mm, $L_2 = 1.3$mm, $L_3 = 1$mm, b) $w_0 = 0.157$mm, $w_1 = 0.1$mm, $w_2 = 0.1$mm, $w_3 = 0.1$mm, $L_1 = 2$mm, $L_2 = 2$mm, $L_3 = 2$mm

3.4.3 Comparison with commercially available models

Most of the commercial tools dedicated to design of microwave components have own libraries of commonly used discontinuities. However, most of them uses quite old, standard closed-form models which accuracy is often limited, compared to electromagnetic simulation results.

To show the advantage of surrogate models based on the results of the electromagnetic simulations two microstrip elements were modelled using the technique proposed in this thesis: a section of microstrip line and an open-end stub. The parameters assumed for the microstrip line were as follows: frequency $f \in (1GHz - 40GHz)$, line width $w \in (50\mu m - 2mm)$ and line length $L \in (0.5mm - 2mm)$. The stub has five parameters: frequency $f \in (1GHz - 40GHz)$, width of the input line $w_1 \in (0.5mm - 2mm)$, width of the output line $w_2 \in (0.5mm - 2mm)$, width of the stub $w_3 \in (0.5mm - 2mm)$ and length of the stub $D \in (1mm - 2.5mm)$. The models were created with tolerance $\varepsilon_0 = 0.003$ in the case of the microstrip line and $\varepsilon_0 = 0.01$ in the case of the stub. The cascade connection of the scattering parameters of this basic elements allows one to obtain a fully parameterized model of the structure presented in Fig.3.19.

Figure 3.20 shows a comparison of accuracy of the evaluation of structure response for different structure dimensions. The reference are the characteristics computed with a full-wave tool using method of moments (Agilent's Momentum). In the same figure a response of the structure calculated with the Agilent ADS 2005A circuit simulator is presented. Agilent ADS has a built-in library of surrogate models for a few technologies. However, it can be seen that the models have a limited accuracy and in some frequency ranges the error of the response is high. On the other hand, the response computed with application of the

models developed with the technique proposed in this thesis is very close to electromagnetic response. It has to be noticed, that the computation of structure response using electromagnetic solver (Momentum) takes about 7s for a single frequency point. The application of surrogate models reduces this time to 0,05s (Matlab implementation).

Chapter 4

Equivalent circuits of LTI devices

4.1 Introduction

Linear time-invariant (LTI) devices are basic building blocks of every electronic circuit. Linearity implies that the relation between the inputs and outputs satisfies the superposition property. Time-invariance means that an input affected by a time delay should effect in a corresponding time delay in the output. LTI system is described in time-domain with an impulse response and in frequency domain with transfer function which is a Laplace transform of the system's impulse response.

The LTI devices can be represented in a form of so-called " *equivalent circuits*". Equivalent circuits are representations of complex electronic devices created using lumped elements that accurately approximate the characteristics of the originals. They are essential for computer simulation of high-frequency electronic devices. Construction of the equivalent circuit allows one to include a distributed elements, such as transmission lines, interconnects or other passive elements to SPICE-like circuit simulators. Generally speaking, equivalent circuits can be categorized into two groups:

- Physical models, involving only RLC elements with non-negative values.
- Realizations of the transfer functions.

Physical models are derived from the device's structure and physical effects expected to be present in the device. In general, they are accurate and can ensure passivity, however, they are difficult to construct for an arbitrary structure. Realizations of the transfer functions in a form of rational representations of admittance/impedance or scattering functions are much more versatile, nevertheless some additional effort has to be made to assure the passivity of the circuit. In general, a robust technique of equivalent circuit synthesis should have the following features:

- It should be versatile, i.e. construction of equivalent circuits of an arbitrary devices should be possible;
- The procedure should be as automated as possible;
- It should be capable to construct equivalent circuits based on frequency domain data obtained in result of EM-simulation or measurements.

In this chapter both types of SPICE-compatible equivalent circuit construction of linear, time-invariant networks are investigated.

4.2 Physical equivalent circuits

Knowledge of device's physical structure can be exploited for construction of equivalent circuit. From this knowledge a general scheme of the frequency-independent physical equivalent circuit can be deduced which is common for a group of devices (white-box model). This approach is popular in the case of transistors [98], microstrip discontinuities [5] or intergrated inductors [135].

The first step is to find a general circuit topology. For several devices the topology of equivalent circuit is well documented. However it is difficult to find one for an arbitrary structure and this is a main drawback of physical models. A next step is to find the values of equivalent circuit elements (resistances, capacitances and inductances) for a particular structure dimensions. This can be handled using either admittance parameters to extract inductance/capacitance values or with an optimization approach, where the following scalar-valuated cost function is minimized:

$$F = \sum_{i=1}^{N} \sum_{j=1}^{N} \sum_{k=1}^{K} \| S_{ij}(f_k) - \widehat{S}_{ij}(f_k) \| \tag{4.1}$$

where N is a number of ports, K is a number of frequency points, S_{ij} and $\widehat{S}_{ij}$ is the i,j-th element of scattering matrix of the optimized circuit and reference data, respectively. The cost function can be minimized with either gradient or genetic optimization methods [124]. Values of the circuit elements for different structure dimensions can be then parameterized using closed-form physical-based equations.

Physical models are compact, accurate and can be easily incorporated into CAD software like SPICE. On the other hand, the technique itself is not versatile, i.e. there is a limited set of devices that can be described with deducible and simple equivalent circuit.

Illustrative example. For a sake of an illustration an extraction scheme of equivalent circuit of integrated inductor on silicon substrate in a form of physical substrate-coupled model [63] (presented in Fig. 4.1) is investigated. The substrate and a sample structure of the inductor is presented in Fig. 4.2 and Fig. 4.3, respectively.

The circuit has a form of pi-circuit with elements representing skin and proximity effects. The circuit structure corresponds directly to electromagnetic effects that occur in operation of inductor. It consists of 14 elements: capacitances C_{ox1} and C_{ox2} between the wire and the substrate, substrate capacitances C_{si1} and C_{si2}, substrate resistances R_{si1} and R_{si2} in direction perpendicular to the substrate surface, wire inductances L_s and L_{sk}, resistances R_s and R_{sk} describing the skin and proximity effects, capacitance between terminals C_s, substrate resistance R_{sub} and inductance L_{sub} in direction parallel to substrate surface and coupling coefficient M between L_s and L_{sub}.

The circuit was used to represent a 2.5-loop octagonal inductor on BiCMOS substrate in frequency range DC-10GHz. Scattering parameters of the inductor for fixed geometric

dimensions (strip width $w = 12\mu m$, inner radius $R = 70\mu m$, spacing between the loops $s = 5\mu m$) were computed using ADS Momentum electromagnetic solver and used as a reference values for a circuit optimization. The response of the circuit with optimized values of the elements is presented in Fig. 4.4. In the frequency band DC-10GHz the root mean square error E_{RMS} in the case of S_{11} and S_{21} responses is -73.2dB and -70.3dB, respectively, which confirms a good accuracy of the equivalent circuit. The values of extracted circuit are shown in Table 4.1, denoted as IND I. The extracted circuit can be directly incorporated into a circuit simulator.

Since the circuit topology corresponds to physical phenomena that occur inside of the structure, the values of the elements are strongly correlated to structure dimensions. Therefore, changing the structure dimensions one can deduce the increase or decrease of values of lumped circuit. For example, it is expected that the increase of the number of turns of the spiral causes increase of the wire inductance L_s and resistance R_s. To show the relation between the elements of the equivalent circuits and the structure parameters, an inductor with the same dimensions was analyzed with a modified conductivity of the metal strip, which was decrease from $\sigma = 3.4 \cdot 10^7 \frac{S}{m}$ to $\sigma = 3.0 \cdot 10^7 \frac{S}{m}$. From the response of the modified structure the physical equivalent circuit was extracted, shown in Tab. 4.1 and denoted as IND II. One can expect that the decrease of the conductivity should mainly increase the restive element R_s, which is confirmed when one observes the values of the extracted equivalent circuit.

Since the physical circuit exploits the physical effects present inside of the component, it is accurate in a limited frequency range. The increase of the frequency of the interest causes, in general, increase of influence of the parasitic effects on the operation of a device. Additionally, some new effects might occur that had not to be taken into account on lower frequencies, resulting in limitation of the accuracy of the equivalent circuit. For example, Fig. 4.5 shows a wideband (DC-40GHz) response of the octagonal inductor and extracted

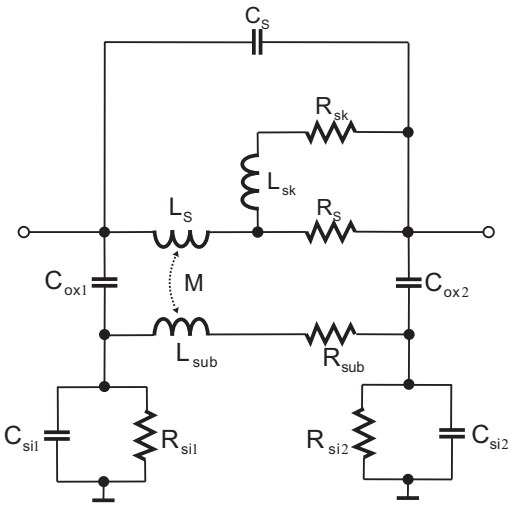

Figure 4.1: General wideband equivalent circuit of integrated inductor on silicon as proposed in [63].

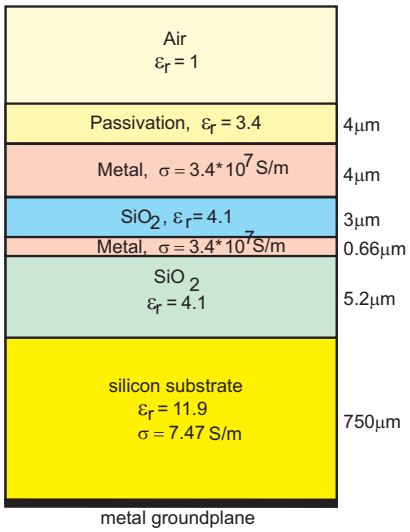

Figure 4.2: Silicon substrate cross-section as simulated in ADS Momentum

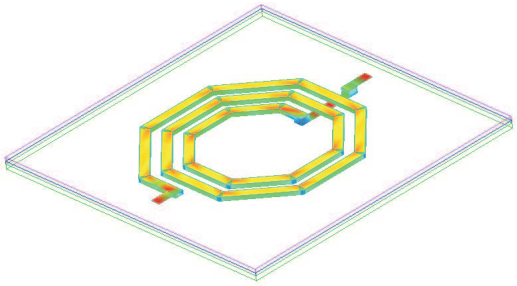

Figure 4.3: Three dimensional field visualization of modelled inductor.

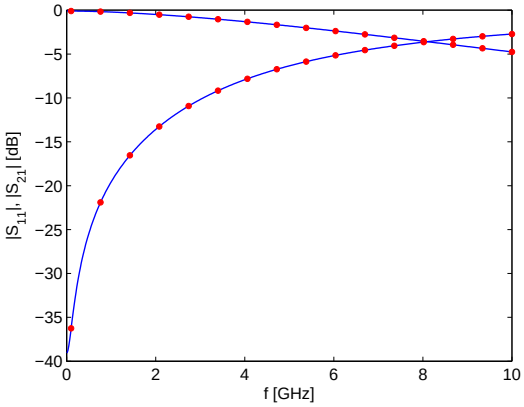

Figure 4.4: Electromagnetic vs. extracted equivalent circuit response.

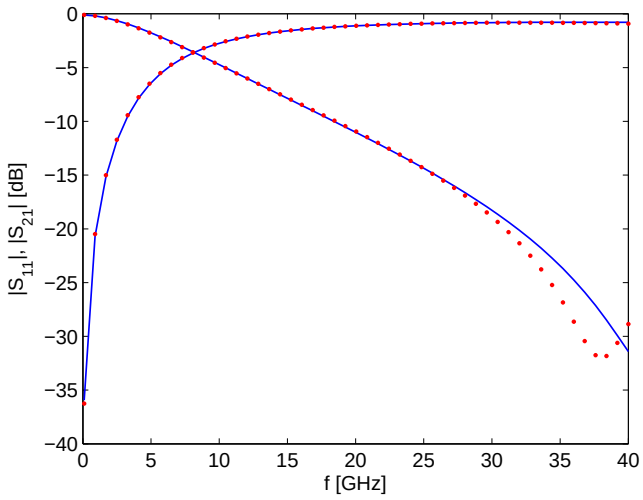

Figure 4.5: Response of substrate-coupled equivalent circuit in wide frequency range: (···) electromagnetic response, (—) extracted circuit response.

substrate-coupled equivalent circuit. It can be observed, that above 25GHz the structure starts to resonate, i.e. the parasitic capacitance strongly increases. However, for such high frequencies the physical circuit does not comply with this phenomenon and loses of the accuracy.

4.3 Realizations of transfer functions

An alternative to the physical equivalent circuits is the realization of the transfer function with lumped elements. This approach is based on a rational representation of the transfer function of multiport component.

Table 4.1: Comparison of equivalent circuit elements extracted from model response and electromagnetic simulation. IND II corresponds to decreased metal conductivity.

Element	IND I	IND II
L_s [nH]	2.033	2.035
R_s [Ω]	144	160
C_s [fF]	3.1	4.7
C_{ox1} [fF]	76	82
C_{ox2} [fF]	76	73
R_{si1} [Ω]	579	615
R_{si2} [Ω]	606	561
C_{si1} [fF]	23.7	22.8
C_{si2} [fF]	17.2	18.5
L_{sub} [nH]	0.562	0.542
R_{sub} [Ω]	4.2	18.4
L_{sk} [nH]	0.913	1.06
R_{sk} [Ω]	5.2	6.2
M	1	1

4.3.1 Rational representation of LTI systems

In general, admittance $\boldsymbol{Y}(s)$, impedance $\boldsymbol{Z}(s)$ or scattering $\boldsymbol{S}(s)$ matrices of linear time-invariant circuit can be represented in a form of a rational function in the frequency domain:

$$\boldsymbol{H}(s) = \begin{bmatrix} \sum_{i=1}^{M} \frac{k_i^{11}}{s+p_i} + c_{11} + s\cdot h_{11} & \sum_{i=1}^{M} \frac{k_i^{12}}{s+p_i} + c_{12} + s\cdot h_{12} & \cdots & \sum_{i=1}^{M} \frac{k_i^{1N}}{s+p_i} + c_{1N} + s\cdot h_{1N} \\ \sum_{i=1}^{M} \frac{k_i^{21}}{s+p_i} + c_{21} + s\cdot h_{21} & \sum_{i=1}^{M} \frac{k_i^{22}}{s+p_i} + c_{22} + s\cdot h_{22} & \cdots & \sum_{i=1}^{M} \frac{k_i^{2N}}{s+p_i} + c_{2N} + s\cdot h_{2N} \\ \vdots & \vdots & \ddots & \vdots \\ \sum_{i=1}^{M} \frac{k_i^{N1}}{s+p_i} + c_{N1} + s\cdot h_{N1} & \sum_{i=1}^{M} \frac{k_i^{N2}}{s+p_i} + c_{N2} + s\cdot h_{N2} & \cdots & \sum_{i=1}^{M} \frac{k_i^{NN}}{s+p_i} + c_{NN} + s\cdot h_{NN} \end{bmatrix} \tag{4.2}$$

where k_p^{ij} is the residue of the matrix element H_{ij} related with p-th pole, M is the function order and $s = j\omega$ is a complex frequency. All elements of the matrix can be described with the same set of common poles (real and complex). Since the time domain response of the device has to be real, the complex poles and corresponding residues have to occur as conjugate complex pairs. A sufficient condition for response to be real is is to ensure that $H_{ij}(s)$ has a form:

$$H_{ij} = \frac{K(s)}{L(s)} \tag{4.3}$$

the polynomials of numerator $K(s)$ and denominator $L(s)$ have a real coefficients. For the sake of simplicity, in further investigations, let $H(s)$ denote any $H_{i,j}$ element of the matrix

$\boldsymbol{H}(s)$.

Stability. Stability is a fundamental issue in electronic engineering. Every stable linear time invariant network need to satisfy the stability condition, of which a general definition is as follow:

Definition 1 *It is said that circuit is stable in* $t \in (0,\infty)$ *if all the inputs reach a steady states for* $t < \infty$*:*

$$\int_{-\infty}^{\infty} \|h(t)\| dt < \infty \tag{4.4}$$

where $h(t)$ *is the impulse response of the circuit.*

From the above definition a sufficient condition for stability of rational representation (4.2) can be derived, which states that all of the poles p_m have to be stable, i.e. $Re(p_m) < 0$.

4.3.2 State-space representation of LTI systems

Every stable LTI device can be represented in a form of continuous time-invariant state-space model [2]. State space representation is a mathematical model of a physical system represented as a set of input, output and state variables related by first-order differential equations:

$$\dot{\boldsymbol{x}} = \boldsymbol{A}\boldsymbol{x} + \boldsymbol{B}\boldsymbol{u} \tag{4.5}$$

$$\boldsymbol{y} = \boldsymbol{C}\boldsymbol{x} + \boldsymbol{D}\boldsymbol{u} \tag{4.6}$$

where $\boldsymbol{A}$ is the state matrix, $\boldsymbol{B}$ relates the input variables to state variables, $\boldsymbol{C}$ relates the state variables to output variables, $\boldsymbol{D}$ relates the inputs directly to the outputs, $\boldsymbol{x}$ is the state vector, $\boldsymbol{u}$ is the input vector, and $\boldsymbol{y}$ is the output vector. The dot denotes time-domain derivative. Both time and frequency domain models are connected by Laplace transform. The response of a frequency domain model can be computed using state-space description as:

$$\boldsymbol{H}(s) = \boldsymbol{D} + \boldsymbol{C}(s\boldsymbol{I} - \boldsymbol{A})^{-1}\boldsymbol{B} \tag{4.7}$$

The rational representation of $\boldsymbol{H}(s)$ in form of (4.2) can be converted to a time domain state-space model (macromodel).

Realization of real poles. In general, a Jordan-canonical realization of state-space model of N-port device described by a transfer function (4.2) with M real poles has a form:

$$\boldsymbol{A} = \begin{bmatrix} \boldsymbol{P_1} & 0 & \cdots & 0 \\ 0 & \boldsymbol{P_2} & \cdots & 0 \\ \vdots & \vdots & \vdots & \vdots \\ 0 & 0 & \cdots & \boldsymbol{P_M} \end{bmatrix} \tag{4.8}$$

$$\boldsymbol{B} = \begin{bmatrix} \boldsymbol{E_1} \\ \boldsymbol{E_2} \\ \vdots \\ \boldsymbol{E_M} \end{bmatrix} \tag{4.9}$$

$$\boldsymbol{C} = \left[\begin{array}{cccc} \boldsymbol{K_1} & \boldsymbol{K_1} & \cdots & \boldsymbol{K_M} \end{array} \right] \tag{4.10}$$

$$\boldsymbol{D} = \left[\begin{array}{cccc} c_{11} & c_{12} & \cdots & c_{1N} \\ c_{21} & c_{22} & \cdots & c_{2N} \\ \vdots & \vdots & \vdots & \vdots \\ c_{N1} & c_{N2} & \cdots & c_{NN} \end{array} \right] \tag{4.11}$$

where $\boldsymbol{P_i}$ is a $N \times N$ matrix with all diagonal elements equal p_i, $\boldsymbol{E_i}$ is a $N \times N$ unitary matrix and $\boldsymbol{K_i}$ is a $N \times N$ matrix of residues associated with the i-th pole.

Realization of conjugated complex poles. If rational model (4.2) is described with a set of complex conjugated poles $p_i = w \pm jz$ ($i = 1 \ldots M$), the direct realization of (4.6) have a form:

$$\boldsymbol{A} = \left[\begin{array}{cc} \boldsymbol{A_1} & 0 \\ 0 & \boldsymbol{A_1^*} \end{array} \right] \tag{4.12}$$

$$\boldsymbol{B} = \left[\begin{array}{c} \boldsymbol{B_1} \\ \boldsymbol{B_1} \end{array} \right] \tag{4.13}$$

$$\boldsymbol{C} = \left[\begin{array}{cccccc} \boldsymbol{K_1} & \boldsymbol{K_1} & \cdots & \boldsymbol{K_M} & \boldsymbol{K_1^*} & \boldsymbol{K_1^*} & \cdots & \boldsymbol{K_M^*} \end{array} \right] \tag{4.14}$$

where matrix $\boldsymbol{A_1}$ is diagonal matrix with form of (4.8) based on poles with $Im(p_i) > 0$ and $\boldsymbol{A_1^*}$ is a complex conjugate of $\boldsymbol{A_1}$. Matrix $\boldsymbol{B_1}$ has structure of (4.9) and $\boldsymbol{D}$ is unchanged. Such a model has to be transformed to eliminate complex values from matrices $\boldsymbol{A}, \boldsymbol{B}, \boldsymbol{C}$ which is necessary to assure a real valuated time domain response. Let us introduce a transformation:

$$\boldsymbol{T} = \left[\begin{array}{cc} \boldsymbol{I} & \boldsymbol{I} \\ j\boldsymbol{I} & -j\boldsymbol{I} \end{array} \right] \tag{4.15}$$

$$\hat{\boldsymbol{x}} = \boldsymbol{T} \cdot \boldsymbol{x} \tag{4.16}$$

where $\boldsymbol{I}$ is a unitary matrix. Applying the transformation $\boldsymbol{T}$ to the original state-space system one obtains model with real matrices $\widetilde{\boldsymbol{A}}, \widetilde{\boldsymbol{B}}, \widetilde{\boldsymbol{C}}, \widetilde{\boldsymbol{D}}$.

$$\widetilde{\boldsymbol{A}} = \boldsymbol{T}\boldsymbol{A}\boldsymbol{T}^{-1} = \left[\begin{array}{cc} Re(\boldsymbol{A_1}) & Im(\boldsymbol{A_1}) \\ -Im(\boldsymbol{A_1}) & Re(\boldsymbol{A_1}) \end{array} \right] \tag{4.17}$$

$$\widetilde{\boldsymbol{B}} = \boldsymbol{T}\boldsymbol{B} = \left[\begin{array}{c} 2\boldsymbol{B_1} \\ 0 \end{array} \right] \tag{4.18}$$

$$\widetilde{\boldsymbol{C}} = \boldsymbol{C}\boldsymbol{T}^{-1} \left[\begin{array}{cccccccc} Re(\boldsymbol{K_1}) & Im(\boldsymbol{K_1}) & Re(\boldsymbol{K_2}) & Im(\boldsymbol{K_2}) & \cdots & Re(\boldsymbol{K_N}) & Im(\boldsymbol{K_N}) \end{array} \right] \tag{4.19}$$

$$\widetilde{\boldsymbol{D}} = \boldsymbol{D} \tag{4.20}$$

Relations between $\boldsymbol{Y}(s)$ and $\boldsymbol{S}(s)$ models. For a given state-space model $\boldsymbol{A},\boldsymbol{B},\boldsymbol{C},\boldsymbol{D}$ of an admittance function $Y(s)$ it is possible to convert the model into a model $\widetilde{\boldsymbol{A}},\widetilde{\boldsymbol{B}},\widetilde{\boldsymbol{C}},\widetilde{\boldsymbol{D}}$ representing a scattering function $\boldsymbol{S}(s)$. Let $\boldsymbol{Z}_0$ denotes reference impedance matrix whose diagonal element Z_{0i} is an impedance of the i-th port. With such assumption the transformation is [23]:

$$\begin{aligned}
\widetilde{\boldsymbol{A}} &= \boldsymbol{A}-\boldsymbol{B}(\boldsymbol{I}+\boldsymbol{D})^{-1}\boldsymbol{C} \\
\widetilde{\boldsymbol{B}} &= \boldsymbol{B}(\boldsymbol{I}+\boldsymbol{D})^{-1}\boldsymbol{Z}_0^{-\frac{1}{2}} \\
\widetilde{\boldsymbol{C}} &= -2\boldsymbol{Z}_0^{-\frac{1}{2}}(\boldsymbol{I}+\boldsymbol{D})^{-1}\boldsymbol{C} \\
\widetilde{\boldsymbol{D}} &= \boldsymbol{Z}_0^{-\frac{1}{2}}(\boldsymbol{I}-\boldsymbol{D})(\boldsymbol{I}+\boldsymbol{D})^{-1}\boldsymbol{Z}_0^{-\frac{1}{2}}
\end{aligned} \tag{4.21}$$

and it is assumed that $(\boldsymbol{I}+\boldsymbol{D})^{\frac{1}{2}}$ exists. Similarly, the following transformation relates the scattering representation $\widetilde{\boldsymbol{A}},\widetilde{\boldsymbol{B}},\widetilde{\boldsymbol{C}},\widetilde{\boldsymbol{D}}$ with the admittance model $\boldsymbol{A},\boldsymbol{B},\boldsymbol{C},\boldsymbol{D}$:

$$\begin{aligned}
\boldsymbol{A} &= \widetilde{\boldsymbol{A}}-\widetilde{\boldsymbol{B}}(\widetilde{\boldsymbol{D}}+\boldsymbol{Z}_0^{-1})^{-1}\widetilde{\boldsymbol{C}} \\
\boldsymbol{B} &= 2\widetilde{\boldsymbol{B}}\boldsymbol{Z}_0^{\frac{1}{2}}(\boldsymbol{I}+\boldsymbol{Z}_0^{\frac{1}{2}}\widetilde{\boldsymbol{D}}\boldsymbol{Z}_0^{\frac{1}{2}})^{-1} \\
\boldsymbol{C} &= -(\boldsymbol{I}+\boldsymbol{Z}_0^{\frac{1}{2}}\widetilde{\boldsymbol{D}}\boldsymbol{Z}_0^{\frac{1}{2}})^{-1}\boldsymbol{Z}_0^{\frac{1}{2}}\widetilde{\boldsymbol{C}} \\
\boldsymbol{D} &= (\boldsymbol{I}-\boldsymbol{Z}_0^{\frac{1}{2}}\widetilde{\boldsymbol{D}}\boldsymbol{Z}_0^{\frac{1}{2}})(\boldsymbol{I}+\boldsymbol{Z}_0^{\frac{1}{2}}\widetilde{\boldsymbol{D}}\boldsymbol{Z}_0^{\frac{1}{2}})^{-1}
\end{aligned} \tag{4.22}$$

assuming the $(\boldsymbol{I}+\boldsymbol{Z}_0^{\frac{1}{2}}\widetilde{\boldsymbol{D}}\boldsymbol{Z}_0^{\frac{1}{2}})^{-1}$ exists.

4.3.3 Lumped realizations of LTI circuits

The state-space notation and rational models can be used for construction of lumped equivalent circuits. Opposite to physical models, the lumped elements of the resulting circuits are not directly related with physical structure and is it very difficult to predict how the change of the structure geometry influences the values of the equivalent circuit.

SPICE network from state-space model. The state-space model (4.6) that represents the admittance or scattering parameters can be directly realized as an electric circuit using resistors, capacitors and voltage/current controlled sources [2]. In general, for an N-port device, the realization of the scattering representation has a form shown in Fig. 4.6. It consists of N input/output and $N \cdot M$ state subcircuits. Additional N input-output circuits are added using the relations between incident and reflected waves a_k, b_k and voltage and current amplitudes v_k, i_k at $k-$th port:

$$b_k = \frac{v_k - Z_{0k} i_k}{2\sqrt{Z_{0k}}} \tag{4.23}$$

$$a_k = \frac{v_k + Z_{0k} i_k}{2\sqrt{Z_{0k}}} \tag{4.24}$$

where Z_{0k} is the characteristic impedance of the $k-$th port.

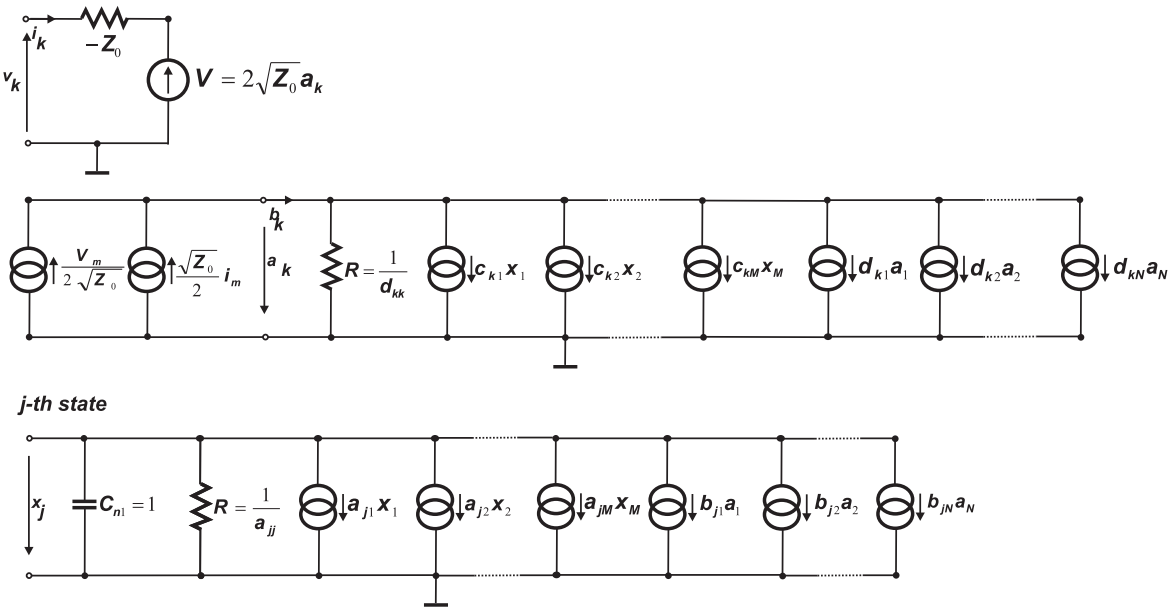

Figure 4.6: Electric networks that realize k-th input/output port and j-th state of state-space model (scattering representation).

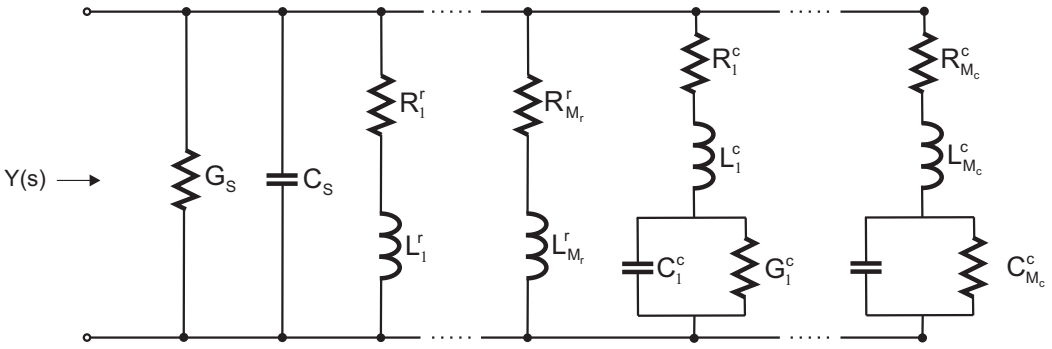

Figure 4.7: An electric network that realizes one-port admittance Y(s)

SPICE network from admittance rational model. From the circuit theory it is well known that an equivalent circuit corresponding to the passive rational model of admittance matrix can be constructed using Foster's or Cauer's realization of the rational function [116]. A one-port equivalent circuit realization of the admittance function:

$$Y(s) = sY_\infty + Y_0 + \sum_{m=1}^{M_r} \frac{r_m}{s - p_m} + \sum_{n=1}^{M_c} \left(\frac{a_n}{s - p_n} + \frac{a_n^*}{s - p_n^*} \right) \tag{4.25}$$

is presented in fig. 4.7. The realization uses the lumped R,L,C elements. The values of the realization can be determined from the following relations [99]:

$$G_s = Y_0 \tag{4.26}$$
$$C_s = Y_\infty \tag{4.27}$$
$$R_m^r = \frac{1}{r_m} \tag{4.28}$$
$$L_m^r = -\frac{p_m}{a_m} \tag{4.29}$$
$$L_n^c = \frac{1}{2\,Re(a_m)} \tag{4.30}$$
$$L_n^c C_n^c \|p_n\|^2 = R_n^c G_n^c + 1 \tag{4.31}$$
$$\frac{G_n^c}{C_n^c} = -\frac{Re(a_n p_n^*)}{Re(a_n)} \tag{4.32}$$
$$\frac{R_n^c}{L_n^c} = -\frac{Re(a_n p_n^*)}{Re(a_n)} - 2\,Re(p_n) \tag{4.33}$$

Since the passivity of the realization is guaranteed, it is acceptable that elements R,L,C have negative values. The one port realization can be generalized to multiport devices and in that case a full admittance matrix $\boldsymbol{Y}_{N\times N}(s)$ can be realized as a complete graph with N-vertices corresponding to N-ports. Each branch of the graph represents an admittance realized as one-port realization. The branch between i,j vertices is a negative value of the admittance $Y_{ij}(s)$. Additionally the m-th port admittance (branch between the port and ground) is the sum of all the admittances in m-th row of admittance matrix.

Example. In section 4.2 it was shown that the physical equivalent circuit of an octagonal inductor is valid in a limited frequency range. The same wideband response was then represented in the form of a rational model, converted to the state-space representation and realized as a SPICE network. The wideband rational model, shown in Table 4.2, has M=6 poles. The error E_{RMS} of the model is equal -89.2dB for S_{11} and -103.2dB for S_{21} parameter, and the accuracy of the constructed equivalent circuit is the same as the one of rational model. It is worth to notice, that the accuracy is significantly higher than what could be achieved in the case of physical substrate-coupled circuit. Fig.4.8 shows the comparison of EM-response and its realization. It is evident that the direct realization of the transfer function is accurate in the whole frequency range, also in the area where the physical model fails, which proves the versatility of the technique.

However, opposite to the physical equivalent circuits, the coefficients of the transfer function (and, in consequence, the elements of the equivalent circuit) can not be directly related to the changes of the modelled structure. For example, the conductance of the metal strip of the inductor was modified in the same manner as in section 4.2. The rational model of the response of the modified structure is shown in Tab. 4.3. It can be seen, that it is impossible to predict which values of the poles and residues change with the modification of the structure.

Table 4.2: Rational model of the octagonal inductor, CASE I.

i	poles p_i	residues k_i^{11}	residues k_i^{21}	residues k_i^{22}
1	-8.7629	-0.0034424	0.045988	-0.062744
2	-17.819	0.88858	0.9803	1.103
3	-52.382	-59.281	58.037	-59.003
4	-223.83	-3.2252	14.082	1.6851
5	-202.56 + 449.49i	-251.53 - 196.65i	132.69 + 64.723i	-197.82 - 189.52i
6	-202.56 - 449.49i	-251.53 + 196.65i	132.69 - 64.723i	-197.82 + 189.52i

Table 4.3: Rational model of the octagonal inductor, CASE II - reduced wire conductivity.

i	poles p_i	residues k_i^{11}	residues k_i^{21}	residues k_i^{22}
1	-15.051	0.48454	0.75525	0.24911
2	-28.557	1.2166	0.037476	2.457
3	-52.294	-61.51	58.97	-63.134
4	-132.19	-2.1707	7.4966	2.8129
5	-193.63 + 407.85i	-224.57 - 195.51i	133.08 + 72.029i	-176.8 - 188.02i
6	-193.63 - 407.85i	-224.57 + 195.51i	133.08 - 72.029i	-176.8 + 188.02i

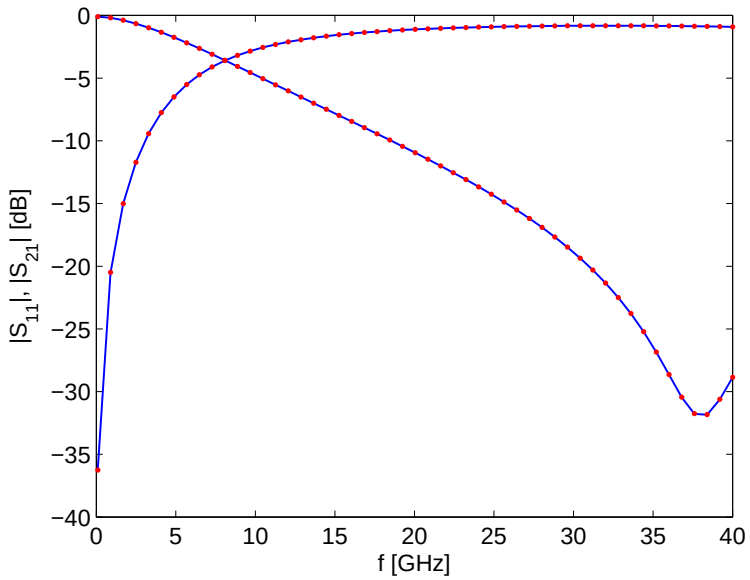

Figure 4.8: Response of circuit being a realization of transfer function (scattering parameters) of octagonal inductor in a wide frequency range: (···) electromagnetic response, (—) equivalent circuit response.

4.4 Techniques of rational data fitting

In practice, the construction of rational representation of the transfer function based on the sampled response in the frequency domain is not a trivial task. Two common techniques that are used for construction of rational representation are:

- Direct interpolation scheme
- Vector fitting

4.4.1 Direct interpolation scheme

Direct interpolation scheme is the most often used technique of rational model construction, commonly used in filter design [3, 36, 76]. With this approach the device response $H(s)$ is interpolated with a rational function as:

$$H(s) \approx \frac{K(s)}{L(s)} = \frac{k_0 + k_1 s + k_2 s^2 + \cdots + k_P s^P}{l_0 + l_1 s + l_2 s^2 + \cdots + l_Q s^Q} \tag{4.34}$$

at a set of discrete frequency points s_i where $i = 1 \ldots I$ and P, Q is the order of numerator and denominator, respectively. A linearized interpolation problem has a form:

$$K(s) - H(s) \cdot L(s) = 0 \tag{4.35}$$

It can be rewritten in a matrix form as:

$$[\boldsymbol{K} \;\; -\boldsymbol{L}] \begin{bmatrix} \boldsymbol{k} \\ \boldsymbol{l} \end{bmatrix} = 0 \tag{4.36}$$

where:

$$\boldsymbol{K}_{I\times P} = \begin{bmatrix} 1 & s_1 & s_1^2 & \ldots & s_1^P \\ 1 & s_2 & s_2^2 & \ldots & s_2^P \\ \ldots & \ldots & \ldots & \ddots & \ldots \\ 1 & s_I & s_I^2 & \ldots & s_I^P \end{bmatrix} \tag{4.37}$$

$$\boldsymbol{L}_{I\times Q} = \begin{bmatrix} H(s_1) & S(s_1)\cdot s_1 & H(s_1)\cdot s_1^2 & \ldots & H(s_1)\cdot s_1^Q \\ H(s_2) & S(s_2)\cdot s_2 & H(s_2)\cdot s_2^2 & \ldots & H(s_2)\cdot s_2^Q \\ \ldots & \ldots & \ldots & \ddots & \ldots \\ H(s_I) & S(s_I)\cdot s_I & H(s_I)\cdot s_I^2 & \ldots & H(s_I)\cdot s_I^Q \end{bmatrix} \tag{4.38}$$

$$\boldsymbol{k} = [\; k_0 \quad k_1 \quad \ldots \quad k_P \;]^T \tag{4.39}$$

$$\boldsymbol{l} = [\; l_0 \quad l_1 \quad \ldots \quad l_Q \;]^T \tag{4.40}$$

Since the response $H(s)$ is a complex valued function, an additional modification is required to ensure the poles of the resulting model come out as perfect complex-conjugate pairs. For

that to happen, sufficient is to construct the problem as a real valued one with transformation of the matrices K and L as:

$$\boldsymbol{K}_{2I\times P} = \begin{bmatrix} 1 & Re(s_1) & Re(s_1^2) & \dots & Re(s_1^P) \\ 0 & Im(s_1) & Im(s_1^2) & \dots & Im(s_1^P) \\ \dots & \dots & \dots & \ddots & \dots \\ 1 & Re(s_I) & Re(s_I^2) & \dots & Re(s_I^P) \\ 0 & Im(s_I) & Im(s_I^2) & \dots & Im(s_I^P) \end{bmatrix} \tag{4.41}$$

$$\boldsymbol{L}_{2I\times P} = \begin{bmatrix} Re(H(s_1)) & Re(H(s_1)\cdot s_1) & Re(H(s_1)\cdot s_1^2) & \dots & Re(H(s_1)\cdot s_1^Q) \\ Im(H(s_1)) & Im(H(s_1)\cdot s_1) & Im(H(s_1)\cdot s_1^2) & \dots & Im(H(s_1)\cdot s_1^Q) \\ \dots & \dots & \dots & \ddots & \dots \\ Re(H(s_I)) & Re(H(s_I)\cdot s_I) & Re(H(s_I)\cdot s_I^2) & \dots & Re(H(s_I)\cdot s_I^Q) \\ Im(H(s_I)) & Im(H(s_I)\cdot s_I) & Im(H(s_I)\cdot s_I^2) & \dots & Im(H(s_I)\cdot s_I^Q) \end{bmatrix} \tag{4.42}$$

That ensures the coefficients $\boldsymbol{k}$,$\boldsymbol{l}$ are real, so the poles and the residues come as perfect conjugate complex pairs.

In the case of modelling of multiport devices it is possible to enforce the same set of common poles for each transfer function. For example, in the case of two responses $H_1(s)$ and $H_2(s)$ one gets a problem:

$$\begin{aligned} H_1(s) &\approx \frac{K(s)}{L(s)} = \frac{k_0 + k_1 s + k_2 s^2 + \dots + k_P s^P}{l_0 + l_1 s + l_2 s^2 + \dots + l_Q s^Q} \\ H_2(s) &\approx \frac{N(s)}{L(s)} = \frac{n_0 + n_1 s + n_2 s^2 + \dots + n_L s^W}{l_0 + l_1 s + l_2 s^2 + \dots + l_Q s^Q} \end{aligned} \tag{4.43}$$

$$\begin{aligned} K(s) - H_1(s)\cdot L(s) = 0 \\ N(s) - H_2(s)\cdot L(s) = 0 \end{aligned} \tag{4.44}$$

which is then rewritten in the matrix from as a real problem:

$$\begin{bmatrix} \boldsymbol{K}_{2I\times P} & 0_{2I\times WL} & -\boldsymbol{L}_{2I\times Q} \\ 0_{2I\times P} & \boldsymbol{N}_{2I\times W} & -\boldsymbol{L}_{2I\times Q} \end{bmatrix} \begin{bmatrix} \boldsymbol{k} \\ \boldsymbol{n} \\ \boldsymbol{l} \end{bmatrix} = 0 \tag{4.45}$$

The structure of sub-matrices $\boldsymbol{K}$,$\boldsymbol{N}$ and $\boldsymbol{L}$ is the same as (4.41) and (4.42), respectively. The techniques for solving the equations 4.45 and 4.36 are presented in Appendix B.

Once the problem has been solved, the coefficients of the polynomials of numerator and denominator are obtained. The equation (4.34) can be then rewritten in pole-residue form, similar to 4.2.

The main issue related to direct approach is poor-conditioning of the interpolation problem and bad-scaling, which limits its applications to narrow frequency band responses described by low-order functions.

4.4.2 Vector fitting

Vector fitting and its modifications [29, 42, 44, 48] is a versatile technique of parameter extraction. The resulting rational model has a pole-residue form:

$$H(s) = \sum_{m=1}^{M} \frac{r_m}{s - p_m} + c + s \cdot h \tag{4.46}$$

The technique is iterative as it starts from an initial guess of model poles and then modifies them to improve the model accuracy. It is possible to model single function or groups of functions that form a vector. In the second case all elements of the vector are fitted with the same set of common poles, which is very useful in electronic engineering. Finally, it deals with poor conditioning of direct interpolation. The rational interpolation problem is solved in two stages.

Stage 1. Pole identification. For the assumed set of initial poles $\tilde{p}_m$ the approximation of $H(s)$ in multiplied with unknown function $\sigma(s)$. It is also assumed that $\sigma(s)$ is approximated with a rational function with the same poles as $H(s)$:

$$\begin{bmatrix} \sigma(s) \cdot H(s) \\ \sigma(s) \end{bmatrix} \approx \begin{bmatrix} \sum_{m=1}^{M} \frac{r_m}{s - \tilde{p}_m} + c + s \cdot h \\ \sum_{m=1}^{M} \frac{\tilde{r}_m}{s - \tilde{p}_m} + 1 \end{bmatrix} \tag{4.47}$$

The initial poles are selected as complex conjugate poles $\tilde{p}_m = w \pm jz$ placed in a linear manner over the frequency of interest. The recommended value of poles' real part is $w = \frac{z}{100}$ [48].

The following equation can be derived multiplying the second row of (4.47) with $H(s)$:

$$\left(\sum_{m=1}^{M} \frac{r_m}{s - \tilde{p}_m} + c + s \cdot h \right) \approx \left(\sum_{m=1}^{M} \frac{\tilde{r}_m}{s - \tilde{p}_m} + 1 \right) \cdot H(s) \tag{4.48}$$

which is then rewritten as:

$$\left(\sum_{m=1}^{M} \frac{r_m}{s - \tilde{p}_m} + c + s \cdot h \right) - H(s) \cdot \left(\sum_{m=1}^{M} \frac{\tilde{r}_m}{s - \tilde{p}_m} \right) = H(s) \tag{4.49}$$

This forms a linear problem $\widetilde{\boldsymbol{A}}\tilde{\boldsymbol{x}} = \tilde{\boldsymbol{b}}$ with unknowns $r_m, \tilde{r}_m, c$ and h that can be solved when written for a set of discrete frequencies s_i, $i = 1 \ldots I$. K-th equation of the problem has a form:

$$\widetilde{\boldsymbol{A}}_k = \begin{bmatrix} \frac{1}{s_k - \tilde{p}_1} & \ldots & \frac{1}{s_k - \tilde{p}_M} & 1 & s_k & -\frac{H(s_k)}{s_k - \tilde{p}_1} & \ldots & \frac{H(s_k)}{s_k - \tilde{p}_M} \end{bmatrix} \tag{4.50}$$

$$\tilde{\boldsymbol{x}} = \begin{bmatrix} r_1 & \ldots & r_M & c & h & \tilde{r}_1 & \ldots & \tilde{r}_M \end{bmatrix} \tag{4.51}$$

$$\widetilde{b}_k = H(s_k) \tag{4.52}$$

As in the case of direct interpolation, some additional effort is needed to ensure the conjugacy of the model residues in the case of complex poles. If $\tilde{p}_i$ and $\tilde{p}_{i+1}$ is a pair of conjugated poles $\tilde{p}_i = w + jz$ and $\tilde{p}_{i+1} = w - jz$ with corresponding residues is $r_i = u + jv$ and $r_{i+1} = u - jv$, then the following transformation in (4.50) is applied:

$$\frac{1}{s_k - \tilde{p}_i} \quad \rightarrow \quad \frac{1}{s_k - \tilde{p}_i} + \frac{1}{s_k - \tilde{p}_i^*} \tag{4.53}$$

$$\frac{1}{s_k - \tilde{p}_{i+1}} \quad \rightarrow \quad \frac{1}{s_k - \tilde{p}_i} - \frac{1}{s_k - \tilde{p}_i^*} \tag{4.54}$$

which ensures that the corresponding residues are simply equal u and v, respectively. Additionally, the problem should be written as a real one to enforce the complex poles being conjugate pairs, similarly as in direct approach.

Once the problem has been solved, one gets a rational representation of $H(s)$ in the form:

$$H(s) = h \cdot \frac{\prod_{m=1}^{M+1} s - z_m}{\prod_{m=1}^{M+1} s - \tilde{z}_m} \tag{4.55}$$

where z_m and $\tilde{z}_m$ are the zeros of the fitted approximations of $\sigma(s) \cdot H(s)$ and $\sigma(s)$ respectively. What is important, the calculated poles of the $H(s)$ are the same as zeros of $\sigma(s) \cdot H(s)$, which gives a corrected set of poles $\tilde{p}_m$. The resulting poles are taken as a better estimation of initial poles and the procedure is reiterated.

Stage 2. Residue identification. Once the set of poles is computed, the residues r_m of (4.46) can be calculated as a solution of a linear least squares problem $\widetilde{\boldsymbol{A}}\tilde{\boldsymbol{x}} = \tilde{\boldsymbol{b}}$. To ensure the conjugacy property, the problem is defined as a real-valued one:

$$\begin{bmatrix} Re(\widetilde{\boldsymbol{A}}) \\ Im(\widetilde{\boldsymbol{A}}) \end{bmatrix} \tilde{\boldsymbol{x}} = \begin{bmatrix} Re(\tilde{\boldsymbol{b}}) \\ Im(\tilde{\boldsymbol{b}}) \end{bmatrix} \tag{4.56}$$

4.4.3 Stability enforcement

Both techniques provide a rational representation of fitted data, however it may occur that some poles of the resulting rational model are not stable. In this case the simplest solution is to flip the poles into a left half of s-plane by reversing of the sign of the real parts of unstable poles.

4.4.4 Comparison of fitting techniques

The techniques described in the previous sections were applied to the same set of real-life data to reveal their properties. Figure 4.9 shows a modelled structure, which is a section of a meander microstrip line. The substrate parameters are: dielectric constant $\varepsilon_r = 2.2$, substrate height $h = 0.508$mm, $\tan\delta = 0.002$. Structure dimensions are: strip width $w = 1.57$mm,

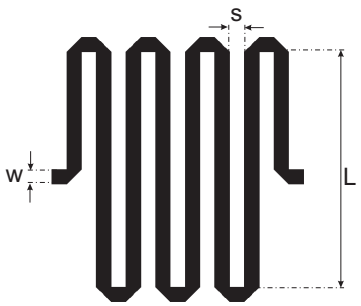

Figure 4.9: Layout of a meander microstrip line.

Table 4.4: Comparison of accuracy of direct and VF interpolation schemes for different model orders M

M	Condition number	E_{RMSDir}	E_{RMSVF}
12	$1.77 \cdot 10^{9}$	-58.32	-60.31
18	$2.78 \cdot 10^{14}$	-77.90	-81.24
24	$4.47 \cdot 10^{19}$	-94.00	-99.74
30	$2.24 \cdot 10^{24}$	-17.36	-101.16

length of the line sections $L = 25$mm and spacing between the lines $s = 1.57$mm. To compute the scattering parameters of the test structure the electromagnetic simulator Agilent ADS Momentum was used. Two cases are investigated, namely narrow- and wide-band modelling. In both cases the S_{11} and S_{21} scattering parameters are fitted with the same set of poles.

Narrowband application The structure was analyzed in the frequency band from DC to 4GHz with the frequency step Δf = 100MHz. The obtained scattering parameters were fitted

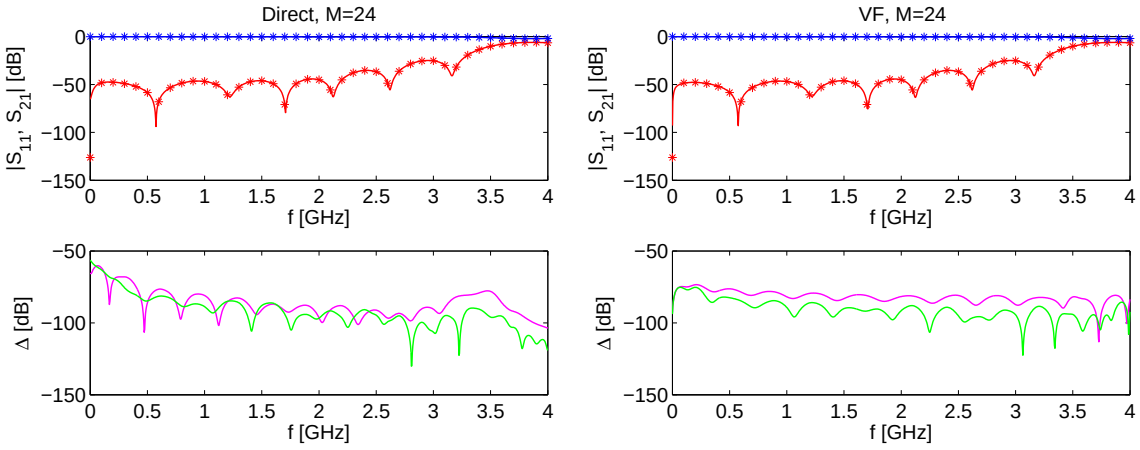

Figure 4.10: Rational models created with direct and vector fitting approach: (—) $\|S_{11}\|$ model, (—) $\|S_{21}\|$ model, (***) $\|S_{11}\|$ reference data, (***) $\|S_{21}\|$ reference data, (—) $\|S_{11}\|$ fitting error, (—) $\|S_{21}\|$ fitting error.

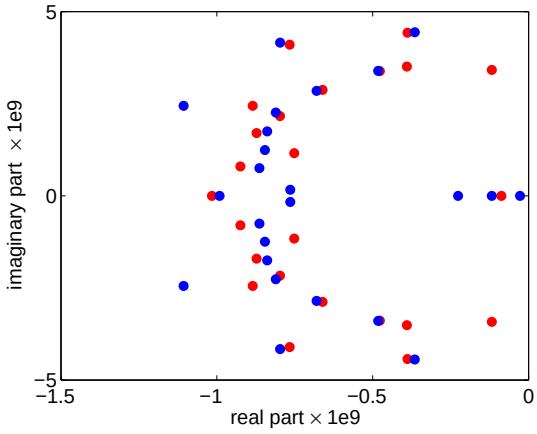

Figure 4.11: Location of poles on the s-plane for models with order M=24: (•) Direct interpolation, (•) Vector fitting.

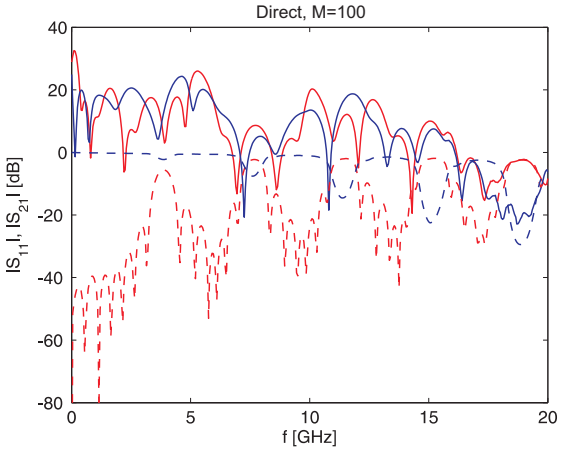

Figure 4.12: Wideband rational model created with direct approach: (—) $\|S_{11}\|$ model, (—) $\|S_{21}\|$ model, (– – –) $\|S_{11}\|$ reference data, (– – –) $\|S_{21}\|$ reference data.

using both described techniques to obtain rational representation with increasing model order M=12,18,24,30. The error E_{RMS} for both models is presented in Table 4.4. In the same table, the condition number κ, computed as the ratio of maximum and minimum singular values of the interpolation matrix (4.44) is shown. In both cases the higher the model order, the higher the accuracy of the fitting. However, in the case of direct approach the ill-conditioning of the interpolation problem appears when the order reaches M=30 and the resulting model is unusable. The vector fitting creates models with better accuracy, and is free of the ill-conditioning problem.

A comparison of the fitting results for a constant model order M=24 along with the error distribution is shown in Fig. 4.10. The real absolute error of the fitting was computed as:

$$\Delta = 20 \cdot \log_{10}(\|S_{ij} - \widehat{S}_{ij}\|) \tag{4.57}$$

for both S_{11} and S_{21} responses, where S_{ij} and $\widehat{S}_{ij}$ is the response of rational model and reference response, respectively. Figure 4.11 shows the pole distribution for the obtained models with M=24 poles. It is worth to notice that despite the similar accuracy of models (error Δ_{max} below -60dB), both representations have noticeably different sets of poles. The rational model is not unique, i.e. there are plenty of rational models described with slightly different sets of poles that approximate the device response with similar accuracy.

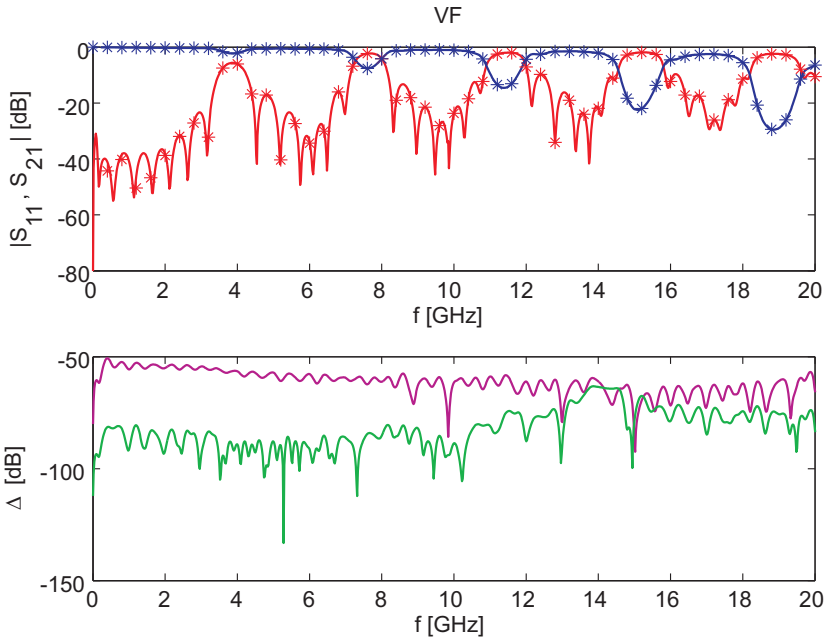

Figure 4.13: Wideband rational model created with vector fitting approach: (—) $\|S_{11}\|$ model, (—) $\|S_{21}\|$ model, (**) $\|S_{11}\|$ reference data, (**) $\|S_{21}\|$ reference data, (—) $\|S_{11}\|$ fitting error, (—) $\|S_{21}\|$ fitting error.

Wideband application The structure was also simulated in a wide frequency band 0 – 20GHz with frequency step Δf = 50MHz. Both techniques were applied to fit the set of scattering parameters. Since the frequency band became wider, the order of the rational model had to be increased. The model order was set as M=100. In this case the condition number of the linear problem solved in the direct approach was very high and equal $7.3 \cdot 10^{41}$, which caused the solution of the problem was inaccurate, as shown in Fig. 4.12. On the other hand, the vector fitting technique was able to create a satisfactory model. The results of the fitting are shown in Fig. 4.13. In this case the error was E_{RMS} = -82.02dB.

Chapter 5

Passive LTI circuits

5.1 Introduction

Passivity implies that a circuit can not generate more energy than it absorbs. A non-stable or non-passive equivalent circuit of a passive device is not physical and leads to improper simulation results. What is important, for a circuit that is composed of smaller subcircuits, the stability of those subcircuits does not ensure the stability of the whole. In fact, the lack of stability of the model can cause two basic problems:

- Stable but not passive circuits may lead to unstable systems when connected to other passive systems
- Transient simulations of non-passive networks may encounter some artificial oscillations

A non-passive device, when loaded with an arbitrary impedance, can lead to a distorted response of the system in frequency domain and to a non-stable simulation in time domain. Therefore, in the case of modelling of passive devices, the rational representation (4.2) should fulfil the stability and passivity conditions. However, the circuit composed of passive subcircuits is guaranteed to be stable [104]. As a result, even a small lack of passivity may influence the results of simulation both in time and frequency domain. A rational representation obtained as a result of rational data fitting can ensure stability and high accuracy of the model in a desired frequency band. However, the fitting techniques cannot ensure the passivity of the model, which is essential in time domain analysis.

As an example, in Fig. 5.1, a very simple structure of a uniform microstrip line is shown. The structure was analyzed using ADS Momentum from DC up to 20GHz and an equivalent circuit of the structure was generated without taking care of its passivity. Then the line was loaded with a passive RC circuit (R=1kΩ and C=1pF) (Fig.5.2) and excited by a sinusoidal voltage source with frequency 18GHz. Figure 5.3 shows the time-domain response of such a circuit. It is seen that the circuit is not stable and the energy in the circuit increases, in contrast to the passive model. The example shows the importance of preserving the passivity of the equivalent circuit if the original device is passive.

In this chapter a techniques of passivity enforcement of the model are investigated.

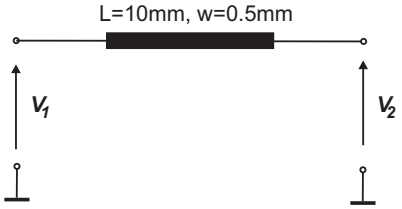

Figure 5.1: Modelled microstrip line

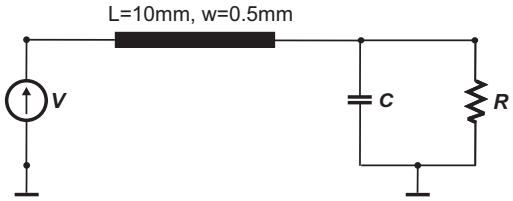

Figure 5.2: Modelled microstrip line loaded with RC circuit

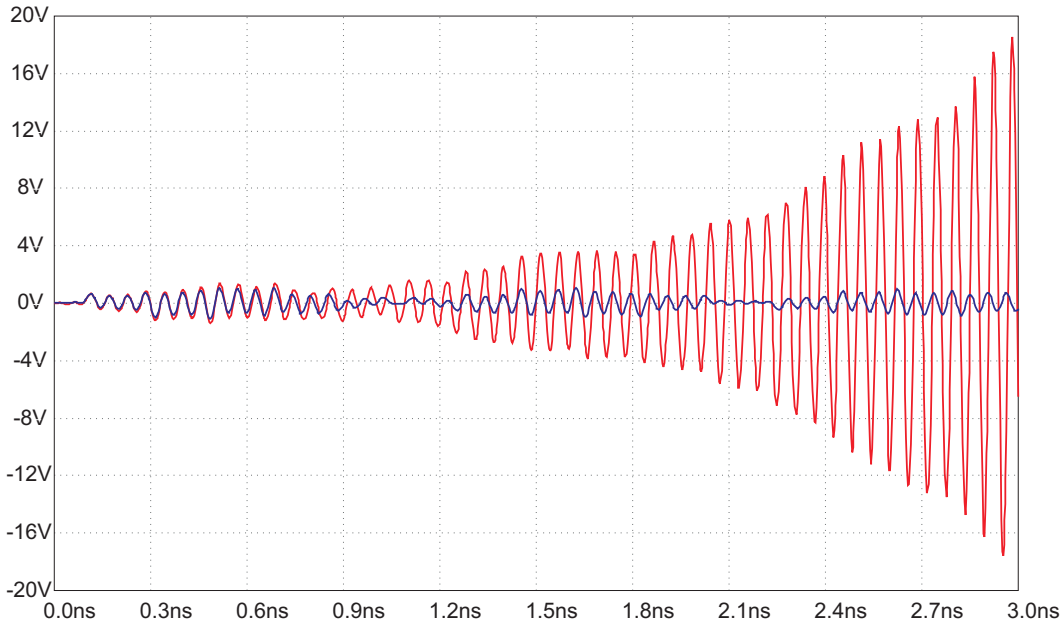

Figure 5.3: Time domain simulation results of passive (—) and non-passive (—) equivalent circuits of microstrip line, both loaded with the same impedance

5.2 Passivity criteria

The most general definition of passivity in electronics engineering is as follows [104, 123]:

Definition 2 *Electronic circuit is said to be passive if energy absorbed by the network via its terminals is grater than energy stored inside for every time period* $t_1 \geq t_0$*:*

$$\int_{t_0}^{t_1} \boldsymbol{v}^T(t) \cdot \boldsymbol{i}(t) dt \geq e(t_1) - e(t_0) \tag{5.1}$$

where v and i denotes the voltage and current vectors in n-port terminals and $e(t)$ *is energy stored inside the circuit.*

5.2.1 PR and BR criteria

In the case of impedance/admittance rational representation this definition is equivalent to positive-realness (PR) condition. The function $\boldsymbol{H}(s)$ is positive real when [7]:

$$\overline{\boldsymbol{H}(s)} = \boldsymbol{H}(\overline{s}) \tag{5.2}$$

$$\boldsymbol{H}(s) + \boldsymbol{H}(s)^H \geq 0 \text{ in} \{s : Re(s) > 0\} \tag{5.3}$$

where $\geq$ denotes the semi-definiteness. A system described with scattering parameters is passive if the rational representation $\boldsymbol{H}(s = j\omega)$ of $\boldsymbol{S}(j\omega)$ is bounded real (BR) [7]:

$$\forall\omega \quad \boldsymbol{I} - \boldsymbol{H}(j\omega)^H \boldsymbol{H}(j\omega) \geq 0 \tag{5.4}$$

which is equivalent to the condition:

$$\forall\omega \quad \max(\sigma(\boldsymbol{H}(j\omega))) \leq 1 \tag{5.5}$$

where $\sigma(\boldsymbol{H}(j\omega))$ denotes the singular values of matrix $\boldsymbol{H}(j\omega)$. Both PR and BR criteria are defined in frequency domain, therefore to check passivity properties of $\boldsymbol{H}(s)$ the frequency-sweep test has to be done. However, for accurate test, dense sampling of the frequency domain is required, which is a significant drawback of this criterion.

5.2.2 Hamiltonian based criteria

More robust passivity criteria are based on a state-space representation $\boldsymbol{A},\boldsymbol{B},\boldsymbol{C},\boldsymbol{D}$ of the system. The basic theory of these criteria was proposed in [18]. Let us consider a Hamiltonian matrix derived from a scattering representation:

$$\boldsymbol{H}_m = \begin{bmatrix} \boldsymbol{A} - \boldsymbol{B}\boldsymbol{R}^{-1}\boldsymbol{D}^T\boldsymbol{C} & -\boldsymbol{B}\boldsymbol{R}^{-1}\boldsymbol{B}^T \\ \boldsymbol{C}^T\boldsymbol{Q}^{-1}\boldsymbol{C} & -\boldsymbol{A}^T + \boldsymbol{C}^T\boldsymbol{D}\boldsymbol{R}^{-1}\boldsymbol{B}^T \end{bmatrix} \tag{5.6}$$

where $\boldsymbol{Q} = (\boldsymbol{D}^T\boldsymbol{D} - \boldsymbol{I})$ and $\boldsymbol{R} = (\boldsymbol{D}\boldsymbol{D}^T - \boldsymbol{I})$. As shown in [43] the state-space model is guaranteed to be passive only if matrix $\boldsymbol{H}_m$ has no imaginary eigenvalues. Additionally, if $j\omega_0$ is the eigenvalue of $\boldsymbol{H}_m$ and a maximum singular value of matrix $\boldsymbol{H}(s)$ crosses value 1 at $j\omega_0$, then ω_0 is a frequency which denotes the cross-over from a non-passive frequency band to a passive one.

The same criterion can be applied for admittance/impedance state-space representation. In this case the appropriate Hamiltonian has a form:

$$\boldsymbol{H}_m = \begin{bmatrix} \boldsymbol{A} + \boldsymbol{B}\boldsymbol{Q}^{-1}\boldsymbol{C} & \boldsymbol{B}\boldsymbol{Q}^{-1}\boldsymbol{B}^T \\ -\boldsymbol{C}^T\boldsymbol{Q}^{-1}\boldsymbol{C} & -\boldsymbol{A}^T - \boldsymbol{C}^T\boldsymbol{Q}^{-1}\boldsymbol{B}^T \end{bmatrix} \tag{5.7}$$

where $\boldsymbol{Q} = -(\boldsymbol{D} + \boldsymbol{D}^T)$ and the passivity constraints imposed on eigenvalues of the H_m are the same as in the case of scattering matrix.

5.3 Passivity enforcement

5.3.1 Existing solutions

Several techniques of passivity enforcement have already been proposed. In this section the most important ones are shortly introduced.

5.3.1.1 QP approach

Gustavsen and Semlyen in [49] propose a passivity enforcement technique which uses quadratic programming (QP) technique. The technique uses positive-definiteness criterion of the admittance matrix, which states that the power absorbed by multiport device is positive if matrix $\boldsymbol{G} = Re(\boldsymbol{Y})$ is positive definite (PD):

$$\forall\ \omega \quad Re(\boldsymbol{Y}(s)) \geq 0 \tag{5.8}$$

The technique is based on a rational representation of admittance matrix in form (4.2) and modifies the residues of the system to restore the PD condition at discrete frequencies.

The optimization problem uses a linearized relation between the model response $\boldsymbol{Y}(s_k)$ stored in vector $\boldsymbol{y}$ and the model parameters (residues) stored in vector $\boldsymbol{x}$:

$$\boldsymbol{\Delta y} = \boldsymbol{M}\boldsymbol{\Delta x} \tag{5.9}$$

This relation is used to relate real parts of $\boldsymbol{y}$ and $\boldsymbol{x}$:

$$\boldsymbol{\Delta g} = Re(\boldsymbol{\Delta y}) = Re(\boldsymbol{M})\boldsymbol{\Delta x} = P\boldsymbol{\Delta x} \tag{5.10}$$

Additionally a linearized relation between eigenvalues of matrix $\boldsymbol{G}$ stored in vector $\boldsymbol{\lambda}$ and vector $\boldsymbol{g}$:

$$\boldsymbol{\Delta\lambda} = \boldsymbol{Q}\boldsymbol{\Delta g} \tag{5.11}$$

These relations can be combined to form:

$$\boldsymbol{\Delta\lambda} = \boldsymbol{Q}\,\boldsymbol{P}\,\boldsymbol{\Delta x} = \boldsymbol{R}\,\boldsymbol{\Delta x} \tag{5.12}$$

Assuming that reference admittance parameters are stored in matrix $\widehat{\boldsymbol{Y}}$ and associated vector $\hat{\boldsymbol{y}}$, the problem is defined as:

$$\hat{\boldsymbol{y}} - (\boldsymbol{y} + \boldsymbol{M}\boldsymbol{\Delta x}) = 0 \tag{5.13}$$

with an additional condition imposed on eigenvalues λ of $\boldsymbol{G} = Re(\boldsymbol{Y})$ to make them positive:

$$\boldsymbol{\Delta\lambda} = \boldsymbol{R}\,\boldsymbol{\Delta x} \geq -\boldsymbol{\lambda} \tag{5.14}$$

This problem is treated as a quadratic programming problem, that minimizes the expression

$$\frac{1}{2}\boldsymbol{\Delta x}\,\bar{\boldsymbol{H}}\,\boldsymbol{\Delta x} - \boldsymbol{f}^{\boldsymbol{T}}\boldsymbol{\Delta x} \tag{5.15}$$

with respect to condition:

$$-\boldsymbol{R}\boldsymbol{\Delta x} < \boldsymbol{\lambda} \tag{5.16}$$

where:

$$\bar{\boldsymbol{H}} = \boldsymbol{M}^T\boldsymbol{M} \quad \boldsymbol{f} = \boldsymbol{M}^T(\hat{\boldsymbol{y}} - \boldsymbol{y}) \tag{5.17}$$

The solution of the quadratic problem gives a correction of model parameters $\Delta\boldsymbol{x}$ and the model $\boldsymbol{x}$ is updated $\boldsymbol{x} = \boldsymbol{x} + \Delta\boldsymbol{x}$. This procedure is iterated until the passivity is restored.

The technique described above is easy to implement, however it suffers from a significant limitation: the passivity is checked and restored only locally on a set of discrete frequency points s_k. It does not guarantee that the resulting model does not violate the passivity at other frequencies.

5.3.1.2 Filter theory approach

The rational representation of the transfer function can be treated as connection of: low-pass, band-pass and all-pass filters, as described in [35,88]. Since a connection of passive elements is passive, passivity enforcement simply enforces the simple subnetworks are passive. Let us transform a matrix valuated rational function $\boldsymbol{H}(s)$ to a form:

$$\begin{aligned} \boldsymbol{H}(s) &= \sum_{m=1}^{LPN} \frac{\boldsymbol{R}_m}{s - p_{mr}} \\ &+ \sum_{n=1}^{BPN} \frac{2\boldsymbol{\alpha}_n(s - p_{nr}) - 2\boldsymbol{\beta}_n p_{ni}}{(s - p_{nr})^2 + p_{ni}^2} + \boldsymbol{\delta} + \boldsymbol{\eta} \cdot s \end{aligned} \tag{5.18}$$

where: LPN is a number or low-pass networks related to real poles p_{mr} and corresponding residues $\boldsymbol{R_m}$, BPN is a number of band-pass networks connected to conjugate complex poles $p_n = p_{nr} \pm j p_{ni}$ and corresponding residues $\boldsymbol{R}_n = \boldsymbol{\alpha_n} \pm \boldsymbol{\beta_n}$. With this notation and applying the positive semi-definiteness condition (5.8), the device is passive if:

$$\begin{aligned} \text{eigenvalues of } \boldsymbol{R}_m &\geq 0 \\ \text{eigenvalues of } [-\boldsymbol{\alpha}_n p_{nr} \pm \boldsymbol{\beta}_n p_{ni}] &\geq 0 \\ \text{eigenvalues of } \boldsymbol{\delta} &\geq 0. \end{aligned} \tag{5.19}$$

For compensating of negative eigenvalues the matrices $\boldsymbol{R_m}$, $\boldsymbol{\alpha}_n$,$\boldsymbol{\beta}_n$ and $\boldsymbol{\delta}$ can be slightly modified.

The advantage of the technique is a global passivity enforcement since the perturbed matrices are free of frequency dependence. However, there is no method for automated correction of the model.

5.3.1.3 Convex optimization approach

In [22] the passivity enforcement problem is organized as a convex optimization scheme that is based on positive-realness (PR) passivity constraints. The Positive Real Lemma (or Kalman-Yakubovich-Popov-Anderson lemma) states that a system $\boldsymbol{H}(s)$ described with state-space representation $\boldsymbol{A},\boldsymbol{B},\boldsymbol{C},\boldsymbol{D}$ is positive real if exists such a matrix $\boldsymbol{K} = \boldsymbol{K}^T$ that linear matrix inequalities:

$$\begin{bmatrix} -\boldsymbol{A}^T\boldsymbol{K} - \boldsymbol{K}\boldsymbol{A} & -\boldsymbol{K}\boldsymbol{B} + \boldsymbol{C}^T \\ -\boldsymbol{B}^T\boldsymbol{K} + \boldsymbol{C} & \boldsymbol{D} + \boldsymbol{D}^T \end{bmatrix} \geq 0 \tag{5.20}$$

$$\boldsymbol{K} \geq 0 \tag{5.21}$$

are satisfied. The convex optimization problem is formulated to determine matrices $\boldsymbol{C}$,$\boldsymbol{D}$ with a cost function defined with inequalities (5.20) and (5.21) and additional weighted least-squares constraints imposed on frequency response of the model:

$$\sum_{k=1}^{N} w_{k,p,q} \| H_{p,q}(s_k) - \widehat{H}_{p,q}(s_k) \| < t_{p,q} \tag{5.22}$$

where $H_{p,q}$ and $\widehat{H}_{p,q}$ are the (p,q) elements of the model and reference data matrices, s_k is a complex frequency and $t_{p,q}$ is an absolute error constraint imposed on (p,q) element of $H(s_k)$. The technique does not perturb the poles of the system.

The advantages of the technique is control of the frequency domain response of the system and global passivity enforcement. However, the convex optimization of the residues (matrix $\boldsymbol{C}$) involves high numerical cost which strongly reduces its applications to simple systems described with low number of states (below 100).

5.3.1.4 Hamiltonian based technique

The most robust and versatile technique was proposed by Talocia in [43] and then extended in [45, 108]. The technique uses the Hamiltonian passivity criterion described in section 5.2.2 to localize a non-passive frequency bands. A correction $\boldsymbol{\Delta C}$ of matrix $\boldsymbol{C}$ is computed minimizing the cumulative energy of the impulse responses perturbations:

$$E = \int_0^{\infty} \| \boldsymbol{dh}(t) \|^2 dt \tag{5.23}$$

which guarantees a minimal deviation of the system responses in time domain:

$$\boldsymbol{dh}(t) = \mathcal{L}^{-1}\{\boldsymbol{dH}(s)\} \tag{5.24}$$

The minimizing of the perturbation of impulse responses is equivalent to minimizing the perturbation $\boldsymbol{\Delta C}$ of system matrix $\boldsymbol{C}$. Perturbation $\boldsymbol{\Delta C}$ influences the hamiltonian matrix $\boldsymbol{H}_m$:

$$\boldsymbol{H}_m^p = \boldsymbol{H}_m + \boldsymbol{\Delta H}_m \tag{5.25}$$

In the case of scattering representation (5.6), neglecting the second order terms, the perturbation has a form:

$$\boldsymbol{\Delta H}_m = \begin{bmatrix} -\boldsymbol{B}\boldsymbol{R}^{-1}\boldsymbol{D}^T\boldsymbol{\Delta C} & \boldsymbol{0} \\ \boldsymbol{C}^T\boldsymbol{Q}^{-1}\boldsymbol{\Delta C} + \boldsymbol{\Delta C}^T\boldsymbol{Q}^{-1}\boldsymbol{C} & \boldsymbol{\Delta C}^T\boldsymbol{D}\boldsymbol{R}^{-1}\boldsymbol{B}^T \end{bmatrix} \tag{5.26}$$

The perturbation $\boldsymbol{\Delta H}_m$ can be applied in order to shift the pure imaginary eigenvalues of $\boldsymbol{H}_m$ off the imaginary axis. With such formulation the model correction $\boldsymbol{\Delta C}$ is computed as a solution of a linear least-squares problem. The procedure is iterative and in each iteration the correction $\boldsymbol{\Delta C}$ is computed and applied to the system, until the passivity of the system is restored.

The main drawback of such approach is that minimization of functional (5.23) does not allow one to control the distortion of the frequency response of the system. Therefore the technique is useful in the case of small violations of the passivity.

Table 5.1: Comparison of passivity enforcement techniques, N-number of ports, M-number of poles

Feature	QP	Filter theory	Convex	Hamiltonian	Proposed
Optimized var.	N^2M	N^2M	N^2M	N^2M	M
Guaranteed passivity	No	Yes	Yes	Yes	Yes
Max. states	tens	tens	tens	hundreds+	hundreds+
FD control	Yes	Yes	Yes	No	Yes
Automated	Yes	No	Yes	Yes	Yes
Implementation	Easy	-	Difficult	Difficult	Easy

5.3.2 Optimization scheme with frequency response control

In Table 5.1 the comparison of features of existing passivity enforcement techniques is shown. It can be seen that all the techniques have some disadvantages. The most powerful technique is the one developed by Talocia, as it makes possible to enforce the passivity of large systems and assures the passivity for all frequencies. However, the technique optimizes the residues of the rational model, which leads to high number of variables. Additionally, the method does not control the distortion of the frequency response and if the passivity violation is large, it may produce inaccurate results.

In this section a novel optimization-based technique of passivity enforcement is introduced. As shown in Table 5.1, the technique has several advantages over the former ones. The technique optimizes the locations of poles instead of residues, which significantly reduces the number of variables. It exploits the Hamiltonian criterion to check the passivity and assures the global passivity. Finally, it controls the frequency response of the resulting macromodel and can be applied to models with strong violation of passivity.

The basics of the technique were published in [72, 73]. The technique has several advantages over the alternative techniques mentioned previously, such as:

- It controls accuracy of frequency response while enforcing passivity;
- It can enforce passivity of the model even if input data is strongly non-passive;
- It allows one to create a passive equivalent circuit of complex passive device with a large number of states;
- It is easy to implement.

The passivity enforcement procedure can be divided into three major elements:

- Identification of the frequency bands where model is not passive
- Correction of model parameters (poles and/or residues) in the optimization loop
- Implementation of the constraints that minimize disturbance of the frequency response

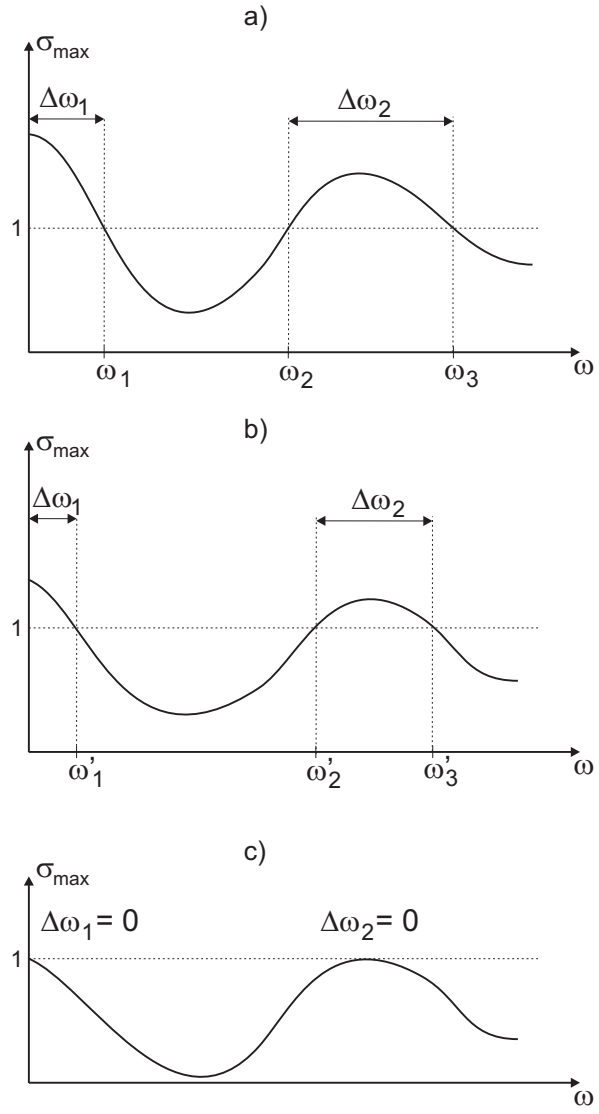

Figure 5.4: Example: Three pure imaginary eigenvalues of H and corresponding non-passive frequency ranges.

5.3.2.1 Passivity test

To test the passivity of the model the Hamiltonian-based criterion (5.6) is used. Using this criterion one can not only detect if the model is passive, but also obtain the frequency bands in which the passivity condition is violated. Such a passivity test is much more reliable and efficient than a standard procedure of testing if the scattering matrix is bounded real in the frequency domain. To find the eigenvalues of the Hamiltonian matrix in an efficient and accurate manner a dedicated solver HAPACK [16] can be used, as described in Appendix A.

5.3.2.2 Model correction

The approach described here can optimize the perturbation of common poles and/or residues. However, the optimization of poles only reduces the number of variables - it needs only M

variables compared to N^2M in the case of residues. Let us introduce vector $\mathbf{\Delta\Omega}$:

$$\mathbf{\Delta\Omega} = \begin{bmatrix} \Delta\omega_1 \\ \Delta\omega_2 \\ \cdots \\ \Delta\omega_P \end{bmatrix} \tag{5.27}$$

where element $\Delta\omega_i$ is the i-th frequency band of passivity violation. Two special cases have to be investigated:

- if the model is not passive from DC to ω_1, then $\Delta\omega_1 = \omega_1$
- if the model is not passive from ω_P to infinity, then $\Delta\omega_P = \omega_P$

Figure 5.4a shows definition of the elements of vector $\mathbf{\Delta\Omega}$ in the case of two non-passive frequency bands, one from DC to ω_1 and second from ω_1 to ω_2.

The procedure of passivity restoration can be organized as an optimization problem. The goal of the optimization is to minimize the values of $\mathbf{\Delta\Omega}$, as shown in Fig. 5.4b. In particular, if condition $\Delta\omega_i = 0$ is fulfilled for $i = 1 \ldots P$, the model is guaranteed to be passive for every ω (Fig. 5.4c).

5.3.2.3 Preservation of the frequency response

Let $\boldsymbol{S}_{N\times N}(\omega)$ be the N-port scattering matrix computed at frequency ω and $\hat{\boldsymbol{S}}_{N\times N}(\omega)$ be the scattering matrix obtained from the state-space model. To minimize the distortion of the frequency domain response due to passivity enforcement an additional condition is imposed:

$$\|\hat{\boldsymbol{S}}(\omega_i) - \boldsymbol{S}(\omega_i)\| \leq \xi \cdot \|\boldsymbol{S}(\omega_i)\| \tag{5.28}$$

at a set of discrete frequency points ω_i. Parameter ξ is defined as an acceptable difference between the reference data and the state space model response and allows one to control the accuracy of the model after the passivity enforcement. The condition presented above enforces the relative error for the created passive model to be less than ξ. On the other hand, one may be interested in enforcing the absolute error of the created model be less than ξ. In this case the condition should be modified to:

$$\|\hat{\boldsymbol{S}}(\omega_i) - \boldsymbol{S}(\omega_i)\| \leq \xi \tag{5.29}$$

Both conditions are implemented as nonlinear inequality constraints of mini-max optimization. Additionally, the accuracy ξ does not have to be the same for every ω_i. One can set a different weight of ξ at each frequency ω_i, setting the different response accuracy over different frequency bands.

In such a case, the optimization routine minimizes the bands of passivity violations and, at the same time, maximizes the model accuracy.

5.3.2.4 Optimization algorithm

Passivity is enforced when all elements of vector $\mathbf{\Delta\Omega}$ are equal zero. In other words, passivity is obtained when the norm of $\mathbf{\Delta\Omega}$ reaches minimum, i.e. zero.

In general, any optimization algorithm can be applied to minimize the values of $\mathbf{\Delta\Omega}$ provided it can handle non-linear constraints. One of them is a gradient based mini-max optimization routine, which finds the minimum of a problem specified as:

$$\min_{p} \max_{\mathbf{\Delta\Omega}} \mathbf{\Delta\Omega}(p) \tag{5.30}$$

with a non-linear condition:

$$\boldsymbol{C}(p) \leq 0 \tag{5.31}$$

where p is a real-valued vector of optimized model parameters (real and imaginary values that describe locations of poles) and $\boldsymbol{C}(p)$ is a function that realizes the condition (5.28) or (5.29). Mini-max optimization technique is implemented in Matlab Optimization Toolbox as *fminimax*, based on publications of Powell and Han [50, 97].

As it is stated above, the procedure finishes successfully if all of the values of $\mathbf{\Delta\Omega}$ are set to zero. Because the proposed procedure is based on an optimization scheme, it is not guaranteed to converge with arbitrary accuracy ξ. Therefore, in case the optimization does not converge to a passive model, it is recommended to relax the accuracy parameter ξ in (5.28) or (5.29).

5.3.2.5 Gradient computation

Minimax optimization involves gradients. In the passivity enforcement technique presented above it is possible to compute an analytic gradient of the goal function. Let us analyze a perturbed unsymmetric eigenvalue problem [40]:

$$(\boldsymbol{H}_m + \Delta\boldsymbol{H}_m)\boldsymbol{x}_p = \lambda_p \boldsymbol{x}_p \tag{5.32}$$

Assume that λ is a simple eigenvalue of $\boldsymbol{H}_m$ and $\bar{\boldsymbol{x}}$ ($\bar{\boldsymbol{y}}$) is the right (left) eigenvector corresponding to λ. Assuming the perturbation of matrix $\boldsymbol{H}$ is small, one can obtain the first-order approximation of eigenvalue λ_p of the perturbed matrix as:

$$\lambda_p = \lambda + \frac{\bar{\boldsymbol{y}}^H \Delta\boldsymbol{H}_m \bar{\boldsymbol{x}}}{\bar{\boldsymbol{y}}^H \bar{\boldsymbol{x}}} \tag{5.33}$$

Additionally, since both matrices $\boldsymbol{H}_m$ and $\Delta\boldsymbol{H}_m$ are hamiltonians, the following relation between the left and right eigenvector exists [43]:

$$\bar{\boldsymbol{y}} = \bar{\boldsymbol{x}}^H \boldsymbol{J} \tag{5.34}$$

$$\boldsymbol{J} = \begin{bmatrix} 0 & \boldsymbol{I} \\ -\boldsymbol{I} & 0 \end{bmatrix} \tag{5.35}$$

The formula can be utilized for fast computation of the gradient of goal function. To obtain full gradient information one needs to compute a set of purely imaginary eigenvalues and

the corresponding left and right eigenvectors only once. In the case of optimization based only on poles (not residues) of model, perturbation of pole location influences only matrix A, therefore:

$$\Delta \boldsymbol{H} = \begin{bmatrix} \Delta \boldsymbol{A} & 0 \\ 0 & -\Delta \boldsymbol{A}^T \end{bmatrix} \tag{5.36}$$

Finally, the sensitivity of the eigenvalue λ_i to the perturbation of pole p_i can be computed as:

$$\frac{\partial \lambda_i}{\partial p_i} = \frac{\bar{\boldsymbol{x}}^H \boldsymbol{J} \boldsymbol{P} \bar{\boldsymbol{x}}}{\bar{\boldsymbol{x}}^H \boldsymbol{J} \bar{\boldsymbol{x}}} \tag{5.37}$$

where $\boldsymbol{P}$ is a matrix of size of perturbation matrix $\Delta \boldsymbol{H}_m$ with elements $P_{ij} = sign\,(\Delta H_{ij})$.

5.3.2.6 Flow chart

In fig. 5.5 a general flow-chart of the described technique is shown. The procedure starts with the frequency domain scattering parameters of a device. Then a rational model of its transfer function is created and tested for passivity violation. If the model is not passive, the algorithm of passivity enforcement is started in an optimization loop. Once the passivity is restored, the equivalent circuit of the device can be generated, using the techniques described in section 4.3.3.

5.4 Comparison of various techniques of passivity enforcement

In this section, a comparison of accuracy of selected passivity enforcement techniques is presented. Three techniques were selected: QP-approach (denoted as QP-PE), technique based on Hamiltonian criterion that minimize the distortion of response in time or frequency domain (denoted as HTD-PE) and proposed Hamiltonian-based optimization technique with frequency response control (denoted as HFD-PE).

5.4.1 Small passivity violation

The first test structure is a microstrip meander line introduced in section 4.4.4. The wideband scattering parameters of the structure in frequency range DC-20GHz with frequency step Δf=200MHz were considered.

QP-PE. At first, an attempt to restore the passivity using QP-approach was made. The wideband rational model of admittance parameters of meander line was created using the VF technique. The model order was set as M=100 poles. The resulting model is very accurate - the root mean square error E_{RMS} of the model is smaller than -75dB in the case of both S_{11} and S_{21} responses. Since the technique relies on PD criterion, a frequency sweep of eigenvalues of admittance matrix at discrete 201 frequency points was performed. The result of such a passivity test is shown in figure 5.6, which shows the model is not passive at

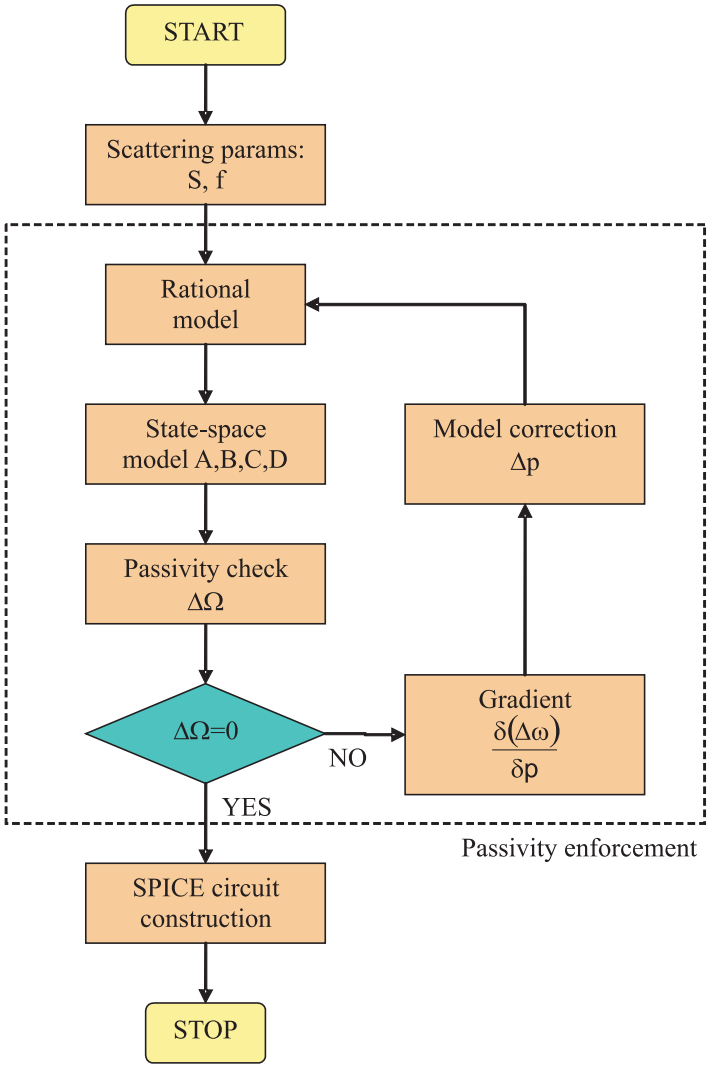

Figure 5.5: Flow chart of the complete algorithm

few frequency points. Then the QP-approach was used to enforce passivity of the model on non-passive frequency points. Three iterations of QP-approach were needed to restore the passivity. The result is presented in Fig. 5.6, which shows that despite the fact that the model has become passive for all discrete frequencies, a few frequency bands still exist within which the passivity is violated. The example proves that the QP-approach does not assure the global passivity of the model.

HTD-PE technique. The same data were used to compute the rational model of scattering parameters. The hamiltonian criterion was applied to determine that the model is not passive in frequency band DC-45.7MHz. Then a HTD-PE technique, developed by Talocia, was used to restore the passivity of the model. The correction of the model parameters (residues) succeeded, and the accuracy results are presented in Tab. 5.2. It is seen that the accuracy of the passive model is very high, since the maximum error Δ_{max} is smaller than -75dB.

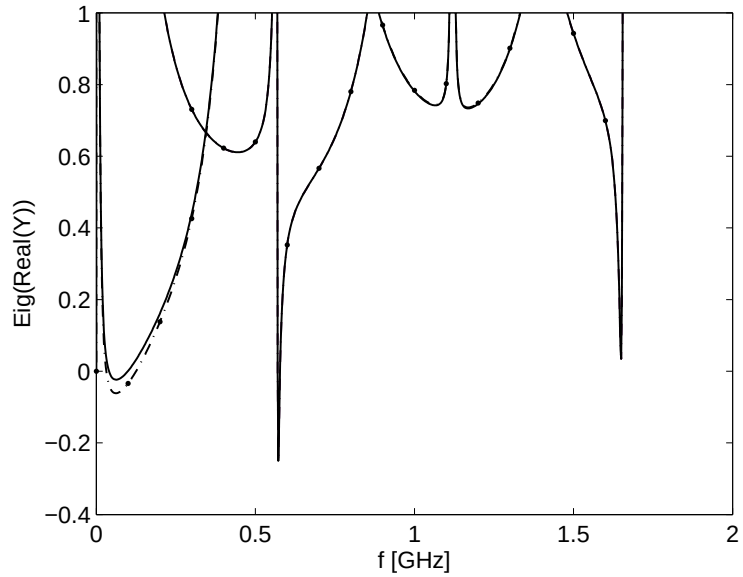

Figure 5.6: Meander line example: PD criterion test result before $-.-.-$ and after — passivity enforcement with QP technique.

HFD-PE technique. The same rational model was enforced to be passive with the HFD-PE technique proposed in this thesis. The technique was run with two different constraints imposed on the frequency domain response of the final model. In the first case (denoted as HFD-PE I) the condition of absolute error (5.28) with the tolerance set as $\xi = 0.0002$ was used. In the second one (denoted as HFD-PE II) the relative error condition was used (5.29) with the same tolerance value. In table 5.2 the errors introduced by both passivity enforcement techniques to the original model are presented.

The first option gives a very accurate model with maximum absolute error smaller than -74dB, similarly to the HTD-PE approach. The results are presented in Fig. 5.7. The minimization of the frequency response distortion based on the relative error produces slightly different results. In this case the accuracy of S_{11} response is increased, while S_{21} slightly decreased.

To conclude, both HTD-PE and HFD-PE approaches gave accurate models which are passive for every frequency. When the model passivity is violated only marginally, both techniques produce similar results. The advantages of HFD-PE technique are seen when the violation of passivity increases and the model is strongly non-passive. This case will be discussed next.

5.4.2 Strong passivity violation

The same techniques were applied to a strongly non-passive response of microwave filter. The non-passive response is a result of the application of non-passive parameterized surrogate models for the evaluation of filter response in the frequency domain in a form of scattering parameters. The data are strongly non-passive since the maximum singular value

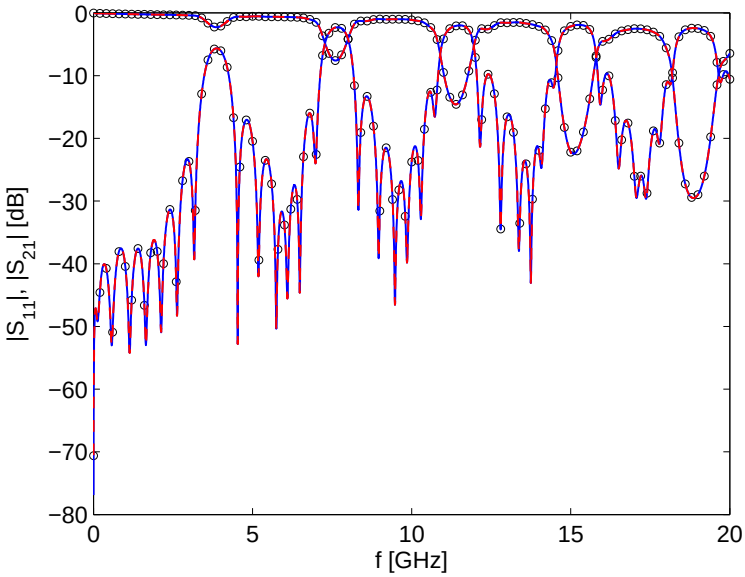

Figure 5.7: Passivity enforcement results with hamiltonian-based technique HFD-PE I: (○) electromagnetic response, (−) passive circuit response.

Table 5.2: Meander line example: Model distortion in the case of passivity enforcement with TD and FD techniques

Error [dB]	HTD-PE		HFD-PE I		HFD-PE II	
	S_{11}	S_{21}	S_{11}	S_{21}	S_{11}	S_{21}
Δ_{max}	−76.3	−76.3	−74.0	−74.0	−94.5	−70.6
Δ_{mean}	−110.3	−110.3	−92.0	−94.2	−105.2	−90.2
E_{RMS}	−116.2	−116.2	−105.2	−106.1	−122.8	−102.63

of the scattering matrix in-band of the filter passband reaches 1.06.

QP-PE technique issues. Since several techniques, like the QP or the convex optimization approach are based on admittance parameters, the first step is to obtain the accurate rational representation of admittance parameters derived from scattering parameters. However, it is often not possible to construct such representation when the passivity violation is strong. To illustrate this two situations are investigated: passive and non passive responses of a microwave filter. In both cases the scattering parameters were transformed to admittance parameters and fitted to the rational form with the VF technique. At this stage, a problem of model accuracy occurs with non-passive data. The RMS error of the fitting of passive response is below -160dB, while in the case of non-passive response the accuracy of the fitting is much worse and the RMS error is greater than -50dB. What is important, the increase of the model error, in the case of non-passive data, does not lead to accuracy improvement. Such high an error of the rational model of admittance parameters makes the model practically useless. The results are shown in Fig. 5.8. Figures 5.8a and 5.8c show the fitted admittance

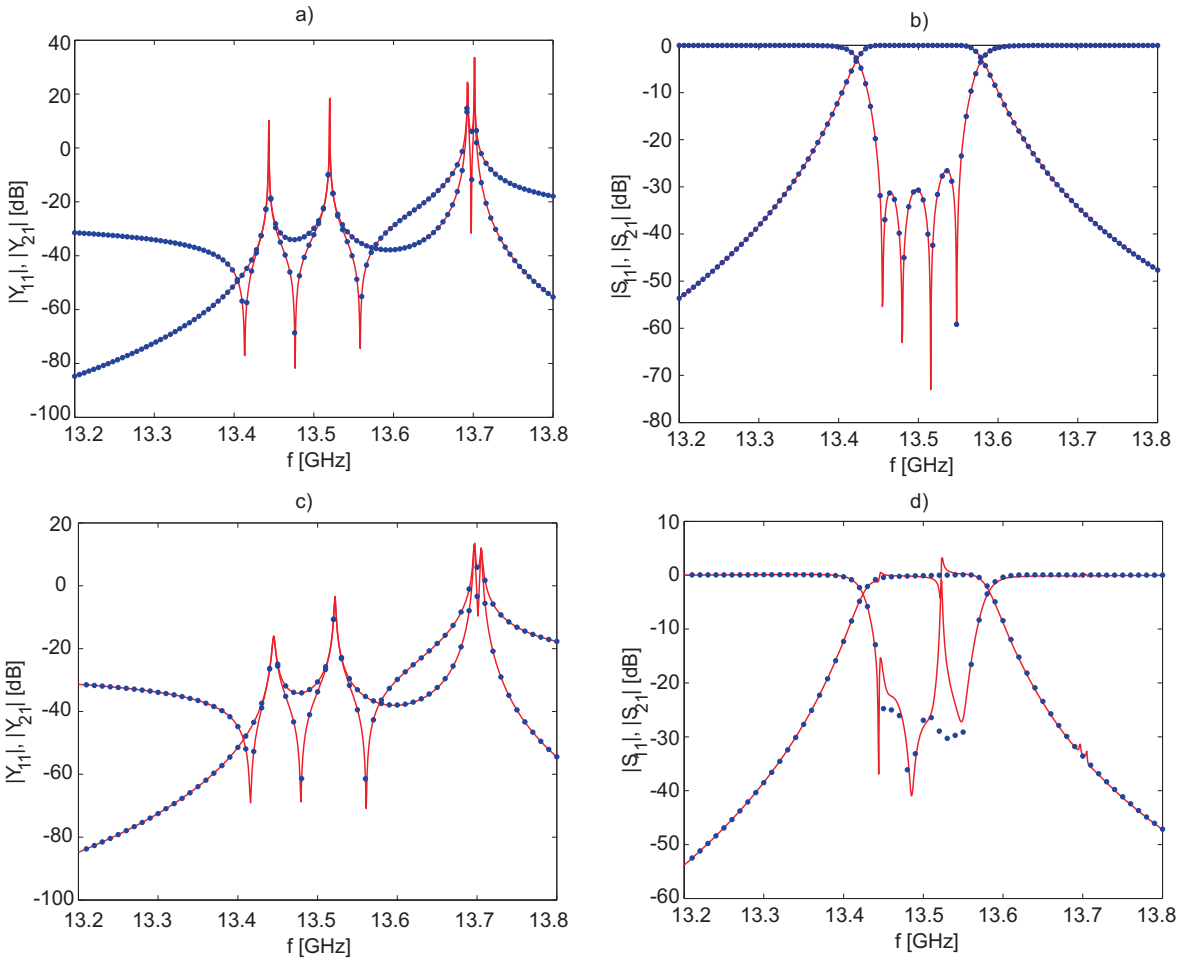

Figure 5.8: Comparison of accuracy of rational model in the case of the passive and non-passive data. Case I: admittance parameters and a rational model of a passive response (a) and scattering parameters computed from the rational model (b). Case II: admittance parameters and a rational model of a non-passive response (c) and scattering parameters computed from the rational model (d).

parameters for passive and non-passive data, respectively. Figures 5.8b and 5.8d show the comparison of the original scattering parameters with the ones computed from the model of admittance parameters. It is seen, that in the case of the non-passive response the limited accuracy of the fitting strongly influences the scattering parameters. The problem manifests itself strongly in a filter passband, where the response has a resonant character. This example shows that in the case of admittance-based techniques like the QP-PE, one of the basic issues is the construction of accurate rational model of admittance parameters. When the passivity is strongly violated, the model has poor accuracy and the passivity enforcement has no chance to succeed.

HTD-PE and HFD-PE techniques. Both Hamiltonian-based techniques were applied to enforce the passivity of non-passive rational model of scattering parameters of a microwave filter. Since both techniques operate on scattering representation, the problem described

Table 5.3: Strong passivity violation: Rational model accuracy and response distortion in the case of passivity enforcement with HTD-PE and HFD-PE techniques.

Error [dB]	Rational		HTD-PE		HFD-PE	
	S_{11}	S_{21}	S_{11}	S_{21}	S_{11}	S_{21}
Δ_{max}	-55.7	-68.0	-16.9	-16.0	-24.6	-21.6
Δ_{mean}	-64.7	-82.2	-30.8	-31.0	-35.0	-37.7
E_{RMS}	-84.3	-96.0	-47.0	-46.3	-53.7	-51.0

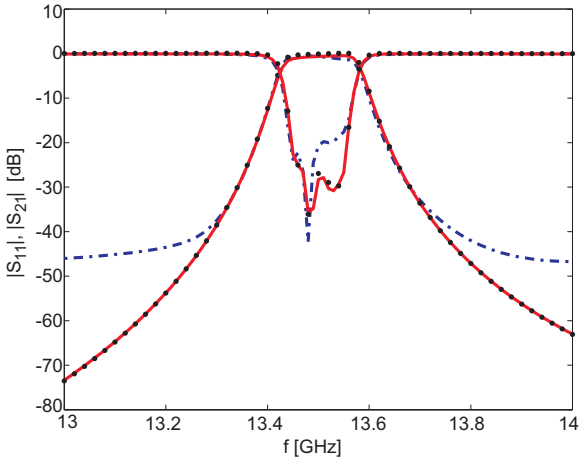

Figure 5.9: Input non-passive data (···) and results of passivity enforcement with proposed technique (—) and presented in [43] (-·-)

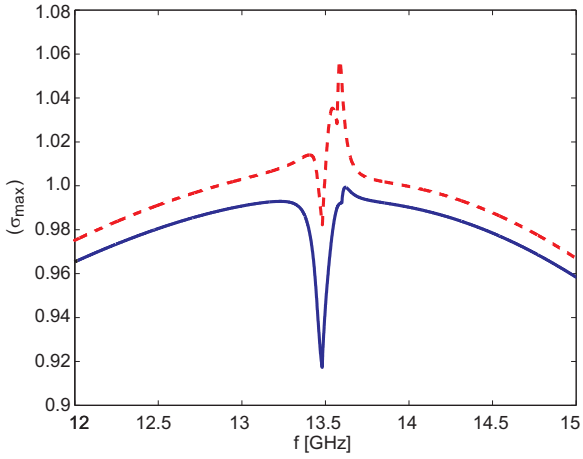

Figure 5.10: Maximum singular value of scattering matrix of microwave filter before (···) and after (–) passivity enforcement

the in previous section does not affect them. The accuracy of the created rational model with M=10 poles is presented in table 5.3. The model is not passive in the frequency range 12.86GHz-13.46GHz and 13.49GHz-13.98GHz (Fig. 5.10).

The plots of the scattering parameters after the passivity enforcement are shown in Fig. 5.9. With the frequency domain approach one gets a passive network with the response much closer to the original non-passive data. In Tab. 5.3 the comparison of accuracy of both passive models are shown. The alternative technique that minimizes distortion of time-domain response gives a model with higher error, which means that the condition for minimization of distortion of the time-domain response is not optimal for non-passive input data. The plot of the σ_{max} vs. frequency before and after model correction is shown in Fig. 5.10 and proves the passivity of the resulting model.

The time needed for passivity enforcement was 2.5 seconds on 1,5GHz laptop PC. The example shows that even in the case of highly non-passive resonant circuits the perturbation of poles with frequency domain procedure yields passive circuits with satisfactory accuracy.

5.4.3 Patch antenna example

The miniaturization of modern microwave circuits has a significant impact on to design of antenna elements. The technology allows one to integrate the antenna with other active components of the system, leading to *active antenna* philosophy [83]. Such a strategy eliminates

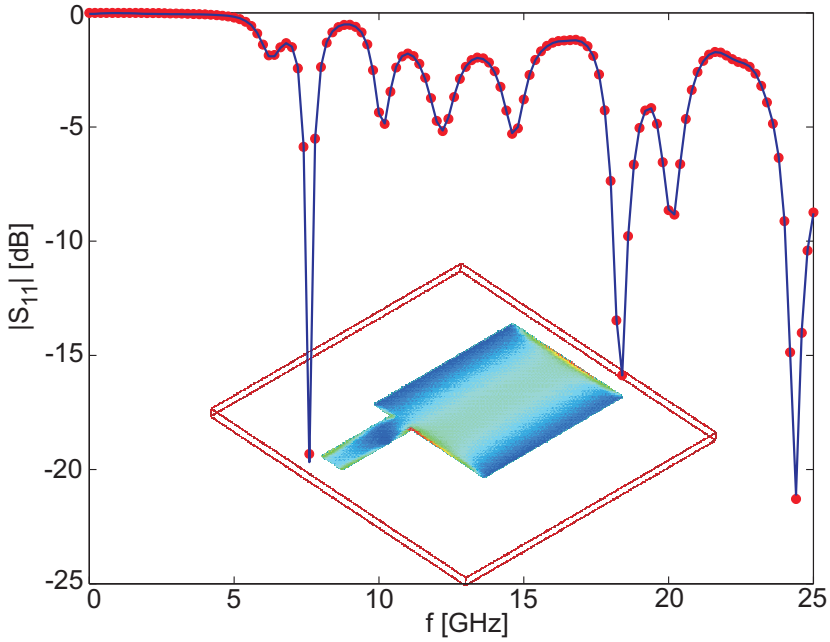

Figure 5.11: Reflection coefficient of patch antenna: (—) passive circuit response, (○) electromagnetic simulator results.

feeding line losses and connectors. The active antennas have a potential in low-cost, wireless applications and radar solutions.

In contrary to classic, stand-alone radiators, the design of active antenna is tightly connected to design of the active subsystems. Since the active devices are mostly analyzed using SPICE simulator, there is a need to include the antenna element into SPICE simulations. In general, from the point of view of input impedance of the antenna, the antenna can be represented as an RLC resonant circuit. However, such a single resonance model is valid in a narrow frequency band close to the resonant frequency. More general circuits involve transmission models (TLM) [37], however they can not be directly incorporated into the SPICE simulator.

What is therefore needed for active antenna design is a versatile technique that can provide a wideband equivalent circuit of the antenna. Since the design involves analog nonlinear elements, such as transistors, the equivalent circuit should be valid for several higher harmonics of the operating frequency. Additionally, the circuit should be suited for time-domain simulation. The method proposed in this thesis is capable of providing such models.

For example, let us investigate a rectangular patch antenna feed by a microstrip line. The antenna structure was described in detail in [126], where one can find the structure dimensions. The antenna was simulated using ADS Momentum in the frequency range from DC up to 25GHz with frequency step 200MHz. The scattering parameter S_{11} was then fitted with VF technique, the order of rational interpolation was M=36. The model accuracy is shown in Tab. 5.4. What is important, the model has turned out to be not passive in the frequency range from 0.36GHz to 1.83GHz.

The passivity of the model was then enforced with HTD-PE and HFD-PE. The accuracy

Table 5.4: Antenna example: Accuracy comparison of non-passive rational model and result of passivity enforcement

Error [dB]	Rational model	HTD-PE	HFD-PE
Δ_{max}	-48.3	-44.5	-46.9
Δ_{mean}	-56.6	-57.3	-52.1
E_{RMS}	-76.5	-76.3	-72.4

of resulting passive models is shown in Tab. 5.4. Both techniques provide a passive models with comparable accuracy. Figure 5.11 shows a comparison of EM simulation results and the response of passive circuit. The wideband equivalent circuit can be now used for analysis within SPICE.

Chapter 6

Advanced examples and applications

In this chapter some advanced examples of the applications of the techniques proposed in this thesis are presented. To illustrate flexibility of the models created with adaptive multivariate rational interpolation technique, models of complex planar and non-planar devices were created. Models with up-to seven variables are shown along with the benefits of the application of the surrogate models for automated design of microwave components.

Next the advanced examples of the construction of passive equivalent circuits of complex, multiport microwave devices are presented. Then the technique of multivariate modelling is combined with a scheme of equivalent circuit construction with guaranteed passivity. It is used to obtain SPICE-compatible parameterized equivalent circuits suitable for time-domain simulation. Such parameterized circuits can be applied to tuning and optimization of non-linear components or signal-integrity analysis on the system level within SPICE.

Finally, the application of models in automated design of selected microwave components is shown. A commercial viability of the models is shown on an example of the first ever commercial tool for rapid synthesis of combline filters.

6.1 Advanced surrogate models

The benefit of application of parameterized surrogate models is apparent when the modelled device has a complex structure and it takes a long time to evaluate its response. This is the case when planar/multilayer elements are analyzed with the MoM technique, using a structured mesh (ADS Momentum).

6.1.1 Spiral inductor in SiGe BiCMOS technology

Structure overview of an octagonal spiral inductor is presented in Fig. 6.1. Figure 6.2 shows a three dimensional view of the structure along with current visualization on the surface of the inductor. The inductor consists of 2.5 loop spiral with an uniform strip at the top layer and metal bridge at lower layer. The structure is described by three geometric parameters: strip width w, gap width s and inner spiral radius R. The model of such structure was computed in the frequency range from DC to 10GHz. Three scattering parameters were modelled: S_{11}, S_{21} and S_{22}. The range of model parameters is presented in Table 6.1. The selected

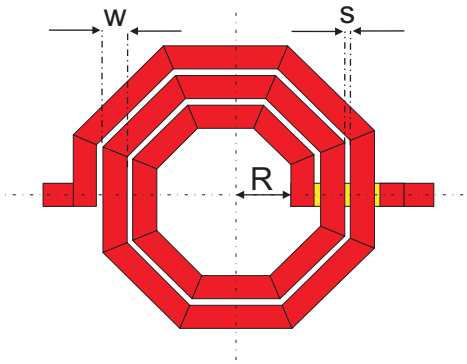

Figure 6.1: Structure and dimensions of modelled octagonal inductor.

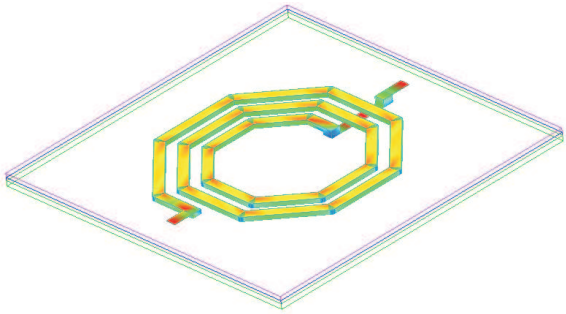

Figure 6.2: Three dimensional field visualization of modelled inductor.

Table 6.1: Range of input parameters of spiral inductor model

Parameter	Range
frequency (f)	0GHz - 10GHz
strip width (w)	$10\mu m$ - $25\mu m$
gap width (s)	$5\mu m$ - $20\mu m$
inner radius (R)	$30\mu m$ - $100\mu m$

parameter range corresponds to approximate inductor die area range from $150\mu m \times 150\mu m$ up to $470\mu m \times 470\mu m$. The required tolerance was set as ε=0.001, and the automated procedure needed 285 support points to build the models. The time of a single analysis was from 3 to 5 minutes on a 1.5GHz PC depending on structure size, so the whole procedure took about 20 hours.

A set of 500 randomly distributed data points in the model domain was generated and used for verification of the accuracy of the model. The mean error computed over the set was -67.3dB, while maximum error reached -55dB. Figure 6.3 shows a histogram and a cumulative distribution function of the S_{11} model error. It can be seen, that for 90% of samples the error is below -63dB. Additionally, the histogram and cumulative distribution function of error of Q factor computed from the model response is presented in Fig.6.4. Although the models of scattering parameters have good accuracy, the error of extracted Q factor can be high. The high error appears very close to the inductor resonance and in this region the parasitic capacitance of the inductor dominates. In fact this region of inductor operation is out of applications.

The advantages of model construction are obvious - while the analysis of the structure at a single frequency point takes a few minutes on a PC, the time of model evaluation is merely 0.02s. The speed-up of order of thousands is then achieved.

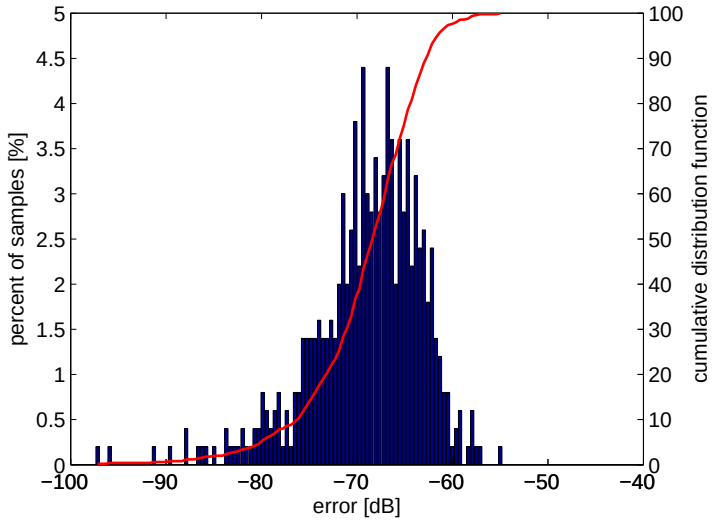

Figure 6.3: Histogram and cumulative distribution function of S_{11} model of octagonal inductor.

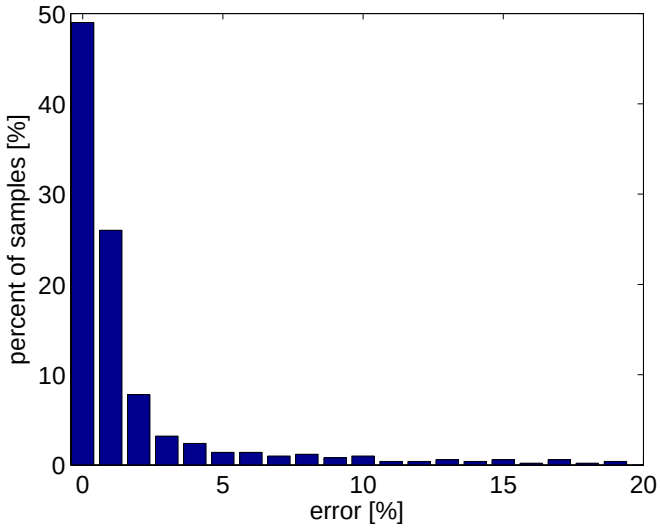

Figure 6.4: Histogram and cumulative distribution function of Q-factor error of rational model of octagonal inductor.

6.1.2 Interdigital capacitor in MCM-D technology

The next example is an MCM-D interdigital capacitor. Thin film MCM-D technology has many advantages over traditional hybrid technologies. It assures high precision components, repeatability of manufacturing complex microwave structures and integration of analog and digital circuits.

A layout of an interdigitated capacitor is shown in Fig. 6.5. A model of six variables (frequency and five geometric dimensions) was created. The ranges of the model parameters are presented in Table 6.2. The substrate parameters are as follows: thickness $45\mu m$, dielectric permittivity $\varepsilon_r = 2.65$, dielectric losses $\tan\delta = 0.002$, metal thickness $3\mu m$, metal conductivity $\sigma = 4.525 \cdot 10^7 \frac{S}{m}$ (gold).

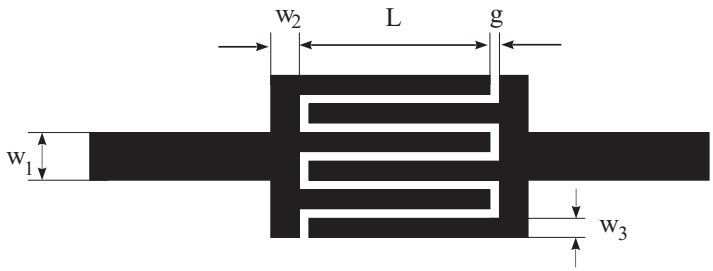

Figure 6.5: Layout of interdigitated capacitor

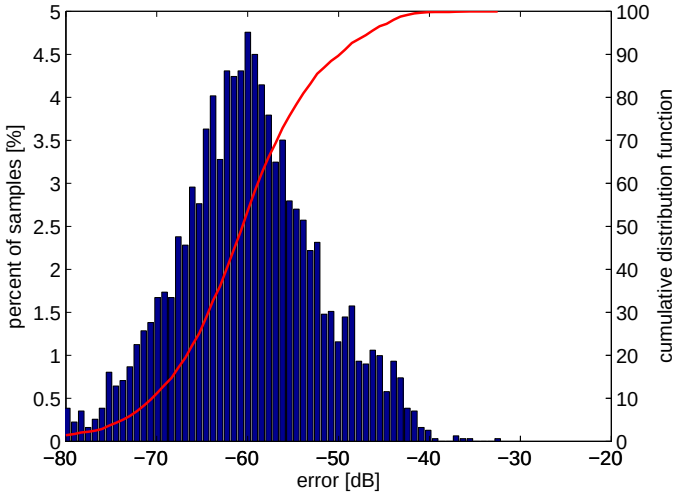

Figure 6.6: Histogram and cumulative distribution function of model error for interdigitated capacitor

Table 6.2: Range of input parameters of interdigitated capacitor model

Parameter	Range
frequency (f)	10GHz - 90GHz
input line width (w_1)	$50\mu m$ - $150\mu m$
cap. line width (w_2)	$10\mu m$ - $25\mu m$
finger length (L)	$100\mu m$ - $250\mu m$
finger line width ($w3$)	$10\mu m$ - $20\mu m$
gap width (g)	$10\mu m$ - $25\mu m$

The requested modelling error was ε =0.001=-60dB. The procedure started using a sparse grid with D=3 (729 support points) and initial orders $V = [2\ 2\ 2\ 2\ 2\ 2]$. Adding 1402 data points and increasing orders to $V = [3\ 4\ 3\ 4\ 4\ 4]$ gives the mismatch between both models below the requested 0.001. To verify the model accuracy a set of 3000 randomly distributed data points was computed using an electromagnetic simulator and compared with the model response. The histogram and cumulative distribution function of the model error

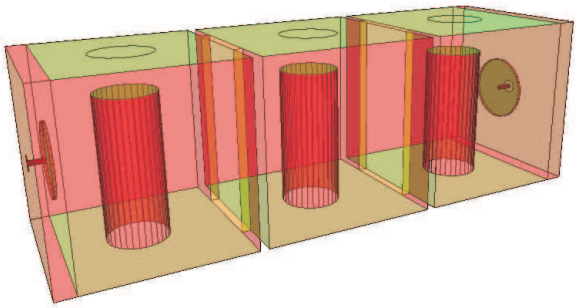

Figure 6.7: Third order combline filter used to create 7-variate models of coupling matrix.

are depicted in Fig. 6.6. The maximum error of created model was -32.5dB and mean error reached -56.5dB. In the case of 90% of test samples the error was below -50dB and for 54% of samples the error was below -60dB.

6.1.3 Models of coupling coefficient

The technique of parameterized model construction can be also applied to model various parameters of electronic circuits, such as the coupling coefficients and resonant frequencies between microwave resonators [52,64,65]. The coupling coefficient is widely used for design of microwave filters and multiplexers. The low-pass filter prototype can be represented in the form of coupling matrix $\boldsymbol{M}$, which elements $m_{i,j}$ determine the couplings between i-th and j-th resonators [19, 58, 70].

Each element $m_{i,j}$ of coupling matrix $\boldsymbol{M}$ can be interpolated with function $f_{i,j}(x_1, x_2, \ldots, x_N)$, where $x_1, \ldots, x_N$ are geometric parameters which influence the coupling matrix elements. The scheme of model construction is similar as in the case of modelling of scattering parameters. The difference is the polynomial (not rational) form of the created model. The modelled coupling matrix is extracted from the electromagnetic simulator response of the modelled coupled resonators using the technique presented in [69].

For a sake of illustration, the technique was used to construct a 7-th variate model of the coupling coefficient between combline resonators. The modelled structure, which is a 3-rd order combline filter, is presented in Fig. 6.7. In this case, the extracted coupling matrix has the following form:

$$\boldsymbol{M} = \begin{bmatrix} 0 & m_{S1} & 0 & 0 & 0 \\ m_{1S} & \Delta\omega_1 & m_{12} & 0 & 0 \\ 0 & m_{21} & \Delta\omega_2 & m_{23} & 0 \\ 0 & 0 & m_{32} & \Delta\omega_3 & m_{3L} \\ 0 & 0 & 0 & m_{L3} & 0 \end{bmatrix} \tag{6.1}$$

where m_{S1} (m_{3L}) is coupling of the source (load) to the first (third) resonator and $\Delta\omega_i$ is resonant frequency of i-th resonator. If the symmetry of the structure is assumed, then $m_{S1} = m_{1S} = m_{L3} = m_{3L}$, $m_{12} = m_{21} = m_{23} = m_{32}$ and $\Delta\omega_1 = \Delta\omega_3$. The models of the coupling of the source with the first resonator m_{S1}, coupling of the first and the second resonator m_{12} and resonant frequencies of the first and the second resonator $\Delta\omega_1$, $\Delta\omega_3$ were created with the

Table 6.3: Accuracy of the models of elements of coupling matrix in the case of combline resonators.

Element	Max. error [%]	Mean error [%]
m_{12}	2.15	0.55
m_{S1}	10.3194	3.286
$\Delta\omega_1$	0.573	0.117
$\Delta\omega_2$	0.580	0.117

proposed modelling approach.

The models parameters are as follow: coupling window width $w \in (0.4-0.9)$,diameter of a resonator post $R \in (0.05-0.2)$, height of a resonator post $H \in (0.6-0.8)$, coupling window thickness $d \in (0.025-0.1)$, electric probe tap diameter $e_2 \in (0.1-0.4)$, electric probe tap length $l_2 \in (0.01-0.05)$ and length of the inner coax wire to which the tap is mounted $l_1 \in (0.05-0.15)$ (all dimensions are normalized to length of resonator wall). The total number of support points used to create all the models was 3378. The accuracy of the model was verified on 1000 randomly distributed points and the results are presented in Tab. 6.3. Created models of elements m_{12},$\Delta\omega_1$ and $\Delta\omega_2$ have accuracy which is enough in most cases. As for the m_{S1} element both models used in the adaptive sampling technique converged to function which slightly differs from the original data, as stated in sec. 3.3.3.1. The high error of the m_{S1} function influences mainly the return loss level in the filter passband. In fact, this effect can be easily removed on stage of final tuning of the design.

6.2 Integration with commercial tools

The models, once computed, can be used for design of various microwave components, in the same manner as models present in the commercial circuit simulators. Additionally, it is possible to integrate the created rational models with the industry standard circuit simulators, like ADS from Agilent or Microwave Office from AWR.

In the ADS, external models can be integrated as user-compiled models. User has to define the parameters of the model, define the symbol of the model and provide the code in C that computes the admittance parameters of the device. Since the proposed modelling scheme involves the rational form of the model, this task can be done easily even by a non-experienced programmer. The the code is compiled with a C compiler and the model is ready to use. As an example, Fig. 6.9 shows the component library appended with the model of the MCM-D capacitor described in sec. 6.1.2.

In the Microwave Office the integration of the external model is done using Model Wizard from the Software Development Kit. The modeling wizard generates a C++ description of the model that can be compiled as a dynamically linked model. The whole procedure is similar to the ADS case.

It is worth to notice, that the possibility of models integration gives one an opportunity to prepare commercial libraries of non-standard, user-specific structures with the application of the technique described in this thesis.

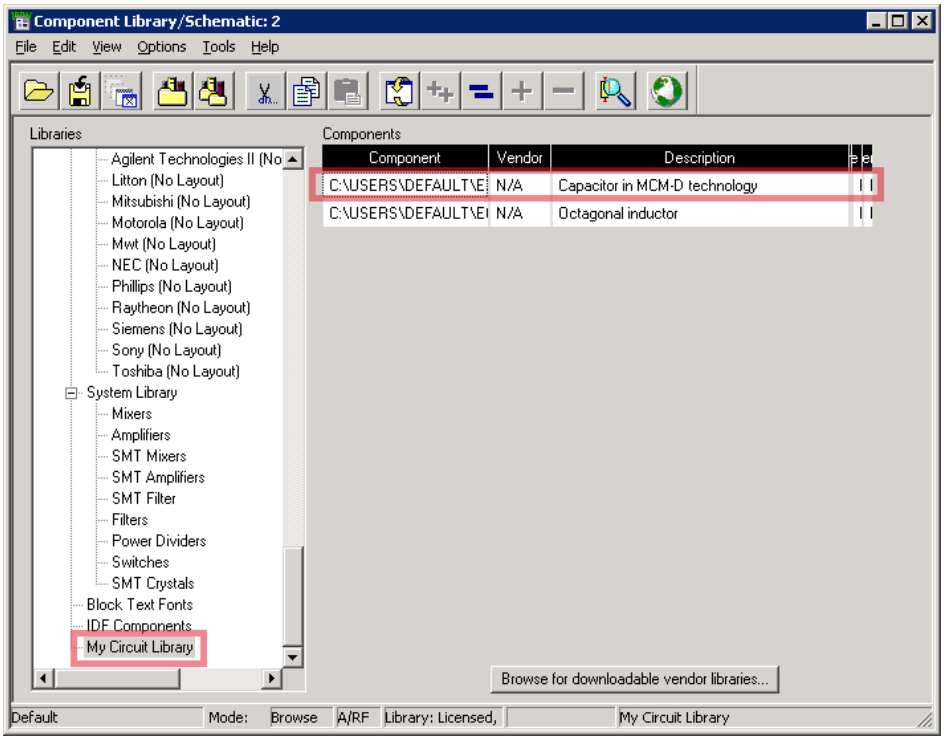

Figure 6.8: View of ADS Component Library window in schematic showing user-compiled models.

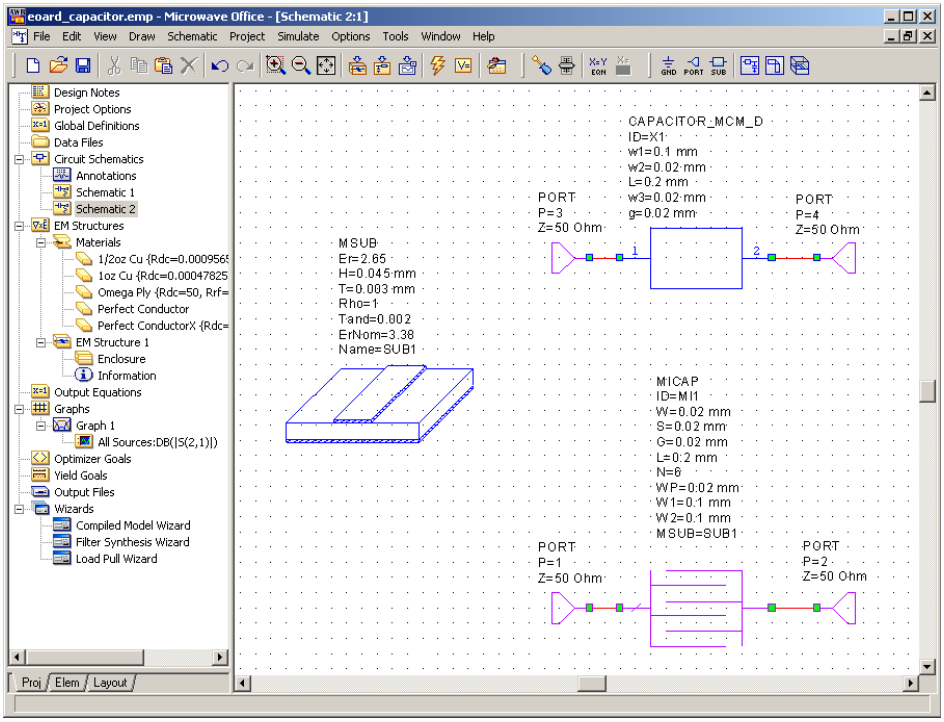

Figure 6.9: MCM-D capacitor integrated with Microwave Office circuit simulator.

Table 6.4: BGA example: Accuracy comparison of non-passive rational model and result of passivity enforcement

Error [dB]	Rational model	Passive circuit
Δ_{max}	-40.8	-32.0
Δ_{mean}	-70.1	-56.7
E_{RMS}	-114.1	-98.4

Table 6.5: BGA example: Location of poles before and after passivity enforcement

Poles	Non-passive	Passive
p_1	-0.0978	-0.1023
p_2	-8.3281	-8.4042
p_3	-24.3026 + 4.9986i	-24.6404 + 5.1439i
p_4	-24.3026 - 4.9986i	-24.6404 - 5.1439i
p_5	-58.1730 +61.7147i	-59.2346 +62.3010i
p_6	-58.1730 -61.7147i	-59.2346 -62.3010i

6.3 Passive equivalent circuits

In this section a few advanced examples are shown that illustrate the versatility of the technique of equivalent circuit construction. The presented structures are very complex not only from a physical point of view, but also show complex responses. To represent their transfer functions the state-space representation must have hundreds of states. This fact disqualifies some techniques, like convex optimization or filter theory approaches, which are not capable of dealing with such big problems. The extended version of Hamiltonian based technique presented in [45] allows one to handle large macromodels, however it is based on sparse-matrix theory and, in result, is difficult to implement.

6.3.1 BGA package

The Ball Grid Array (BGA) package was developed out of the need to have a more robust and convenient package for integrated circuits with large numbers of pins. The conventional quad flat pack style packages had very thin and close spaced pins, and these were very easy to damage. In the BGA the pins are placed in a grid pattern (hence the name Ball Grid Array) on the surface of the chip carrier. Also, rather than having pins to provide the connectivity, pads with balls of solder are used as the method of connection. On the printed circuit board (PCB), onto which the BGA device is to be fitted, there is a matching set of copper pads to provide the required connectivity.

Figures 6.10 and 6.11 show a ball grid array (BGA) package with 96 pins. The package was simulated with the Agilent Momentum RF electromagnetic simulator over the frequency range from DC up to 10GHz. The package structure and localization of the package ports are presented in Fig. 6.12.

The passivity enforcement technique described above can be obviously used to create a passive equivalent circuit of the device directly from simulation results. It is an important

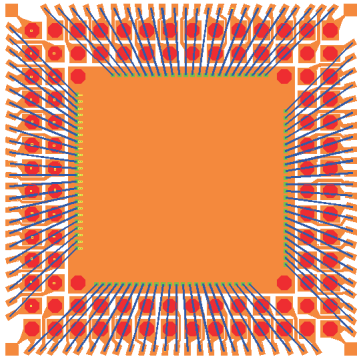

Figure 6.10: Two-dimensional view of 96-pin BGA package

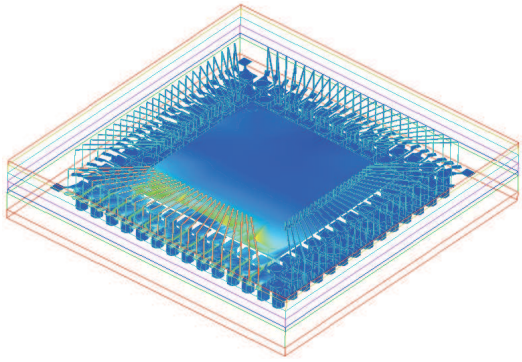

Figure 6.11: Three-dimensional view of 96-pin BGA package

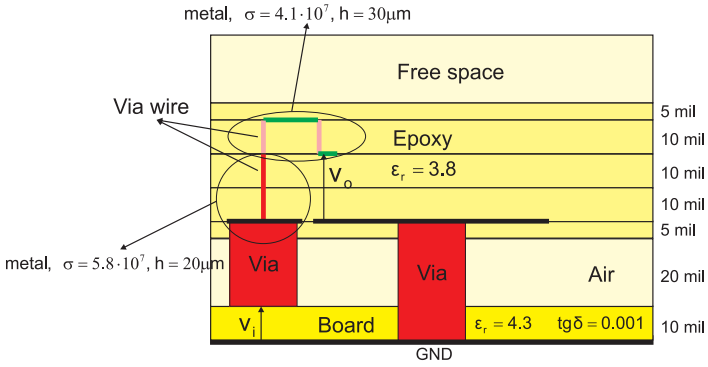

Figure 6.12: Cross-section of BGA package as simulated in ADS Momentum.

issue, because in several cases the rational representation of a device response derived from passive data might became non-passive.

The rational model of the response of 1/4 the device (one side of the package) was created. Despite the input data being passive, the resulting rational model was not, as shown in Fig. 6.14. To create the passive equivalent circuit of the package the proposed technique that preserves the frequency domain response was utilized.

Figure 6.13 shows the comparison of the results of electromagnetic simulation of the package and the response of the equivalent circuit with enforced passivity. The accuracy tests details are presented in Table 6.4. Good agreement between both responses can be observed. Additionally in Table 6.5 the locations of poles of non-passive and passive models are shown. It can be seen that proposed technique slightly shifted the poles to the left of the complex plane. At the same time the imaginary parts of the poles were shifted to ensure the minimal distortion of frequency response.

The created equivalent circuit of the 1/4 of BGA package maintains its validity up to 10GHz and is guaranteed to be passive for every frequency. It can be used for the estimation of the crosstalk between selected pins of the package, or time domain simulation of a whole chip that takes into consideration the performance of the BGA package.

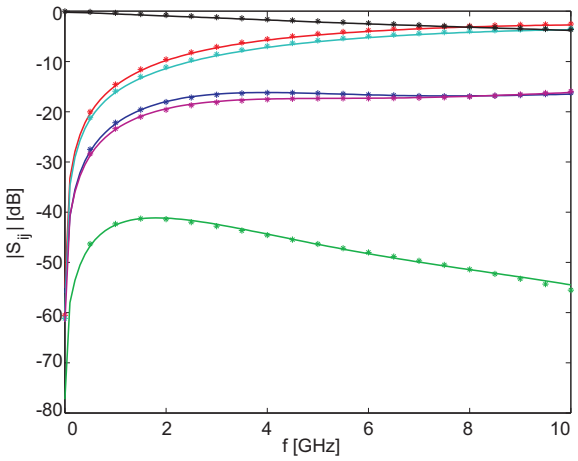

Figure 6.13: BGA example: Comparison of scattering parameters before and after passivity enforcement

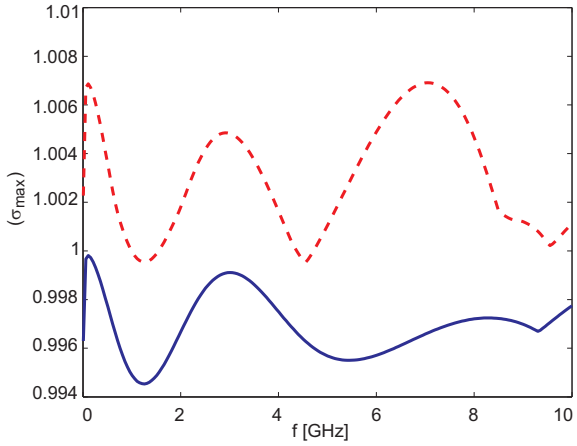

Figure 6.14: BGA example: Maximum singular value of scattering matrix before and after passivity enforcement

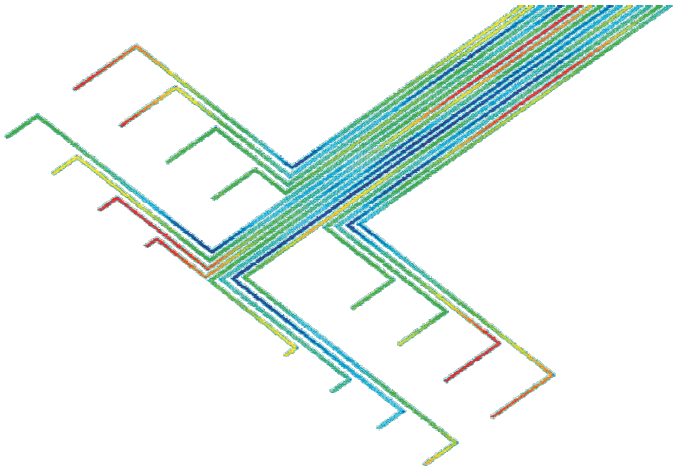

Figure 6.15: 3D overview of printed circuit board lines as simulated in ADS Momentum.

6.3.2 Printed Circuit Board lines

Transmission lines between various system components are often realized as printed circuit board (PCB) connections. In high-speed digital networks the quality of the PCB design can determine the success of the entire system. A designer has to take into account as many parasitic effects as possible. The crucial element of system design is signal integrity analysis, which allows one to verify the functioning of a system as a whole. At this stage, crucial system elements have to be represented in a form suitable for time-domain simulation. A possible solution is to use the presented technique to construct a passive equivalent circuit of main PCB transmission lines.

For a sake of an example, a structure of 16 coupled PCB lines on the FR4 substrate (32-port device) was analyzed with ADS Momentum in the frequency band DC-2GHz with 25MHz frequency step. The length of the lines is 130*mm*. The structure overview is presented in Fig. 6.15.

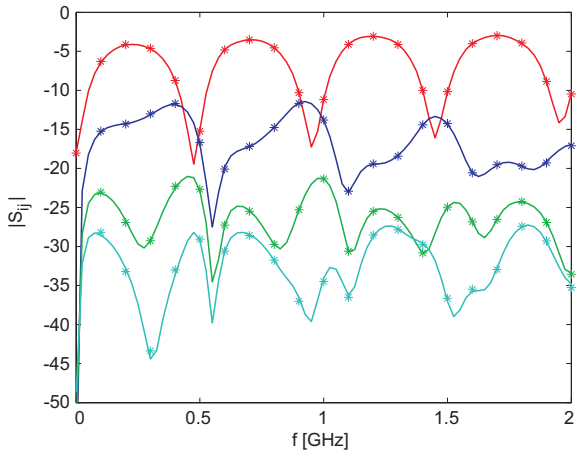

Figure 6.16: PCB example: Comparison of selected scattering parameters before and after passivity enforcement

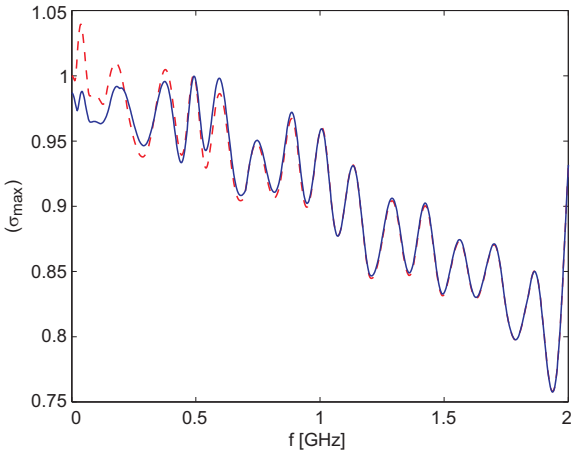

Figure 6.17: PCB example: Maximum singular value of scattering matrix before and after passivity enforcement

Table 6.6: PCB example: Accuracy comparison of non-passive rational model and result of passivity enforcement

Error [dB]	Rational model	Passive circuit
Δ_{max}	-33.0	-32.5
Δ_{mean}	-62.0	-59.8
E_{RMS}	-106.3	-103.9

The resulting scattering parameters were fitted with the vector fitting technique to the rational representation with $M = 30$ poles, which took about 6 hours on 1,5GHz laptop PC. In this case, the state-space representation has 960 states. The model is not passive in frequency bands: DC-1.86MHz, 16.1MHz-60.4MHz, 153.9MHz-200MHz, 363MHz-390MHz, 488MHz-493MHz. The plot of maximum singular value (BR test) is shown in Fig. 6.17.

The results of the passivity enforcement are shown in Fig. 6.16 and Table 6.6 shows a comparison of accuracy of the non-passive and passive model. The perturbation of the poles introduced very small modification of the response. The time of the passivity enforcement was 15 min on the same PC (Matlab implementation of the technique).

6.3.3 SPICE networks from measurements

Applications of modern digital systems are dedicated to a fast processing of digital data (audio/video data streams) or high speed data transmission. Such applications enforce increase of bandwidth of transmitted signals and parasitic effects have to be taken into account to a obtain successful design. At the same time the complexity of circuits increases because of high integration of structures. With a rapid increase of complexity of modern devices also new tools for electromagnetic simulation of circuits are being developed. However, in many cases the structure complexity is so high that even the increase of processing power of computers is not sufficient to perform a successful simulation in a reasonable time. The solution for that is to set up a measurement environment and observe the electric performance of the

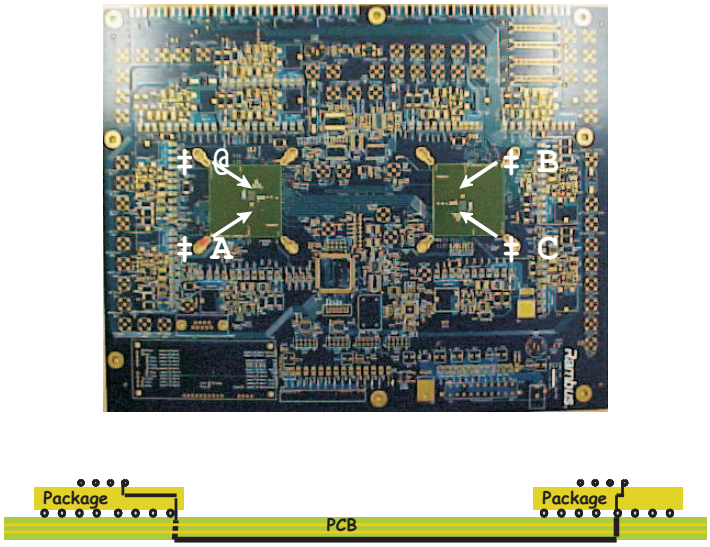

Figure 6.18: RAMBUS processor bus structure overview.

Table 6.7: RAMBUS example: Accuracy comparison of non-passive rational model and result of passivity enforcement

Error [dB]	Rational model	Passive circuit
Δ_{max}	−27.4	−27.4
Δ_{mean}	−45.7	−45.5
E_{RMS}	−81.9	−81.7

circuit. The measurement results (for example scattering parameters) can then be directly incorporated into a circuit simulator as frequency domain data. To convert the data into a passive equivalent circuit (SPICE compatible) one can apply the procedure described above. Such a procedure is very useful, because it allows one to generate a passive equivalent circuit based on measured data which can be directly used for time-domain analysis. The created model, that includes all the parasitic effects, can then be used to perform the final simulation of the system (signal integrity analysis).

6.3.3.1 RAMBUS FlexIO processor bus

Processor bus design and realization are critical for system operation. The bus plays a central role, both inside the chip, where a bus connects the CPU to a controllers, and external to the chip, where busses connect a device to external peripherals. The RAMBUS FlexIO[1] processor bus is a chip-to-chip interface technology that offers signal bandwidth of 400 MHz up to 8.0 GHz. It is dedicated to intra-board processor, chipset and networking parallel connections in consumer electronics (game consoles and HDTV), computing (PC) and networking (routers and switches).

An example structure of the FlexIO bus is presented in Fig. 6.18. The channel consists of

[1]Measurements results and pictures courtesy of W.T. Beyene from RAMBUS Inc.

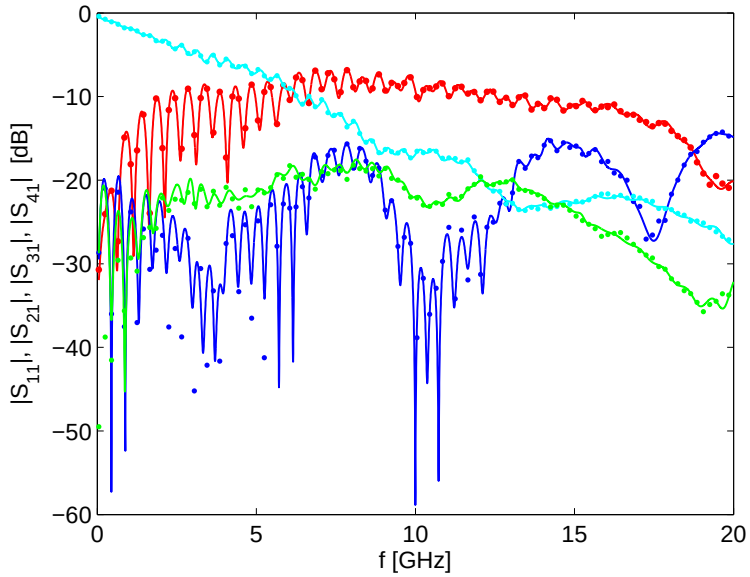

Figure 6.19: Input data (···) and response of passive equivalent circuit created with proposed technique (—) of RAMBUS FlexIO channel.

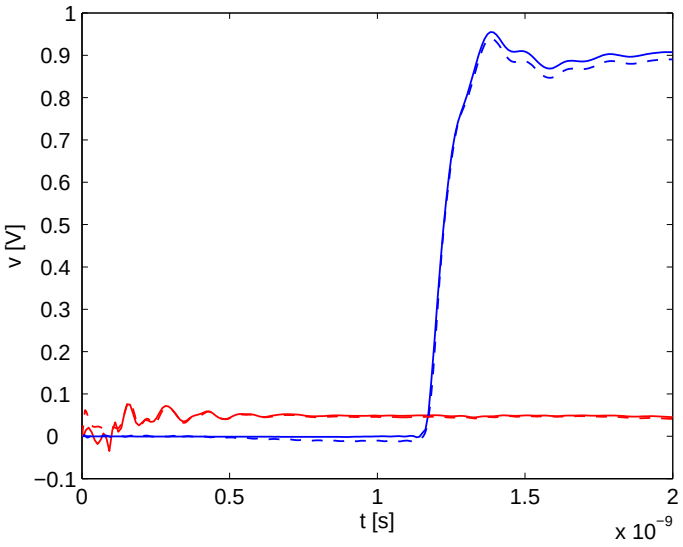

Figure 6.20: Time domain simulation results: (—) convolution technique, (- - -) passive SPICE network

two 12 inches long meandered lines made on the FR4 PCB substrate and two PCB/package vias [17]. Because of the complexity of the structure making it hard to simulate with an electromagnetic solver, the performance of the design has to be verified by the measurements. It is highly recommended to include the measurement data to a circuit simulator (like SPICE) for further simulation of the device and signal integrity analysis. With the proposed scheme, the passive equivalent circuit of the bus can be created from measured frequency domain

data.

4-port measurements of scattering parameters of FlexIO bus were performed in the band 50MHz - 20GHz and the DC parameters were obtained from a simulation of the structure in ADS Momentum. The whole set of data was used to generate a rational representation of the scattering parameters using the Modified Vector Fitting (MVF) technique [47]. Due to high complexity of the device and the parasitic effects (like ringing) the order of the function has to be very high (M=100 poles). The rational model turned out to be not passive in the frequency range 58MHz-157MHz and 188MHz-237MHz. The proposed technique was utilized to restore the passivity of the model, which took 5 minutes on 1,5GHz laptop PC. The number of states in state-space representation was 400.

The comparison of the input data and the final passive model is shown in Fig. 6.19 and summarized in Table 6.7. Presented results prove that even for high-complexity circuits, such as FlexIO channel, it is possible to construct a passive SPICE-compatible circuit, which can be useful in further analysis of the devices that use the measured structure. For example, Fig. 6.20 shows a comparison of the structure time-domain response calculated with the convolution technique and using time-domain simulation in SPICE. The circuit was excited with voltage pulse 1V with rise time 10ps. The picture shows good agreement between the responses. A small difference between traces is mainly caused by the accuracy of the rational model. The responses of non-passive and passive rational models are indistinguishable.

6.4 Parameterized passive equivalent circuits

In Chapter 3 the approach of multivariate surrogate model construction was presented. The time of computing of the surrogate model response is insignificant compared to the time required by a EM solver. The drawback of surrogates is the lack of passivity of computed response, especially in the case of complex models. However, the surrogate model can be combined with techniques of equivalent circuit construction discussed in Chapter 4. As a result one can create create a parameterized passive SPICE network from the response of surrogate models. Two cases are possible: parameterized physical equivalent circuits and parameterized realizations of transfer functions. In the latter case one can use the techniques of passivity enforcements that were described in Chapter 5 to assure the passivity of the circuit. However, if the passivity violation is strong and one of the previously reported passivity enforcement techniques is applied, the corrected model may have disturbed frequency response, as it was shown in the same chapter (sec. 5.4.2).

The technique of passivity enforcement presented in this work allows one to create a passive circuit from data with disturbed passivity and, at the same time, preserving the frequency response. Combining this technique with surrogate models one obtains a parameterized SPICE network with guaranteed passivity. Such circuits can be useful in many applications, such as analysis and tuning of RFIC devices on post-layout stage of design.

The scheme of construction of parameterized surrogate models with guaranteed passivity is depicted in Fig. 6.21. For a specific structure, a parameterized surrogate model is created. The response of the model is then used to construct an equivalent circuit of the device in a form of a physical (RLC) circuit or by realization of its rational representation. In the second

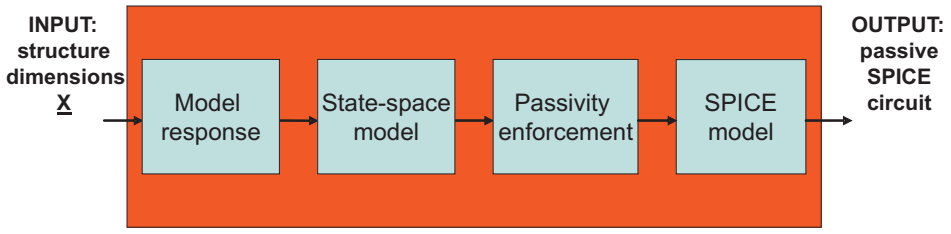

Figure 6.21: Proposed technique of construction of parameterized passive SPICE networks.

case, a rational model of the response of surrogate model is used as an input to the passivity enforcement routine. Once the passivity of the model has been restored, the rational model can be realized as a lumped equivalent circuit. It has to be noted that the accuracy of the equivalent circuit is affected by two sources of errors:

- the error of the surrogate model itself,
- the perturbation of the model response during the passivity enforcement.

It is impossible to estimate a-priori the influence of both elements on the final circuit. However, one may expect the more accurate the parameterized model is, the more accurate final equivalent circuit is, as the passivity violation of a high accuracy surrogate model is smaller.

In this section two examples are shown to illustrate the idea and to indicate possible ways of using of such parameterized circuits.

6.4.1 Parameterized physical equivalent circuit of integrated inductor

A parameterized surrogate model of the integrated inductor on BiCMOS presented in section 6.1.1 was used to evaluate the scattering parameters of the inductor for its various geometric dimensions. The model response was then used to extract an equivalent circuit of the inductor using RLC circuit structure and parameter extraction technique described in section 4.2. Table 6.8 shows the accuracy of the extracted equivalent circuit for various geometric dimensions of the inductor. The plots of the scattering parameters are shown in Fig. 6.22. It can be seen that the accuracy of the extracted circuits is very high. Table 6.9 shows the comparison of values of extracted elements in the case of the model and the electromagnetic response. The inductor dimensions were set as R = 70μm, w = 12μm and s = 5μm. The results show a very good agreement.

The time of response computation of parameterized model at 21 frequency points is 0.4s, the estimated mean time of optimization of elements of physical equivalent circuit is 3s (1.6 GHz PC). As a result, the total time of extraction of accurate equivalent circuit for given dimensions of the inductor is below 4s. It is extremely fast, comparing to the time of electromagnetic simulation (few minutes for a single frequency point).

It is worth to notice, that incorporation of surrogate models with a fast parameter extraction scheme results in a parameterized physical equivalent circuit. The technique presented in this example can be then introduced to any device that can be described by a compact, lumped, RLC equivalent circuit.

Table 6.8: Accuracy of extracted substrate-coupled equivalent circuit of an inductor for different structure dimensions

R [μm]	w [μm]	s [μm]	$E_{RMS}^{S_{11}}$ [dB]	$E_{RMS}^{S_{21}}$ [dB]
40	10	5	-55.6	-58.1
60	10	10	-88.5	-80.5
70	12	5	-87.8	-84.1
80	10	5	-84.7	-85.2
90	15	5	-86.3	-84.9
90	20	15	-73.6	-71.2

Table 6.9: Comparison of equivalent circuit elements extracted from model response and electromagnetic simulation

Element	EM	Model
L_s [nH]	2.033	2.030
R_s [Ω]	144	146.8
C_s [fF]	3.1	3.0
C_{ox1} [fF]	76	81
C_{ox2} [fF]	76	70
R_{si1} [Ω]	579	621
R_{si2} [Ω]	606	567
C_{si1} [fF]	23.7	22.6
C_{si2} [fF]	17.2	18.6
L_{sub} [nH]	0.562	0.554
R_{sub} [Ω]	4.2	22
L_{sk} [nH]	0.913	0.792
R_{sk} [Ω]	5.2	4.4
M	1	1

6.4.2 RF application

If a physical circuit involves only RLC elements, passivity enforcement is not needed. To show the application of the technique with passivity enforcement, a microwave filtering structure made in MCM-D technology was analyzed with the application of models created with adaptive multivariate rational interpolation scheme, described in section 3.4.3.

In Figure 6.23a) the original non-passive surrogate model response, the rational approximation obtained with vector fitting and the result of passivity enforcement are presented. The order of rational interpolation used is M=14. To correct the passivity only the locations of poles were perturbed and it took 3.4 seconds to find the solution of the optimization problem. Fig. 6.23 presents the frequency sweep of the maximum singular value of the scattering matrix before and after the passivity correction. For comparison, Fig. 6.23a) shows also the

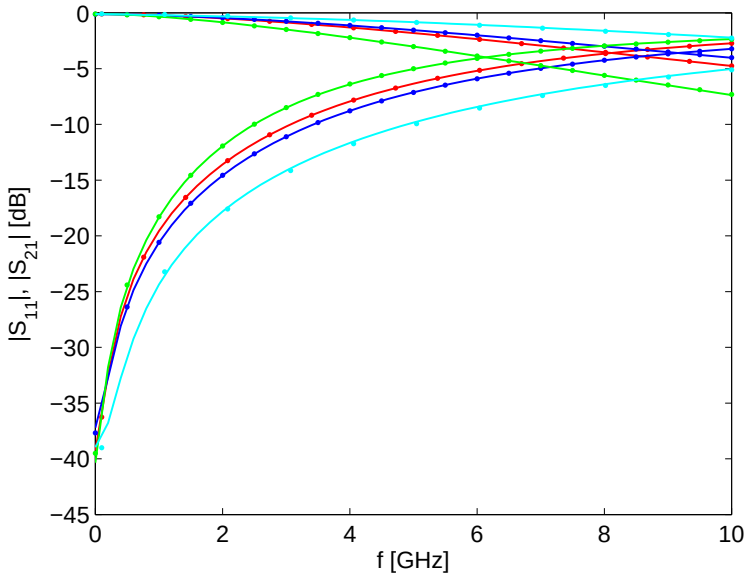

Figure 6.22: Comparison of parameterized equivalent circuit response and electromagnetic simulator: (– – –) R = 70μm, w = 12μm, s = 5μm, (– – –) R = 60μm, w = 10μm, s = 10μm, (– – –) R = 90μm, w = 20μm, s = 15μm, (– – –) R = 40μm, w = 10μm, s = 5μm.

Table 6.10: Accuracy of the developed parameterized equivalent circuit of filtering structure compared to models response from ADS circuit simulator (all errors in decibels).

Structure dimensions [mm]							Non-passive		Passive		ADS built-in	
w_0	w_1	w_2	w_3	L_1	L_2	L_3	$E_{RMS}^{S_{11}}$	$E_{RMS}^{S_{21}}$	$E_{RMS}^{S_{11}}$	$E_{RMS}^{S_{21}}$	$E_{RMS}^{S_{11}}$	$E_{RMS}^{S_{21}}$
0.13	0.1	0.15	0.1	1.5	2	2	-55.7	-50.8	-53.0	-48.8	-40.8	-42.2
0.18	0.1	0.15	0.2	1.5	1.5	1.8	-52.9	-51.4	-52.7	-48.6	-37.3	-36.7
0.1	0.05	0.05	0.1	2.5	2	2	-47.6	-47.0	-46.7	-47.5	-35.8	-37.1
0.157	0.1	0.1	0.1	2	2	2	-53.1	-49.7	-53.0	-50.0	-37.3	-35.7
0.157	0.157	0.05	0.2	2.5	1.3	1	-53.1	-49.0	-51.8	-49.9	-37.1	-44.2

results obtained using alternative passivity enforcement technique presented in [43]. While the method of [43] gives a passive model, its response differs from original frequency domain data. The presented approach creates a passive macromodel with better quality in the frequency domain. The difference between the original and corrected response is almost indistinguishable. In Table 6.10 comparison of errors of the non-passive, passive and built-in ADS model responses for different structure dimensions are presented. It can be seen, that in each case the proposed scheme gives one a models with accuracy higher than in the case of models included in ADS circuit simulator.

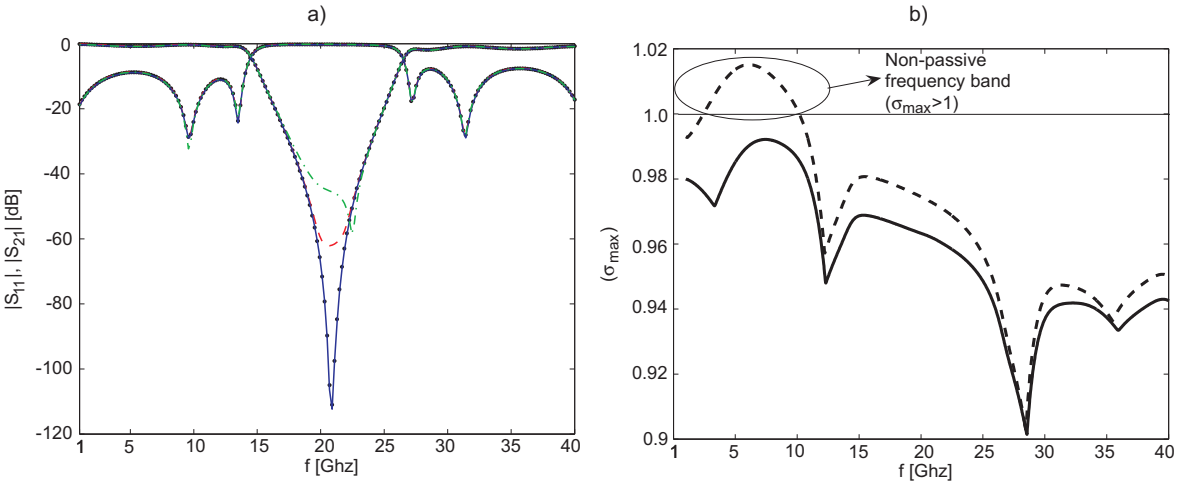

Figure 6.23: RF application: a) results of passivity enforcement: ··· original non-passive data, - - rational model obtained with VF, – . – result of the technique described in [43], — result of the proposed technique, b) Maximum singular value of scattering matrix of non-passive (···) and corrected (–) model.

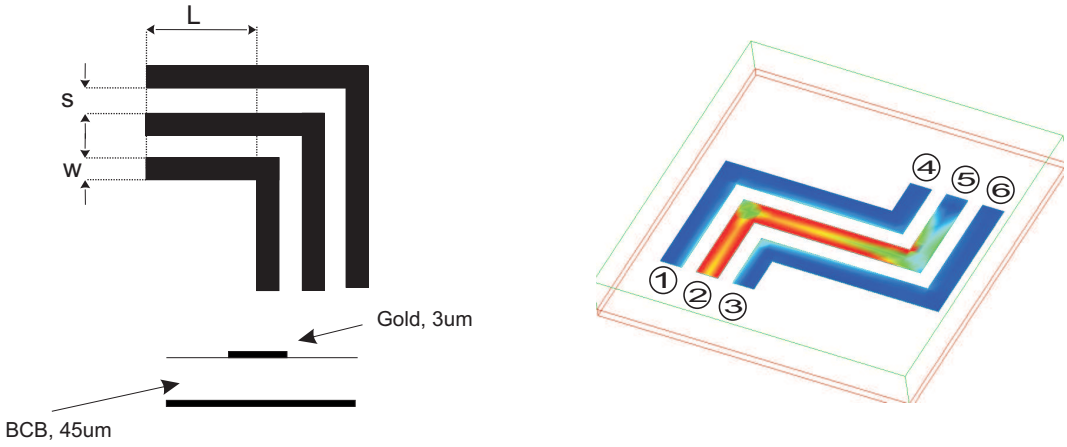

Figure 6.24: Basic three conductor line bend (left) and double-bend interconnect structure (right).

6.4.3 Interconnect application

An area where parameterized SPICE circuits can be applied is the design of mixed analog-digital circuits and interconnects. Accurate modelling of the interconnect circuits, including frequency dependent effects, is one of the most researched problems in RF circuit design [2, 82, 105].

Let us consider a three conductor microstrip line bend on thin-film MCM-D substrate, as shown in Fig. 6.24. A four variate surrogate model of scattering parameters of the structure was created using technique described in this thesis. The reference response of the structure was computed using the Agilent ADS Momentum electromagnetic simulator. The range of model parameters is presented in Table 6.11.

The resulting model was applied to compute the response of a double-bend of a multi-conductor line as shown in Fig. 6.24. Then a passive SPICE circuit was created for different structure dimensions applying the technique proposed in this thesis. The rational model

Table 6.11: Interconnect application: range of model parameters

Parameter	Min. value	Max. value
Frequency [GHz]	0	20
Strip width w [mm]	0.05	0.2
Gap width s [mm]	0.05	0.15
Line length L [mm]	0.1	0.3

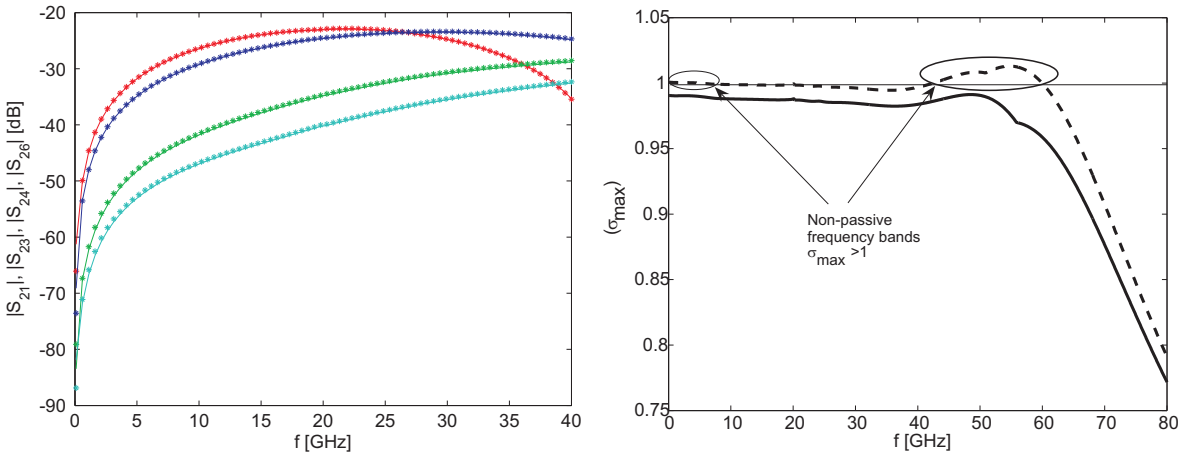

Figure 6.25: Frequency response of non-passive (solid) and passive (dotted) model and maximum singular value of scattering matrix of non-passive (···) and corrected (–) model.

Table 6.12: Accuracy of the developed parameterized equivalent circuit of double-bend structure (all errors in decibels) compared to electromagnetic response.

Structure dimensions [mm]			Non-passive			Passive		
w	s	L	Δ_{max}	Δ_{mean}	E_{RMS}	Δ_{max}	Δ_{mean}	E_{RMS}
0.12	0.05	0.25	-55.48	-70.52	-99.40	-56.20	-70.04	-99.23
0.10	0.10	0.20	-56.15	-71.05	-99.39	-56.80	-70.69	-99.00
0.20	0.15	0.25	-54.20	-72.13	-98.97	-52.85	-67.51	-94.49
0.07	0.05	0.25	-48.64	-63.23	-91.91	-47.01	-60.56	-89.41
0.07	0.07	0.10	-47.86	-68.67	-95.43	-41.28	-54.17	-81.81
0.15	0.15	0.20	-52.27	-71.25	-97.04	-34.04	-52.79	-77.64

order was M=10 and the state-space model had 60 states. The accuracy of the resulting passive circuits for different structure dimensions is shown in Tab. 6.12. The accuracy of the equivalent circuit varies with the change of the structure dimensions, on the other hand the accuracy achieved is high enough to use the models in a real-life design. Fig. 6.25 shows the response of the model for fixed dimensions (dimensions $w = 0.12$mm, $s = 0.05$mm and $L = 0.3$mm) before and after passivity enforcement. The total time of the passive SPICE model construction for the specified structure dimensions is a few seconds on a 1,6GHz PC.

The created passive SPICE network can be now utilized for various types of analyses. For

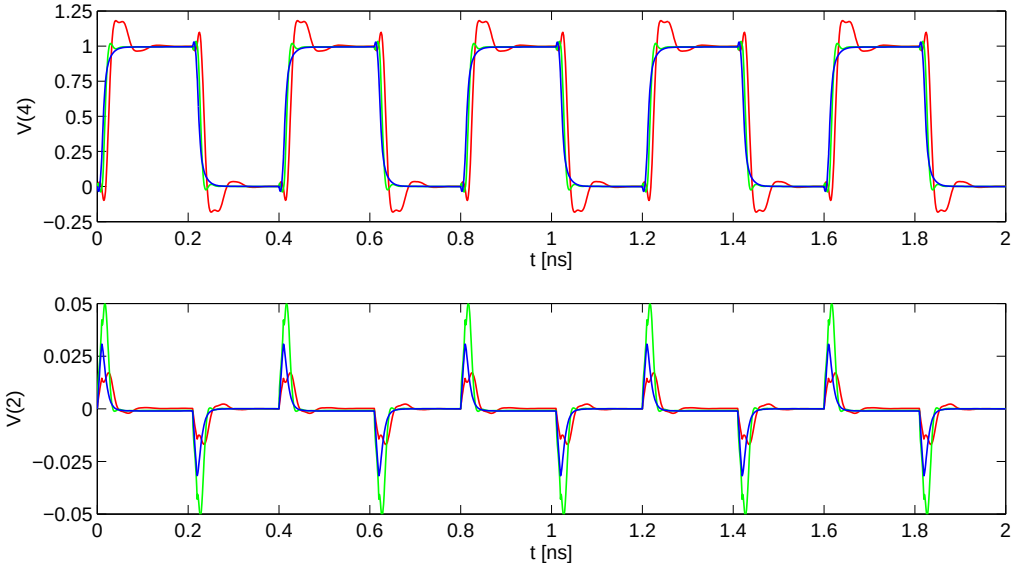

Figure 6.26: Time domain analysis of parameterized equivalent circuit of double-bend MCM-D structure for different structure dimensions: (—) $w = 20\mu m$, $s = 15\mu m$, $L = 30\mu m$, (—) $w = 12\mu m$, $s = 5\mu m$, $L = 25\mu m$, (—) $w = 7\mu m$, $s = 7\mu m$, $L = 10\mu m$.

example, one can estimate crosstalk between strips for excitation with voltage pulse source (digital circuit) for different structure dimensions. Fig. 6.26 shows time-domain voltage waveforms collected form ports 2 and 4 of double-bend structure for various dimensions when port 1 is excited with pulse voltage source (pulse period 0.4ns, time on 0.2ns, rise/fall time 10ps).

Without surrogate models and fast passivity enforcement technique, the parametric analysis of cross-talk effect in this structure would require full-wave simulations (using e.g. FDTD solver) every time the dimensions have changed.

6.5 Automated design of microwave components

The design-by-optimization philosophy has became recently popular [10, 27, 54, 100, 133]. In this approach dimensions of the designs are computed in an automated way using optimization routines with suitably defined cost functions. A common factor of all optimization based approaches is multiple evaluation of cost function, which often must be done hundreds or thousands times. It is obvious, that straight incorporation of an electromagnetic solver makes the time of optimization long. Usually it takes hours or days to find an acceptable solution.

Using the techniques of surrogate modelling one can create a library of models made in various technologies, e.g. waveguide, microstrip, coplanar or multilayer. The computation of model response is very fast, therefore they are suitable for design-by-optimization methods. The responses of models can be very close to the results of an electromagnetic solver,

therefore, the design usually requires only a small tuning to fulfill the requirements.

Using the automated design techniques, a designer has to provide only the knowledge about structure geometry that is able to realize the requested transfer function. Most of the techniques involve cost functions based on direct comparison of reference, ideal response and response of structure being optimized [10, 32]. More advanced solutions use more complex cost functions, like zero-pole based technique presented in [36, 59] suitable for filter design.

To show the efficiency of the design-by-optimization approach and accuracy of surrogate models created using adaptive multivariate rational scheme a few design examples are presented below. In all examples the design is automatic and takes very short time. Most examples involves filters. Filters are a good example to illustrate the importance of fast and robust automated design procedure. Many applications (e.g. UMTS, GSM) require filters with generalized Chebyshev response (i.e. finite, real and/or complex transmission zeros). Modern, narrow-band filter structures involve complex shaped, high quality cavities. To successfully perform a design all the field effects have to be taken into account, with enforces the application of electromagnetic simulators. That is why a complete filter design cycle may take several weeks or months.

6.5.1 Waveguide filter with dispersive stubs

The first example is a 5-th order microwave filter with two dispersive stubs and generalized Chebyshev response shown in Fig. 6.27 [6]. The standard design procedure is based on the classical inverter approach of direct-coupled bandpass filters. In this approach, the inverters are frequency invariant, therefore the procedure is modified to ensure the proper inverter value in the filter passband and enforce the location of the transmission zeros in stopband. Such a procedure gives one a very coarse initial dimensions of the structure, which have to be then optimized to fit the filter response to design requirements. As an alternative to the classic approach, one can apply the automated technique using an optimization scheme based on zeros and poles of transmission and reflection functions described in [59]. The optimization algorithm uses a cost function in form:

$$C = \sum_{i=1}^{M} \|(Z_i - Z_i^{'})\|^2 + \sum_{i=1}^{M} \|(P_i - P_i^{'})\|^2 \tag{6.2}$$

where P_i (Z_i) are the roots of denominator (numerator) of ideal, Chebyshev transfer function and $P_i^{'}$ $(Z_i^{'})$ are the roots of the denominator (numerator) of filter's response rational approximation.

For the purpose of design, the structure was divided into separate discontinuities that have been modelled using the proposed approach. Two structures were modelled: a stub and an iris. The range of the input parameters in the case of the stub is: frequency $f \in (10GHz - 12GHz)$, stub length $l \in (36mm - 46mm)$ and width $d \in (12mm - 19mm)$. The iris was considered having the parameters: frequency $f \in (10GHz - 13GHz)$, iris width $l \in (3mm - 9mm)$ and length $d \in (0.5mm - 8mm)$. Scattering parameters S_{11} and S_{21} were modelled with the same accuracy tolerance ε_0=-60dB.

The models were then used for design of the filter with the following specification: return loss 20dB in passband 11GHz-11.2GHz and two transmission zeros at 10.88GHz and

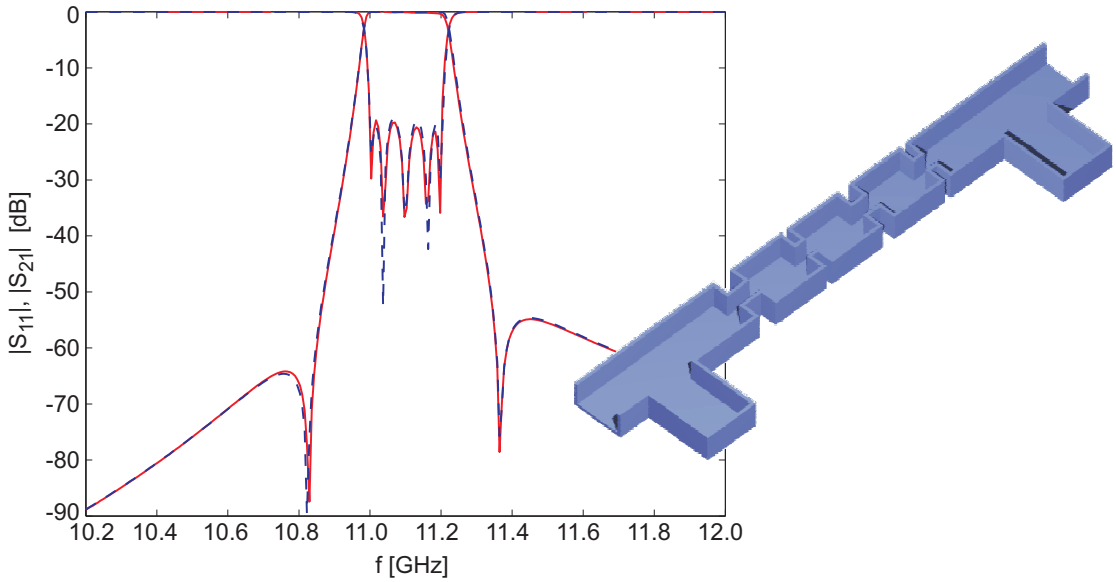

Figure 6.27: Waveguide filter structure and the comparison of model response with the results of electromagnetic simulator (mode-matching).

11.32GHz. The optimization-based technique presented in [59] was used. All 17 variables that fully describe the filter dimensions were optimized. A random set of dimensions was used as a starting point. The optimization of the structure took 500s on 1.6GHz PC.

Figure 6.27 shows a comparison of the model and electromagnetic (mode-matching) responses of the optimized structure. In can be seen that the filter response based on the the models is very accurate. What is important, it takes 0.01s to evaluate the response of the filter at a single frequency point using surrogate models, compared to 0.6s in the case of mode-matching simulation. It gives the speed-up about 60 times without noticeable loss of accuracy. If a full wave solver was used for automated filter design, the design cycle would last about 8 hours.

6.5.2 Dual-mode filter design

Most of applications of surrogate models are limited to fundamental mode response. However, in many cases the signal is transferred by higher order modes. Therefore they also have to be taken into account to get a proper simulation result. In some applications, the presence of higher order modes is even required. In [75] it was shown that the technique of surrogate models construction can be also applied for scattering parameters connected to higher-order modes.

In Figure 6.6 the structure of 4-th order microwave dual-mode filter is shown. The filter exploits a dual-mode cavity which operates with modes TE_{102} and TE_{201} [46]. The standard design procedure involves the separate design of dual-mode cavities, which are then cascaded and the whole structure is optimized using the electromagnetic simulator [46]. The procedure takes several steps and is hard to automate.

To automatically design the filter, using only electrical specification as a starting data,

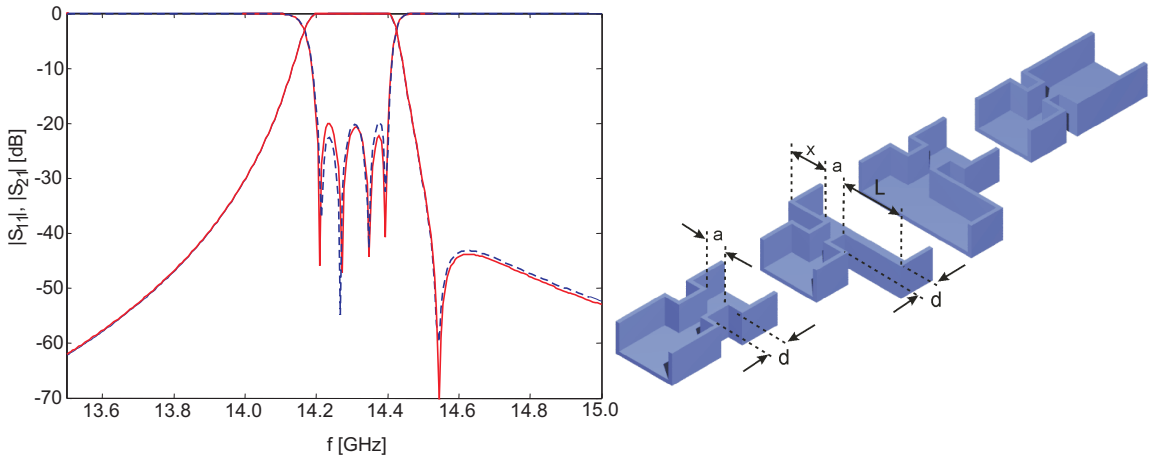

Figure 6.28: Accuracy comparison and the structure of 4-th order dual mode filter design

the structure is partitioned into two separate discontinuities: a symmetric inductive iris and a transition between the input waveguide and the dual-mode cavity. The discontinuities were again simulated using mode-matching technique. The response of each discontinuity was modelled as multivariate rational function. In the case of the iris the fundamental mode response S_{21} and S_{11} was modelled within model domain: frequency $f \in (13GHz - 15GHz)$, iris width $a \in (6mm - 14mm)$ and iris thickness $d \in (1mm - 10mm)$. The maximum absolute error of the models is below -50dB and the number of support points is 101. The model of the waveguide transition was created as a two-mode model (TE_{10} and TE_{20}). In this case the scattering matrix has size 4×4 with 10 unique elements. The model domain was: frequency $f \in (13GHz - 15GHz)$, iris width $a_1 \in (5mm - 12mm)$, wider waveguide width $a_2 \in (24mm - 29mm)$ and iris shift $x \in (2mm - 7mm)$. Iris thickness was set as $d = 2mm$. At first the model of the S_{11} parameter of the fundamental mode was created. With 202 support point the accuracy of the model reached -55dB. The resulting set of support point was then used to build the remaining 9 models. For each model, the set of support points was appended using an adaptive sampling technique. In summary, to build all 9 models with similar accuracy, 90 points were appended to the initial set.

The models, were then used for design of a dual-mode filter. With the mode-matching technique the evaluation of the filter response at a single frequency point takes 0.68s, while the application of surrogate models reduces the time to 0.02s, which gives 34 speed-up of computation. As in the previous example the models were used for optimization of the filter with the technique described in [59]. In this case the filter specification is 20dB return loss in passband 14.2GHz-14.4GHz and one transmission zero on 14.55GHz. The optimization lasted 4min on 1.6GHz PC. Again random dimensions were used as a starting point.

The results are presented in Fig. 6.28. It is seen that the filter's response based on the models is very close comparing to EM simulations. The average time of the filter optimization starting from random filter dimensions was 4 min using surrogate models comparing to over 2h in the case of electromagnetic analysis. This shows the advantage of application of the surrogate models over full-wave simulations.

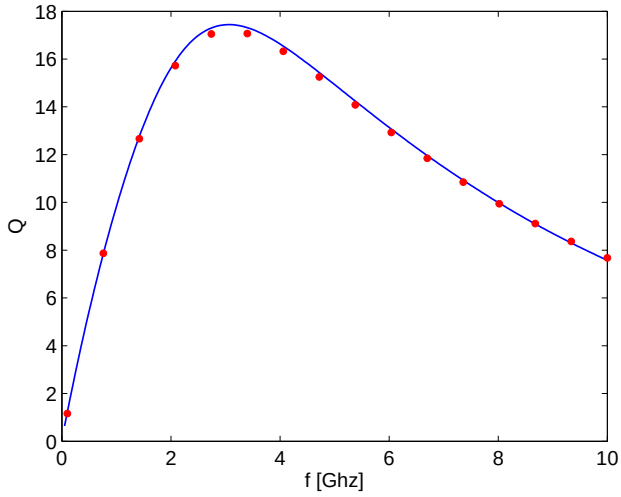

Figure 6.29: Q-factor comparison between model (—) and electromagnetic response (···) of optimized inductor.

6.5.3 Inductor design

Design of high Q inductors is one of the problems in on-chip solutions for RF and microwaves. It is a common problem for designers to find an inductor that at frequency f realizes an inductance L_0 and at the same time minimize the inductor's area S and/or maximize the Q. There exist several design rules for inductor with the same value of inductance L_0 and different values of quality factor and size. Several authors have investigated the inductor optimization problem [85, 90, 109, 135]. These authors propose to create a simple closed-form model of inductor parameters, like in [109, 135], but such models are difficult to find for multivariate case.

By transforming the scattering parameters to the corresponding admittance matrix, one can extract the frequency dependent inductance L and quality factor Q of inductor:

$$L(f,\underline{X}) = \frac{1}{2\pi f \cdot Im(Y_{11}(f,\underline{X}))} \tag{6.3}$$

$$Q(f,\underline{X}) = \frac{Re(1/Y_{11}(f,\underline{X}))}{Im(1/Y_{11}(f,\underline{X}))} \tag{6.4}$$

If one uses the model response to evaluate the scattering parameters of inductor, then one gets a parameterized model of the inductor quality factor $Q(f,\underline{X})$ and inductance $L(f,\underline{X})$.

Both parameters, L and Q of an inductor depend on frequency f and dimensions of the structure $\underline{X} = [x_1\ x_2\ \ldots\ x_N]$. The procedure of the inductor search is organized as a simple optimization routine with goal function G defined as:

$$G(f_0,\underline{X}) = \|L(f_0,\underline{X}) - L_0\| - Q(f_0,\underline{X}) + F(\underline{X}) \tag{6.5}$$

where L_0 is a desired inductor inductance at frequency f_0 and $F(\underline{X})$ is a vector valuated function that determines the size of the inductor.

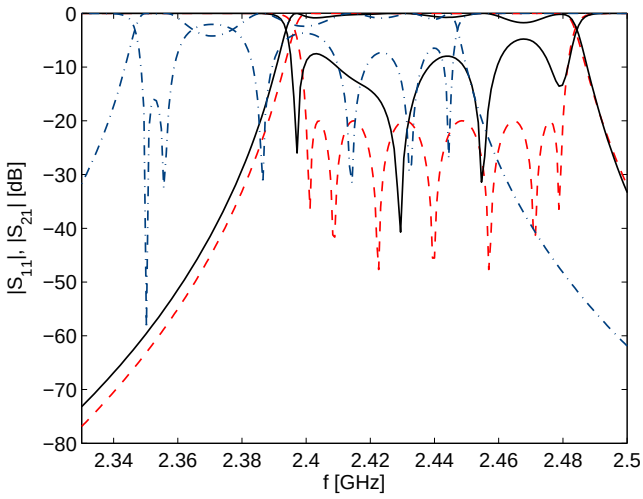

Figure 6.30: 7-th order combline filter synthesis results: (—) synthesis response with application of surrogate models, (-.-) classic synthesis response, (—) optimized filter response

The goal function G has to be minimized over the range of model geometric parameters. The minimum of the goal function gives the value of L as close as possible to the required one and assures the smallest inductor size and the highest Q factor. As an optimization algorithm any gradient based method can be used. Obviously, such a search would be time consuming if an electromagnetic simulator was involved to compute the inductor parameters. The advantage of the surrogate model is thus evident.

To prove the usefulness of the proposed approach, the model of an octagonal inductor was used for automated inductor design by optimization. The requested specification of the inductor was $L_0 = 2$nH at frequency 2.1GHz. The optimized inductor dimensions are: R = 67.5μm, w = 12.1μm and s = 5μm. The comparison of quality factor between model and electromagnetic response is shown in Fig. 6.29. What is important, the total inductor design time was 0.5 seconds. It is extremely fast comparing to the electromagnetic approach since the EM-simulation of the inductor response at a single frequency takes a few minutes.

6.5.4 Automated synthesis of combline filters

The final is an example of a recently developed commercial application which is entirely based on the parameterized, surrogate models of coupling coefficients (sec. 6.1.3). With classic approach of synthesis of inline coupled-resonator filters, all the resonators are adjusted to resonate at the frequency being center of the passband. Then the cavities are modified to introduce the required couplings, which can disturb the resonant frequencies. Since the model involves not only the coupling coefficients, but also the resonant frequencies of loaded cavities, the synthesis scheme involving surrogate models [74] improves the estimation of initial filter dimensions when compared to the classic approach [64,67,74]. The proposed synthesis scheme using surrogate models gives a very good starting point for further final tuning of the design, for example using the technique described in [59].

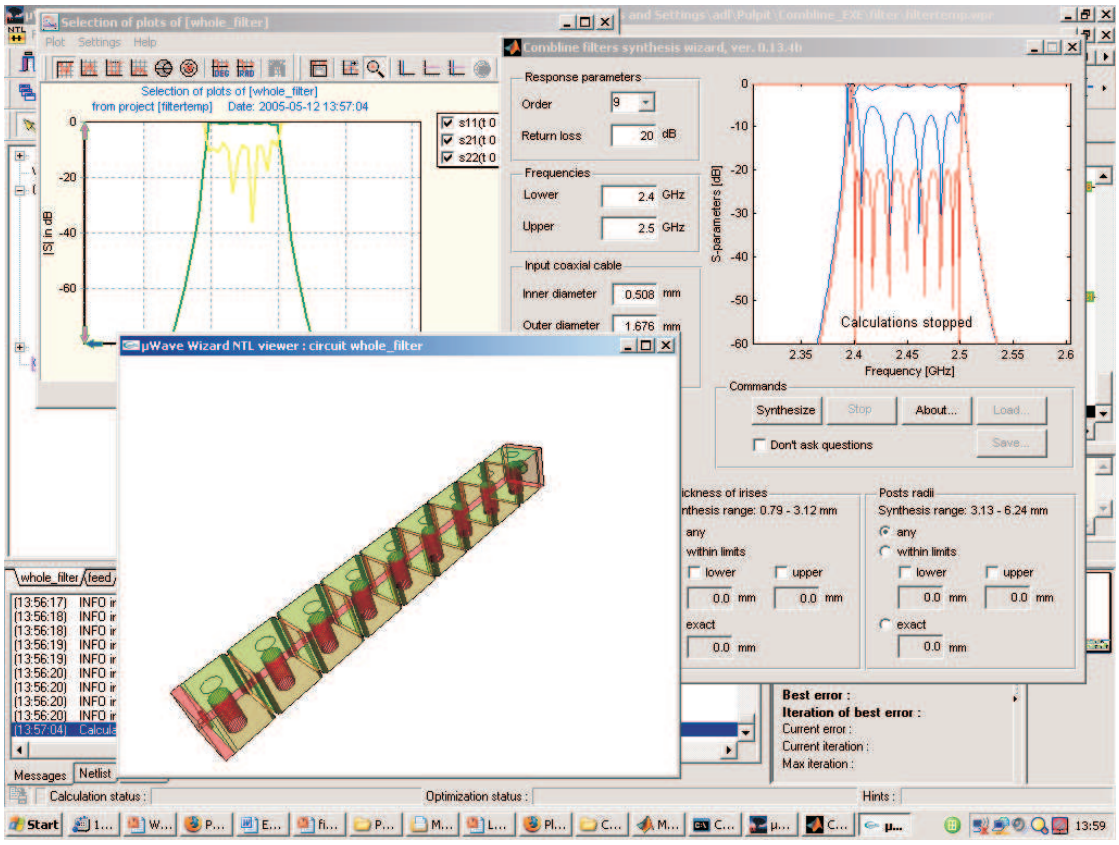

Figure 6.31: Developed commercial software for rapid design of combline filters.

The advantage of a design based on surrogate models is illustrated on an example of a 7-th order combline filter for the ISM band 2.40GHz-2.48GHz and return loss 20dB. The response of the synthesized filter using surrogate models is depicted in Fig. 6.30(in red). For comparison, the same figure (blue curve) shows a results of filter synthesis with standard technique, that does not take into account the phenomenon of detuning of the resonator when the coupling is introduced. Is can be seen that the response is shifted to lower frequencies. It has to be noted that the total time of synthesis of 7-th order filter with application of models was only two seconds on 1.6GHz PC.

The models, once constructed, can be applied to rapid synthesis of combline filters with different specifications. The models used in the example described above were incorporated into a commercial application for automated design of combline filters (Fig.6.31), developed at the WiComm Center of Excellence at the Gdansk University of Technology [67] in a cooperation with the company Mician, GmbH [129]. The final product would be available soon on the world market.It has to be underlined that no other software tool offers a similar feature.

Chapter 7

Conclusions and outlook

The thesis discusses construction methodology of various models of microwave components that are essential for automation of high-frequency circuit design. Both equivalent circuits and parameterized, mathematical models are covered. The former can be constructed either by considering physical effects which can be predicted from component structure or as a direct realization of transfer functions (scattering or impedance/admittance rational functions). The latter can be realized as complex expressions derived by the application of various schemes of multidimensional interpolation or in non-evident form as artificial neural networks.

It is shown, that surrogate models and equivalent circuits can be combined and, as a result, one obtains parameterized, passive equivalent circuits suitable for time-domain simulation in SPICE. The results of this work open up the way to substantially expand the capabilities of popular high frequency circuit simulators. With the application of the described techniques the optimization of complex, high frequency devices has become possible in SPICE.

This work has advanced the state-of-the-art of surrogate models and passive equivalent circuits in the following ways:

- A new technique of passivity enforcement of rational model was developed [68, 75]. The technique disturbs the model parameters (poles and/or residues) to restore its passivity and at the same time preserves the device's response in the frequency domain. The technique is applicable to large macromodels, described by hundreds of states, that most other techniques cannot handle.

- A novel technique of construction of parameterized, multivariate surrogate models was proposed. The method exploits multivariate rational interpolation scheme that, together with adaptive sampling, allows one to create the models with several parameters. Numerical tests and comparisons with alternative techniques were showed that the technique requires by far fewer electromagnetic simulations than alternative solutions. As a result, for the first time it was possible to construct high quality parameterized models with as many as six (or even seven) variables. This is twice as many parameters as the previous approaches were shown to be able to handle.

- Practical utility of surrogate models was confirmed by the development of a first ever

commercial tool for rapid synthesis of a combline cavity filters.

- The application of surrogate models gives a significant speed-up of the circuit analysis. It is shown, that in the case of complex structures, such as an octagonal inductor on SiGe BiCMOS substrate, the speed-up factor reaches thousands.

- It was shown, that the models are well-suited for automated design of microwave components using various optimization strategies. Due to fast evaluation of cost function one can start the optimization with far from optimal (even random) initial dimensions of the structure.

- It was demonstrated that both techniques, i.e. parameterized surrogates and equivalent circuits can be combined. This way one obtains a parameterized equivalent circuit well suited for time and frequency domain, active and passive, linear and non-linear circuit simulations combined with fast geometry optimization. Such a feature, while desirable, can not be found in any commercial electronic design tool available on the market.

The results presented in this thesis show possible applications of surrogate models. A commercial potential of high accuracy models is very large. In section 6.5.4 an example of a commercial tool for combline filter synthesis developed with the application of surrogate models presented in this thesis is shown. Work is under way at the WiComm Center of Excellence at the Gdansk University of Technology to develop new commercial tools for design of very complex structures, such as multi-channel multiplexers, dual-mode filters with generalized Chebyshev response etc. In all cases the design involves surrogate models for various building blocks. Also, as shown in sec. 6.2, the models can be incorporated in the industry standard circuit simulators (ADS and Microwave Office).

The recommendations for future work are as follows:

- Extension of the modelling technique to active components.

- Enhancement of the interpolation algorithm in order to enable even more variables, for instance using the technique used in the alternative approach [79].

- Development of software environment that allows one to perform an easy layout/geometry optimization using SPICE circuit simulator with application of parameterized equivalent circuits.

- Development of other commercial tools dedicated to rapid design of various microwave elements, for example dielectric resonator filters.

It has to be pointed out that surrogate models and passivity enforcement techniques are attractive also for advancement in computational techniques. For example, in the Method of Moments, significant numerical cost is related to the computation of impedance matrix at each frequency point. Recently, a new approach to reduce the calculation time was introduced, that uses the interpolation of the impedance matrix in the frequency domain [89]. However it seems possible to create more complex, multivariate surrogate models of the

impedance matrix that take into account the changes of structure parameters. Similarly, passivity enforcement technique opens up the way to create hybrid methods combining time domain analysis (FDTD) with frequency domain techniques, e.g. MoM.

To conclude, the techniques proposed in this thesis are applicable to a wide spectrum of simulation problems that occur in high frequency circuit design. They shorten the design time, which is essential in tightening time-to-market constraints.

About the Author

Adam Lamęcki was born in Strzelno, Poland, in 1977. He received the M.S.E.E. degree from the Gdansk University of Technology (GUT), Gdańsk, Poland, in 2002, and in the same year started working towards Ph.D. under supervision of prof. Michał Mrozowski.

His research interests include surrogate models and their use in the CAD of microwave devices, SPICE equivalent circuits, RFIC/MMIC, computational electromagnetics and filter design.

He had co-authored 5 reviewed journal papers, 1 monograph chapter and 12 conference papers. He is a recipient of a Domestic Grant for Young Scientists award founded by Foundation of Polish Science (START programme) in 2006. In the same year he received a scholarship founded by LOTOS S.A. for best Ph.D. students at Gdansk University of Technology.

Acknowledgments

I would like to express my appreciation to my supervisor, prof. Michał Mrozowski, for the scientific education, inspirations and support in many ideas that lead this work to a successful end.

I am very grateful to dr Piotr Kozakowski, for his support on the start of my research and discussions concerning filter design and applications of surrogate models.

I also want to express my thanks to my colleagues: Łukasz Balewski, Piotr Kowalczyk, Rafał Lech, Piotr Sypek and Michał Wiktor, for the time spent together and for all interesting discussions.

Last but not least, words of my appreciation and gratitude to my family, in particular to my wife, parents and my sister, for their constant support, help and patience during my work on this thesis.

This work was sponsored by US Air Force contract no FA8655-05-1-3028, the Polish Ministry of Science and Higher Education under the contract number 3 T11D 024 30. The work was also supported by the Foundation for Polish Science under the Domestic Grants for Young Scientists Scheme (START programme), Senior Scholars Grants (MISTRZ programme) and the TECHNE commercialization programme, and the Polish-Flanders Scientific Bilateral Programme.

Appendix A

Eigenvalues of Hamiltonian matrices

A.1 Hamiltonian matrix definition

The accurate computation of eigenvalues of the Hamiltonian matrix is an essential issue of several engineering problems. A matrix $\boldsymbol{H}$ is the Hamiltonian if it has a form [15]:

$$\boldsymbol{H} = \begin{bmatrix} \boldsymbol{A} & \boldsymbol{G} \\ \boldsymbol{Q} & -\boldsymbol{A}^T \end{bmatrix} \tag{A.1}$$

where

$$\begin{aligned} \boldsymbol{Q} &= \boldsymbol{Q}^T \\ \boldsymbol{G} &= \boldsymbol{G}^T \end{aligned} \tag{A.2}$$

and $\boldsymbol{A}, \boldsymbol{G}, \boldsymbol{Q} \in \mathbb{R}^{n \times n}$. The eigenvalues of Hamiltonian matrix have a special spectral property: the spectrum of H is symmetric with respect to real and imaginary axes.

A.2 Hamiltonian eigenvalue problem

The Hamiltonian eigenvalue problems are fundamental in system and control, especially in stability radius computation, H_∞-norm computation or algebraic Riccati equations [15]. To solve the Hamiltonian eigenvalue problem one can use standard techniques involving reduction to upper Hessenberg form and Schur factorization (like ZGEEV.f from LAPACK, used in Matlab as eig.m). However, these techniques do not exploit the structure of the Hamiltonian matrix and limited machine precision causes that spectral properties are not preserved. It is most evident in the case of pure imaginary and close to imaginary eigenvalues, which are crucial for passivity enforcement technique presented in Chapter 5.

To compute the eigenvalues of Hamiltonian matrix it is advisable to use dedicated eigensolvers, like a Fortran 77 package HAPACK [14, 16]. HAPACK is based on *symplectic URV decomposition*. It allows one to solve the problem in a backward-stable manner, exploits the structure of the matrix and preserves the spectral properties of the Hamiltonian eigenvalues.

Table A.1: Example I. Comparison of selected eigenvalues

eig.m	*haeig.m*
$-0.2582 \cdot 10^{-11} - 21.3857i$	$-21.3857i$
$0.2646 \cdot 10^{-11} - 15.3687i$	$-15.3687i$
$0.1879 \cdot 10^{-11} - 12.2283i$	$-12.2283i$
$-0.2253 \cdot 10^{-11} - 6.6848i$	$-6.6848i$
$-0.2253 \cdot 10^{-11} + 6.6848i$	$6.6848i$
$0.1879 \cdot 10^{-11} + 12.2283i$	$12.2283i$
$0.2646 \cdot 10^{-11} + 15.3687i$	$15.3687i$
$-0.2582 \cdot 10^{-11} + 21.3857i$	$21.3857i$

Table A.2: Example II. Comparison of selected eigenvalues

eig.m	*haeig.m*
$-4.9996 \cdot 10^{-13} + 0.9999999999995i$	$-4.9999 \cdot 10^{-13} - 0.9999999999995i$
$-4.9996 \cdot 10^{-13} - 0.9999999999995i$	$-4.9999 \cdot 10^{-13} + 0.9999999999995i$
$5.0007 \cdot 10^{-13} + 0.9999999999995i$	$4.9999 \cdot 10^{-13} + 0.9999999999995i$
$5.0007 \cdot 10^{-13} - 0.9999999999995i$	$4.9999 \cdot 10^{-13} - 0.9999999999995i$

Techniques comparison. The first example is a non-passive state-space representation of a microstrip line. The model has 20 states (10 poles). To verify the non-passivity the eigenvalues of the Hamiltonian matrix were computed (section 5.2.2) with matlab *eig.m* and HAPACK *haeig.m*. Table A.1 shows the comparison of selected 8 eigenvalues.

Comparing both results it is seen that the real parts of the eigenvalues computed with standard *eig.m* routine are affected with numerical noise. On the other hand the *haeig.m* procedure properly identifies pure imaginary eigenvalues.

The disturbance of real parts of eigenvalues on level below 10^{-11} seems to be very low and one can argue that it is possible to use the standard techniques and assume that if the real part of the eigenvalue is below some level (for example 10^{-10}), then it can be treated as pure imaginary one. However, in several cases, the eigenvalues of H are very close to imaginary, but not pure imaginary. For example let us investigate the state-space system [16]:

$$A = \begin{bmatrix} -\phi & 1 & 0 & 0 \\ -1 & -\phi & 0 & 0 \\ 0 & 0 & \phi & 1 \\ 0 & 0 & -1 & \phi \end{bmatrix} \tag{A.3}$$

$$B = \begin{bmatrix} 1 \\ 1 \\ 1 \\ 1 \end{bmatrix} \tag{A.4}$$

$$C = B^T \tag{A.5}$$

$$D = 0 \tag{A.6}$$

where ϕ a real-valued parameter. When $\phi \to 0$ then eigenvalues of H (pair of complex conjugate eigenvalues) tend to be purely imaginary. Let us assume that $\phi = 10^{-6}$. Computed eigenvalues are presented in Tab. A.2. It is seen that a non-dedicated solver does not preserve the symmetry properties of the eigenvalues. True eigenvalues for this problem are equal $\lambda = \pm 0.5000 \cdot 10^{-13} \pm 0.9999999999995i$ [16]. The eigenvalues are very close to imaginary axis, but not purely imaginary. By computing the eigenvalues with a standard solver it is not possible to decide whether the eigenvalue is purely imaginary or not.

Appendix B

Fitting problem solution

In several data fitting applications, a crucial part is an efficient solution of a linear problem in the form:

$$[\boldsymbol{A} \ \ -\boldsymbol{B}] \cdot \begin{bmatrix} \boldsymbol{a} \\ \boldsymbol{b} \end{bmatrix} = 0 \tag{B.1}$$

where $\boldsymbol{A}$ is a $L \times M_1$ matrix and $\boldsymbol{B}$ is a $L \times M_2$ matrix. To find a non-trivial solution of (B.1) two techniques can be used: the least squares (LS) and the total least squares (TLS).

B.1 Least squares

The solution of the problem in a least-square sense is described in [21,88]. The real-valuated problem (B.1) is transformed to an eigenvalue problem:

$$\boldsymbol{C}^T \cdot \boldsymbol{C} \cdot \boldsymbol{x} = \lambda \boldsymbol{x} \tag{B.2}$$

where

$$\boldsymbol{C} = [\boldsymbol{A} \ \ -\boldsymbol{B}] \tag{B.3}$$

and

$$\boldsymbol{x} = \begin{bmatrix} \boldsymbol{a} \\ \boldsymbol{b} \end{bmatrix} \tag{B.4}$$

The non-trivial solution $\boldsymbol{x}$ is an eigenvector corresponding to minimum eigenvalue λ_{min}.

In the case of the rational/polynomial interpolation, the value of λ_{min} can be used for estimation of the model order, as described in [88].

B.2 Total least squares

The total least squares method is suited to problems in which both the coefficient matrix and the right-hand side are not precisely known. It allows one to filter the noise from interpolated data and improve the quality of resulting solution. The first step is the computation of the *QR* decomposition of the matrix $[\boldsymbol{A} \ -\boldsymbol{B}]$, which results in:

$$\begin{bmatrix} \boldsymbol{R}_{11} & \boldsymbol{R}_{12} \\ \boldsymbol{0} & \boldsymbol{R}_{22} \end{bmatrix} \begin{bmatrix} \boldsymbol{a} \\ \boldsymbol{b} \end{bmatrix} = 0 \tag{B.5}$$

where matrix $\boldsymbol{R}_{11}$ has size $(M_1 \times M_1)$, $\boldsymbol{R}_{12}$ has size $(M_1 \times M_2)$ and $\boldsymbol{R}_{22}$ is $((L - M_1 + 1) \times M_2)$ matrix. The $\boldsymbol{R}_{22}$ matrix is affected by the noise. The equation (B.5) can be written as two separate equations:

$$[\boldsymbol{R}_{11}]\boldsymbol{a} = -[\boldsymbol{R}_{12}]\boldsymbol{b} \tag{B.6}$$

$$[\boldsymbol{R}_{22}]\boldsymbol{b} = 0 \tag{B.7}$$

Computing the singular value decomposition (*SVD*) of $\boldsymbol{R}_{22}$ one obtains:

$$[\boldsymbol{U}][\boldsymbol{\Sigma}][\boldsymbol{V}]\boldsymbol{b} = 0 \tag{B.8}$$

where matrix $\boldsymbol{V}$ is size $(M_2 \times M_2)$. The solution of the problem in TLS sense is proportional to the last column of the matrix $\boldsymbol{V}$, therefore is assumed that $\boldsymbol{b} = [\boldsymbol{V}]_{M_2}$.

Copyright note/Prawo rozpowszchniania

Bibliography

[1] R. Achar, P. K. Gunupudi, M. Nakhla, and E. Chiprout, "Passive Interconnect Reduction Algorithm for Distributed/Measured Networks," *IEEE Transactions on Circuit and Systems*, vol. 2, pp. 287–301, Apr. 2000.

[2] R. Achar and M. S. Nakhla, "Simulation of High-Speed Interconnects," *Proceedings of the IEEE*, vol. 89, pp. 693–728, May 2001.

[3] R. S. Adve, T. K. Sarkar, S. M. Rao, E. K. Miller, and D. R. Pflug, "Application of the Cauchy Method for Extrapolating/Interpolating Narrow-Band System Responses," *IEEE Transactions on Microwave Theory and Techniques*, vol. 45, pp. 837–845, May 1997.

[4] H. Akaike, "A New Look at the Statistical Model Identification," *IEEE Transactions on Automatic Control*, vol. 19, pp. 716–723, Dec. 1974.

[5] N. G. Alexopoulos and S.-C. Wu, "Frequency-Independent Equivalent Circuit Model for Microstrip Open-End and Gap Discontinuities," *IEEE Transactions on Microwave Theory and Techniques*, vol. 42, pp. 1268–1272, July 1994.

[6] S. Amari and J. Bornemann, "Using frequency-dependent coupling to generate finite attenuation poles in direct coupled resonator bandpass filters," *IEEE Microwave Guided Wave Letters*, vol. 9, pp. 404–406, Oct. 1999.

[7] B. D. Anderson and S. Vongpanitlerd, *Network Analysis and Synthesis*. NJ: Prentice-Hall, 1973.

[8] G. Antonini, "SPICE Equivalent Circuits of Frequency-Domain Responses," *IEEE Transactions on Electromagnetic Compatibility*, vol. 45, pp. 502–512, Aug. 2003.

[9] R. Araneo, "Extraction of Broad-Band Passive Lumped Equivalent Circuits of Microwave Discontinuities," *IEEE Transactions on Microwave Theory and Techniques*, vol. 54, pp. 393–401, Jan. 2006.

[10] J. W. Bandler and S. Chen, "Circuit Optimization: The State of the Art," *IEEE Transactions on Microwave Theory and Techniques*, vol. 36, pp. 424–443, Feb. 1988.

[11] J. W. Bandler, D. M. Hailu, K. Madsen, and F. Pedersen, "A Space-Mapping Interpolating Surrogate Algorithm for Highly Optimized EM-Based Design of Microwave Devices," *IEEE Transactions on Microwave Theory and Techniques*, vol. 52, pp. 2593–2600, Nov. 2004.

[12] R. H. Bartels and J. J. Jezioranski, "Least-Squares Fitting Using Orthogonal Multinomials," *ACM Transactions on Mathematical Software*, vol. 11, pp. 201–217, Sept. 1985.

[13] M. S. Basel, M. B. Steer, and P. D. Franzon, "Simulation of High Speed Interconnects Using a Convolution-Based Hierarchical Packaging Simulator," *IEEE Transactions on Components, Packaging and Manufacturing Technology*, vol. 18, pp. 74–82, Feb. 1995.

[14] P. Benner and D. Kressner, "New Hamiltonian eigensolvers with applications in control," in *IEEE Conference on Decision and European Control*, 2005.

[15] ——, "Skew-Hamiltonian and Hamiltonian Eigenvalue Problems: Theory, Algorithms and Applications," in *Proceedings of the Conference on Applied Mathematics and Scientific Computing*. Springer-Verlag, 2005.

[16] ——, "Fortran 77 Subroutines for Computing the Eigenvalues of Hamiltonian Matrices," *ACM Transactions on Mathematical Software*, vol. 32, pp. 352–373, 2006.

[17] W. T. Beyene, J. Feng, N. Cheng, and X. Yuan, "Performance Analysis and Model-to-Hardware Correlation of Multigigahertz Parallel Bus With Transmit Pre-Emphasis Equalization," *IEEE Transactions on Microwave Theory and Techniques*, vol. 53, pp. 3568–3577, Nov. 2005.

[18] S. Boyd, V. Balakrishnan, and P. Kabamba, "A Bisection Method for Computing the H_∞ Norm of a Transfer Matrix and Related Problems," *Math. Control Signals Syst.*, vol. 2, pp. 207–219, 1989.

[19] R. J. Cameron, "General Coupling Matrix Synthesis Methods for Chebyshev Filtering Functions," *IEEE Transactions on Microwave Theory and Techniques*, vol. 47, pp. 433–442, Apr. 1999.

[20] D. Choi and W. Hoefer, "The Finite-Difference Time-Domain method and its application to eigenvalue problems," *IEEE Transactions on Microwave Theory and Techniques*, vol. 32, pp. 1464–1470, Dec. 1986.

[21] K. L. Choi and M. Swaminathan, "Development of Model Libraries for Embedded Passives Using Network Synthesis," *IEEE Transactions on Circuits and Systems-II: Analog and Digital Signal Processing*, vol. 47, no. 4, pp. 249–260, Apr. 2000.

[22] C. P. Coelho, J. Phillips, and L. M. Silveira, "A Convex Programming Approach for Generating Guaranteed Passive Approximations to Tabulated Frequency-Data," *IEEE Transactions on Computer-Aided Design of Integrated Cicruits and Systems*, vol. 23, pp. 293–301, Feb. 2004.

[23] C. P. Coelho, J. R. Phillips, and L. M. Silveira, "Passive Constrained Rational Approximation Algorithm using Nevanlinna-Pick Interpolation," in *Proceedings of the Design, Automation and Test in Europe Conference and Exhibition*, 2002.

[24] G. Conciauro, M. Guglielmi, and R. Sorrentino, *Advanced modal analalysis*. John Wiley & Sons, Ltd, 2000.

[25] G. L. Creech, B. J. Paul, C. D. Lesniak, T. J. Jenkins, and M. C. Calcatera, "Artificial Neural Networks for Fast and Accurate EM-CAD of Microwave Circuits," *IEEE Transactions on Microwave Theory and Techniques*, vol. 45, pp. 794–801, May 1997.

[26] A. Cuyt, R. B. Lenin, S. Becuwe, and B. Verdonk, "Adaptive Multivariate Rational Data Fitting With Applications in Electromagnetics," *IEEE Transactions on Microwave Theory and Techniques*, vol. 54, pp. 2265–2274, May 2006.

[27] D. De Zutter, J. Sercu, T. Dhaene, J. D. Geest, F. J. Demuynck, S. Hammadi, and C.-W. P. Huang, "Recent Trends in the Integration of Circuit Optimization and Full-Wave Electromagnetic Analysis," *IEEE Transactions on Microwave Theory and Techniques*, vol. 52, no. 1, pp. 245–256, Jan. 2004.

[28] D. Deschrijver and T. Dhaene, "Passivity Based Sample Selection and Adaptive Vector Fitting Algorithm for PoleResidue Modeling of Sparse Frequency Domain Data," in *IEEE International Conference on Behavioral Modeling and Simulation Proceedings*, Oct. 2004, pp. 68–73.

[29] ——, "Broadband macromodelling of passive components using orthonormal vector fitting," *Electronisc Letters*, vol. 41, no. 21, pp. 1160–1161, Oct. 2005.

[30] V. K. Devabhaktuni, M. C. E. Yagoub, and Q.-J. Zhang, "A Robust Algorithm for Automatic Development of Neural-Network Models for Microwave Applications," *IEEE Transactions on Microwave Theory and Techniques*, vol. 49, pp. 2282–2291, Dec. 2001.

[31] T. Dhaene, J. Ureel, N. Faché, and D. De Zutter, "Adaptive Frequency Sampling Algorithm for Fast and Accurate S-parameters Modelling of General Planar Structures," in *IEEE MTT-S Internatial Microwave Symposium Digest*, USA, 1995.

[32] X. Ding, V. K. Devabhaktuni, B. Chattaraj, M. C. E. Yagoub, M. Deo, J. Xu, and Q. J. Zhang, "Neural-Network Approaches to Electromagnetic-Based Modeling of Passive Components and Their Applications to High-Frequency and High-Speed Nonlinear Circuit Optimization," *IEEE Transactions on Microwave Theory and Techniques*, vol. 52, no. 1, pp. 436–449, Jan. 2004.

[33] T. A. Driscoll and B. Fornberg, "Interpolation in the limit of increasingly flat radial basis functions," *Computers and Mathematics with Applications*, vol. 43, pp. 413–422, 2002.

[34] K. Eshraghian, "SoC Emerging Technologies," *Proceedings of the IEEE*, vol. 94, no. 6, pp. 1197–1213, June 2006.

[35] R. Gao, Y. S. Mekonnen, W. T. Beyene, and J. E. Schutt-Ain, "Black-Box Modeling of Passive Systems by Rational Function Approximation," *IEEE Transactions on Advanced Packaging*, vol. 28, pp. 209–215, May 2005.

[36] A. Garcia-Lamperez, S. Llorente-Romano, M. Salazar-Palma, and T. K. Sarkar, "Efficient Electromagnetic Optimization of Microwave Filters and Multiplexers Using Rational Models," *IEEE Transactions on Microwave Theory and Techniques*, vol. 52, no. 2, pp. 508–521, Feb. 2004.

[37] R. Garg, P. Bhartia, I. Bahl, and A. Ittipiboon, *Microstrip Antenna Design Handbook*. Artech House, 2001.

[38] J. D. Geest, T. Dhaene, N. Fache, and D. D. Zutter, "Adaptive CAD-model Building Algorithm for General Planar Microwave Structures," *IEEE Transactions on Microwave Theory and Techniques*, vol. 47, pp. 1801–1809, Sept. 1999.

[39] D. E. Goldberg, *Genetic Algorithms in Search, Optimization, and Machine Learning*. Addison-Wesley, 1989.

[40] G. H. Golub and C. F. V. Loan, *Matrix Computation*. The Johns Hopkins University Press, 1996.

[41] P. R. Graves-Morris and T. R. Hopkins, "Reliable rational interpolation," *Numerische Mathematik*, vol. 36, pp. 111–128, 1981.

[42] S. Grivet-Talocia, "Package Macromodeling via Time-Domain Vector Fitting," *IEEE Microwave and Wireless Components Letters*, vol. 13, no. 11, pp. 472–474, Nov. 2003.

[43] ——, "Passivity Enforcement via Perturbation of Hamiltonian Matrices," *IEEE Transactions on Circuits and Systems*, vol. 51, pp. 1755–1769, Sept. 2004.

[44] S. Grivet-Talocia and M. Bandinu, "Improving the Convergence of Vector Fitting for Equivalent Circuit Extraction From Noisy Frequency Responses," *IEEE Transactions on Electromagnetic Comatibility*, vol. 48, no. 1, pp. 104–120, Feb. 2006.

[45] S. Grivet-Talocia and A. Ubolli, "On the Generation of Large Passive Macromodels for Complex Interconnect Structures," *IEEE Transactions on Advanced Packaging*, vol. 29, pp. 39–54, Feb. 2006.

[46] M. Guglielmi, P. Jarry, E. Kerherve, O. Roquebrun, and D.Schmitt, "A New Family of All-Inductive Dual-Mode Filters," *IEEE Transactions on Microwave Theory and Techniques*, vol. 49, pp. 1764–1796, Oct. 2001.

[47] B. Gustavsen, "Improving the Pole Relocating Properties of Vector Fitting," *IEEE Transactions on Power Delivery*, vol. 21, no. 3, pp. 1587–1592, 2006.

[48] B. Gustavsen and A. Semlyen, "Rational Approximation of Frequency Domain Responses by Vector Fitting," *IEEE Transactions on Power Delivery*, vol. 14, pp. 1052–1061, July 1999.

[49] B. Gustavsena and A. Semlyen, "Enforcing Passivity for Admittance Matrices Approximated by Rational Functions," *IEEE Transaction on Power Systems*, vol. 16, pp. 97–104, Feb. 2001.

[50] S. Han, "A Globally Convergent Method For Nonlinear Programming," *Journal of Optimization Theory and Applications*, vol. 22, pp. 297–309, 1977.

[51] R. Haupt, "Comparison Between Genetic and Gradient-Based Optimization Algorithms for Solving Electromagnetics Problems," *IEEE Transactions on Magnetics*, vol. 31, no. 3, pp. 1932–1935, May 1995.

[52] J. S. Hong and M. J. Lancaster, *Microstrip Filters for RF/Microwave Application*. New York: Wiley, 2001.

[53] S. Y. Hui and K. H. Yeung, "Challenges in the Migration to 4G Mobile Systems," *IEEE Communications Magazine*, pp. 54–59, Dec. 2003.

[54] N. Jain and P. Onno, "Methods of Using Commercial Electromagnetic Simulators for Microwave and Millimeter-Wave Circuit Design and Optimization," *IEEE Transactions Microwave Theory and Techniques*, vol. 45, pp. 724–746, May 1997.

[55] J. Jin, *The Finite Element Method in Electromagnetics*. John Wiley & Sons, Ltd, 1993.

[56] J. M. Johnson and Y. Rahmat-Samii, "Genetic Algorithms in Engineering Electromagnetics," *IEEE Antennas and Propagation Magazine*, vol. 39, no. 4, pp. 7–21, Aug. 1997.

[57] M. Kirschning, R. H. Jansen, and N. H. L. Koster, "Measurement and Computer-Aided Modeling of Microstrip Discontinuities by an Improved Resonator Method," in *IEEE MTT-S International Microwave Symposium Digest*, 1983.

[58] P. Kozakowski, A. Lamecki, P. Sypek, and M. Mrozowski, "Eigenvalue Approach to Synthesis of Prototype Filters with Source/Load Coupling," *IEEE Microwave and Wireless Components Letters*, vol. 15, pp. 98–100, Feb. 2005.

[59] P. Kozakowski and M. Mrozowski, "Automated CAD of Coupled Resonator Filters," *IEEE Microwave and Wireless Components Letters*, vol. 12, no. 12, pp. 470–472, Dec. 2002.

[60] S. Koziel, J. W. Bandler, and K. Madsen, "A Space-Mapping Framework for Engineering OptimizationTheory and Implementation," *IEEE Transactions on Microwave Theory and Techniques*, vol. 54, pp. 3721–3730, Oct. 2006.

[61] ——, "Space-Mapping-Based Interpolation for Engineering Optimization," *IEEE Transactions on Microwave Theory and Techniques*, vol. 54, pp. 2410–2421, June 2006.

[62] E. Krol, "Silicon-germanium," *Potentials, IEEE*, vol. 18, pp. 17–19, 1999.

[63] I. C. H. Lai and M. Fujishima, "A New On-Chip Substrate-Coupled Inductor Model Implemented With Scalable Expressions," *IEEE Journal of Solid-State Circuits*, vol. 41, pp. 2491–2499, Nov. 2006.

[64] A. Lamecki, L. Balewski, P. Kozakowski, and M. Mrozowski, "Multivariate models of inter-resonator couplings and their application in filter design," in *XXVIII-th General Assembly of International Union of Radio Science Proceedings*, New Delhi, India, Oct. 2005.

[65] A. Lamecki, L. Balewski, and M. Mrozowski, "Multivariate Models of Inter-Resonator Couplings for Microwave Filter Synthesis," in *International Conference on Adaptive Modeling and Simulation ADMOS*, Barcelona, Spain, 2005.

[66] ——, "High accuracy multidimensional parameterized surrogate models for fast optimization of microwave circuits in the industry standard circuit simulators," *EOARD Grant report, Grant no FA8655-05-1-3028*, 2006.

[67] A. Lamecki, Ł. Balewski, and M. Mrozowski, "Synthesis of combline filters with application of surrogate model of inter-resonator and source-resonator coupling (Synteza filtru *combline* z wykorzystaniem modelu sprzężeń miedzyrezonatorowych i źródło-rezonator," *Zgłoszenie innowacyjne, Politechnika Gdańska*, no. 4/07, Feb. 2007.

[68] A. Lamecki, P. Kozakowski, and M. Mrozowski, "Efficient Implementation of the Cauchy Method for Automated CAD-model Construction," *IEEE Microwave and Wireless Components Letters*, vol. 13, pp. 268–270, July 2003.

[69] ——, "Fast Extraction of Coupling Matrix for Optimization and CAD Tuning Problems," in *Proceedings of the 34th European Microwave Conference*, 2004, pp. 1385–1388.

[70] ——, "Fast Synthesis of Coupled-Resonator Filters," *IEEE Microwave and Wireless Components Letters*, vol. 14, pp. 174–176, Apr. 2004.

[71] A. Lamecki and M. Mrozowski, "CAD-Model Construction Based on Adaptive Radial Basis Functions Interpolation Technique," in *15-th International Conference on Microwaves, Radar and Wireless Communications Mikon*, Warsaw, Poland, May 2004.

[72] ——, "Passive SPICE Networks from Non-Passive Data," in *16-th International Conference on Microwaves, Radar and Wireless Communications Mikon*, Krakow, May 2006.

[73] ——, "Equivalent SPICE Circuits With Guaranteed Passivity From Nonpassive Models," *IEEE Transaction on Microwave Theory and Techniques*, vol. 55, pp. 526–532, Mar. 2007.

[74] ——, "Parameterized surrogate models of combline resonators (Sparametryzowane modele zastępcze dla trójki rezonatorów typu combline)," *Zgłoszenie innowacyjne, Politechnika Gdańska*, no. 1/07, Feb. 2007.

[75] A. Lamecki, P.Kozakowski, and M. Mrozowski, "Multimode, Multiparametric Surrogate Models for Fast Design of Waveguide Components," in *European Microwave Conference Proceedings*, Munich, Germany, Oct. 2003.

[76] A. G. Lamprez, T. K. Sarkar, and M. S. Palma, "Generation of Accurate Rational Models of Lossy Systems Using the Cauchy Method," *IEEE Microwave and Wireless Components Letters*, vol. 14, pp. 490–492, Oct. 2004.

[77] J.-H. Lee, G. DeJean, S. Sarkar, S. Pinel, K. Lim, J. Papapolymerou, J. Laskar, and M. M. Tentzeris, "Highly Integrated Millimeter-Wave Passive Components Using 3-D LTCC System-on-Package (SOP) Technology," *IEEE Transactions on Microwave Theory and Techniques*, vol. 53, no. 6, pp. 2220–2229, June 2005.

[78] Y. Lee and D. S. Filipovic, "ANN Based Electromagnetic Models for the Design of RF MEMS Switches," *IEEE Microwave and Wireless Components Letters*, vol. 15, pp. 823–825, Nov. 2005.

[79] R. Lehmensiek and P. Meyer, "Creating Accurate Multivariate Rational Interpolation Models of Microwave Circuits by Using Efficient Adaptive Sampling to Minimize the Number of Computational Electromagnetic Analyses," *IEEE Transactions on Microwave Theory and Techniques*, vol. 49, pp. 1419–1430, Aug. 2001.

[80] ——, "Using Efficient Multivariate Adaptive Sampling by Minimizing the Number of Computational Electromagnetic Analysis Needed to Establish Accurate Interpolation Models," in *IEEE MTT-S Internatial Microwave Symposium Digest*, USA, 2001.

[81] ——, "Adaptive Sampling Applied to Multivariate, Multiple Output Rational Interpolation Models with Application to Microwave Circuits," *Int Journal RF and Microwave*, pp. 332–340, 2002.

[82] E.-P. Li, E.-X. Liu, L.-W. Li, and M.-S. Leong, "A Coupled Efficient and Systematic Full-Wave Time-Domain Macromodeling and Circuit Simulation Method for Signal Integrity Analysis of High-Speed Interconnects," *IEEE Transactions on Advanced Packaging*, vol. 27, pp. 213–223, Feb. 2004.

[83] J. Lin and T. Itoh, "Active Integrated Antennas," *IEEE Transactions on Microwave Theory and Techniques*, vol. 42, pp. 2186–2194, Dec. 1994.

[84] S. Lin and E. Kuh, "Transient Simulation of Lossy Interconnects Based on the Recursive Convolution Formulation," *IEEE Transactions on Circuits and Systems*, vol. 39, pp. 879–892, Nov. 1992.

[85] J. M. Lopez-Villegas, J. Samitier, C. Cane, P. Losantos, and J. Bausells, "Improvement of the Quality Factor of RF Integrated Inductors by Layout Optimization," *IEEE Transactions on Microwave Theory and Techniques*, vol. 48, pp. 76–83, Jan. 2000.

[86] A. Matsuzawa, "RF-SoCExpectations and Required Conditions," *IEEE Transactions on Microwave Theory and Techniques*, vol. 50, no. 1, pp. 245–253, Jan. 2002.

[87] E. McGibney and J. Barrett, "An Overview of Electrical Characterization Techniques and Theory for IC Packages and Interconnects," *IEEE Transactions on Advanced Packaging*, vol. 29, pp. 131–139, Feb. 2006.

[88] S.-H. Min and M. Swaminathan, "Construction of Broadband Passive Macromodels From Frequency Data for Simulation of Distributed Interconnect Networks," *IEEE Transactions on Electromagnetic Compatibility*, vol. 46, pp. 544–558, Nov. 2004.

[89] M. Mongiardo, R. Sorrentino, and C. Tomassoni, "Efficient Planar Electromagnetic Analysis by Impedance Matrix Interpolation," in *IEEE MTT-S Internatial Microwave Symposium Digest*, USA, 2005.

[90] S. Mukherjee, B. Mutnury, S. Dalmia, and M. Swaminathan, "Layout-Level Synthesis of RF Inductors and Filters in LCP Substrates for Wi-Fi Applications," *IEEE Transactions on Microwave Theory and Techniques*, vol. 53, pp. 2196–2210, June 2005.

[91] E. E. Newman, "Simple Examples of the Method of Moments in Electromagnetics," *IEEE Transactions on Education*, vol. 31, pp. 193–200, Aug. 1988.

[92] R. Neymayer, F. Haslinger, A. Stelzer, and R. Weigel, "Synthesis of SPICE-Compatible Broadband Electrical Models from N-Port Scattering Parameter Data," *IEEE International Symposium on Electromagnetic Compatibility*, vol. 1, pp. 469–474, Aug. 2002.

[93] A. Odabasioglu, M. Celik, and L. T. Pileggi, "PRIMA: Passive Reduced-Order Interconnect Macromodeling Algorithm," *IEEE Trans. Computer-Aided Design*, vol. 17, pp. 645–654, Aug. 1998.

[94] A. C. Parker and S. Hayati, "Automating the VLSl Design Process Using Expert Systems and Silicon Compilation," *Proceedings of the IEEE*, vol. 75, pp. 777–785, June 1987.

[95] S. F. Peik, R. R. Mansour, and Y. L. Chow, "Multidimensional Cauchy Method and Adaptive Sampling for an Accurate Microwave Circuit Modeling," *IEEE Transactions on Microwave Theory and Techniques*, vol. 46, pp. 2364–2371, Dec. 1998.

[96] J. Powell and D. Bannister, "Business Prospects for Commercial mm-Wave MMICs," *IEEE Microwave Magazine*, pp. 34–43, Dec. 2005.

[97] M. Powell, "A Fast Algorithm for Nonlineary Constrained Optimization Calculations," *Springer Verlag Lecture Notes in Mathematics*, vol. 630, pp. 144–175, 1978.

[98] R. L. Pritchard, "Transistor Equivalent Circuits," *Proceedings of the IEEE*, vol. 86, no. 1, pp. 150–162, Jan. 1998.

[99] Z. Qi, H. Yu, P. Liu, S. X.-D. Tan, and L. He, "Wideband Passive Multiport Model Order Reduction and Realization of RLCM Circuits," *IEEE Transactions on Computer-Aided Design of Integrated Circuits and Systems*, vol. 25, pp. 1496–1509, Aug. 2005.

[100] J. E. Rayas-Sanchez, "EM-Based Optimization of Microwave Circuits Using Artificial Neural Networks: The State-of-the-Art," *IEEE Transactions on Microwave Theory and Techniques*, vol. 52, pp. 420–435, Jan. 2004.

[101] S. Rippa, "An algorithm for selecting a good value for the parameter *c* in radial basis function interpolation," *Advances in Computational Mathematics*, vol. 11, pp. 193–210, 1999.

[102] J. J. Rissanen, "Modeling by shortest data description," *Automatica*, vol. 14, pp. 465–471, 1953.

[103] A. R. Rofougaran, M. Rofougaran, and A. Behzad, "Radios for Next-Generation Gigabit Networks," *IEEE Microwave Magazine*, pp. 38–43, Mar. 2005.

[104] R. Rohrer and H. Nostrati, "Passivity considerations in stability studies of numerical integration algorithms," *IEEE Transactions on Circuits and Systems*, vol. 28, pp. 857–866, Sept. 1981.

[105] A. E. Ruehli and A. C. Cangellaris, "Progress in the Methodologies for the Electrical Modeling of Interconnects and Electronic Packages," *Proceedings of the IEEE*, vol. 89, pp. 740–771, May 2001.

[106] D. Saraswat, R. Achar, and M. S. Nakhla, "A Fast Algorithm and Practical Considerations for Passive Macromodeling of Measured/Simulated Data," *IEEE Transactions on Advanced Packaging*, vol. 27, pp. 57–70, Feb. 2004.

[107] ——, "Passive Reduction Algorithm for RLC Interconnect Circuits With Embedded State-Space Systems (PRESS)," *IEEE Transactions on Microwave Theory and Techniques*, vol. 52, pp. 2215–2226, Sept. 2004.

[108] ——, "Global Passivity Enforcement Algorithm for Macromodels of Interconnect Subnetworks Characterized by Tabulated Data," *IEEE Transactions on Very Large Scale Integration (VLSI) Systems*, vol. 13, pp. 819–832, July 2005.

[109] C. B. Sia, B. H. Ong, K. W. Chan, K. S. Yeo, J.-G. Ma, and M. A. Do, "Physical Layout Design Optimization of Integrated Spiral Inductors for Silicon-Based RFIC Applications," *IEEE Transactions on Electron Devices*, vol. 52, pp. 2559–2567, Dec. 2005.

[110] E. S. Siah, M. Sasena, J. L. Volakis, P. Y. Papalambros, and R. W. Wiese, "Fast Parameter Optimization of Large-scale Electromagnetic Objects Using DIRECT with Kriging Metamodeling," *IEEE Transactions on Microwave Theory and Techniques*, vol. 52, pp. 276–285, Jan. 2004.

[111] P. P. Silvester, G. Pelosi, and Eds, *Finite Elements for Wave Electromagnetics*. IEEE Press, 1994.

[112] H. Sobol, "Microwave Communications - An Historical Perspective," *IEEE Transactions on Microwave Theory and Techniques*, vol. 32, pp. 1170–1181, Sept. 1984.

[113] D. Staiculescu, J. Laskar, and E. M. Tentzeris, "Design Rule Development for Microwave Flip-chip Applications," *IEEE Transactions on Microwave Theory and Techniques*, vol. 48, pp. 1476–1481, Sept. 2000.

[114] J. Stoer and R. Bulirsch, *Introduction to Numerical Analysis*. Berlin: Springer-Verlag, 1978.

[115] A. Taflove, *Computational Electromagnetics: The Finite-Difference Time-Domain Method*. Artech House, 1995.

[116] G. C. Temes and J. Lapatra, *Introduction to Circuit Synthesis and Design*. McGraw-Hill, 1977.

[117] S. A. Teo, B. L. Ooi, S. T. Chew, and M. S. Leong, "A Fast PEEC Technique for Full-Wave Parameters Extraction of Distributed Elements," *IEEE Microwave and Wireless Components Letters*, vol. 11, no. 5, pp. 226–228, May 2001.

[118] I. Timmins and K.-L. Wu, "An Efficient Systematic Approach to Model Extraction for Passive Microwave Circuits," *IEEE Transactions on Microwave Theory and Techniques*, vol. 48, pp. 1565–1573, Sept. 2000.

[119] R. R. Tummala, "SOP: What Is It and Why? A New Microsystem-Integration Technology Paradigm-Moores Law for System Integration of Miniaturized Convergent Systems of the Next Decade," *IEEE Transactions on Advanced Packaging*, vol. 27, pp. 241–249, May 2004.

[120] R. R. Tummala, M. Swaminathan, M. M. Tentzeris, J. Laskar, G.-K. Chang, S. Sitaraman, D. Keezer, D. Guidotti, Z. Huang, K. Lim, L. Wan, S. K. Bhattacharya, V. Sundaram, F. Liu, and P. M. Raj, "The SOP for Miniaturized, Mixed-Signal Computing, Communication, and Consumer Systems of the Next Decade," *IEEE Transactions on Advanced Packaging*, vol. 27, no. 2, pp. 250–267, May 2004.

[121] A. Veluswami, M. S. Nakhla, and Q.-J. Zhang, "The Application of Neural Networks to EM-Based Simulation and Optimization of Interconnects in High-Speed VLSI Circuits," *IEEE Transactions on Microwave Theory and Techniques*, vol. 45, pp. 712–723, May 1997.

[122] J. Wang, "Generalised Moment Methods in Electromagnetics," *IEE Proceedings*, vol. 137, pp. 127–132, Apr. 1990.

[123] L. Weinberg, *Network Analysis and Synthesis*. Mcgraw Hill, 1962.

[124] P. L. Werner, R. Mittra, and D. H. Werner, "Extraction of Equivalent Circuits for Microstrip Components and Discontinuities Using the Genetic Algorithm," *IEEE Microwave and Wireless Components Letters*, vol. 8, pp. 333–335, Oct. 1998.

[125] K.-L. Wu, Y.-J. Zhao, J. Wang, and M. K. K. Cheng, "An Effective Dynamic Coarse Model for Optimization Design of LTCC RF Circuits With Aggressive Space Mapping," *IEEE Transactions on Microwave Theory and Techniques*, vol. 52, pp. 393–402, Jan. 2004.

[126] S.-C. Wu, N. G. Alexopoulos, and O. Fordham, "Feeding Structure Contribution to Radiation by Patch Antennas with Rectangular Boundaries," *IEEE Transactions on Antennas and Propagation*, vol. 40, pp. 1245–1249, Oct. 1992.

[127] www.agilent.com.

[128] www.linmic.com.

[129] www.mician.com.

[130] www.mwoffice.com.

[131] L. Yang and G. B. Giannakis, "Ultra Wideband communications - An Idea Whose Time Has Come," *IEEE Signal Processing Magazine*, pp. 26–54, Nov. 2004.

[132] K. Yee, "Numerical Solution of Initial Boundary Value Problems Involving Maxwells Equations in Isotropic Media," *IEEE Transactions on Antennas and Propagation*, vol. 14, pp. 302–307, May 1966.

[133] A. H. Zaabab, Q. J. Zhang, and M. Nakhla, "A Neural Network Modeling Approach to Circuit Optimization and Statistical Design," *IEEE Transactions on Microwave Theory and Techniques*, vol. 43, pp. 1349–1558, June 1995.

[134] Q.-J. Zhang, K. C. Gupta, and V. K. Devabhaktuni, "Artificial Neural Networks for RF and Microwave DesignFrom Theory to Practice," *IEEE Transactions on Microwave Theory and Techniques*, vol. 51, no. 4, pp. 1339–1350, Apr. 2003.

[135] C. Zhen and G. Lihui, "Application of the Genetic Algorithm in Modeling RF On-Chip Inductors," *IEEE Transactions on Microwave Theory and Techniques*, vol. 51, pp. 342–346, Feb. 2003.

Modele zastępcze i automatyczne projektowanie wspomagane komputerem pasywnych elementów mikrofalowych

Adam Lamęcki

Rozprawa doktorska (streszczenie)

Politechnika Gdańska

Wydział Elektroniki, Telekomunikacji i Informatyki

Promotor: Prof. Michał Mrozowski

Gdańsk 2007

Spis treści

1 Wprowadzenie

W najbliższej przyszłości kierunki rozwoju technologii to przede wszystkim zwiększenie oferowanej przepływności transmisji danych i miniaturyzacja wymiarów urządzeń. Połączone to jest ze zwiększaniem się pasma transmitowanych sygnałów oraz wykorzystaniem coraz to wyższych częstotliwości. Transmisja w zakresie pasma mikrofalowego jest bardzo atrakcyjna z punktu widzenia potencjalnych zastosowań. Duże zmiany tłumienności dla różnych częstotliwości powodują, że możliwe jest rozwijanie systemów przesyłania danych zarówno na dalekie jak i krótkie dystanse. W ostatnich latach największe ożywienie obserwować można zwłaszcza w zakresie miniaturyzacji urządzeń i zwiększania stopnia integracji projektowanych układów. Obecnie możliwa jest integracja układów analogowych i cyfrowych w jednym układzie scalonym (*system-on-chip, SoC*) [31]. Równolegle rozwijane są technologie integracji wielu układów w jednej obudowie (*system-on-package, SoP*) [36], takie jak moduły wielochipowe (*Multi Chip Module, MCM*). Powoduje do konieczność projektowania coraz bardziej skomplikowanych połączeń międzyukładowych (*interconnects*), prowadzących do pasywnych układów trójwymiarowych.

Rosnący stopień komplikacji układów wysokiej częstotliwości wymusza konieczność ich analizy przy użyciu narzędzi wykorzystujących pełną analizą elektromagnetyczną. Takie metody analizy charakteryzują się dużą złożonością obliczeniową, co prowadzi do długiego czasu symulacji, mogącej trwać kilka godzin, dni lub nawet tygodni. Czas analizy układu mikrofalowego jest bardzo istotny z punktu widzenia możliwości wdrażania i projektowania nowych elementów. Długi czas analizy pojedynczego układu prowadzi to do wzrostu kosztów projektu (i w konsekwencji produkcji) oraz małej elastyczności producentów na potrzeby rynku.

Możliwe jest zastąpienie analizy elektromagnetycznej przez analizę obwodową, warunkiem jest jednak posiadanie modelu zastępczego danego układu (w postaci modelu matematycznego lub schematu zastępczego). Takie rozwiązanie powszechnie przyjęte jest w dostępnych obecnie komercyjnych symulatorach obwodów mikrofalowych, takich jak Advanced Design Studio (ADS) [37] czy Microwave Office [38]. Symulatory te oferują opracowane przez siebie biblioteki modeli matematycznych różnych nieciągłości mikrofalowych, jednak często ich dokładność jest niewystarczająca w porównaniu z wynikami symulacji elektromagnetycznej. Dodatkowo producenci oprogramowania do projektowania układów i systemów wielkiej częstotliwości wyposażają swoje programy w biblioteki matematycznych modeli zastępczych obejmujące co najwyżej kilkadziesiąt podstawowych nieciągłości wykonanych w kilku dobrze znanych technologiach. W oparciu o istniejące biblioteki można szybko projektować układy typowe, wykonane w dobrze znanych technologiach. Modele matematyczne stosowane w bibliotekach standardowych powstały w wyniku wieloletnich badań i ich rozszerzanie w miarę pojawiania się nowych technologii nie jest proste. Dla rozwiązań nowych i niestandardowych poleca się stosowanie czasochłonnej analizy polowej (elektromagnetycznej) układu.

Rosnący poziom integracji układów mikrofalowych i rozwijanie układów na zakres fal milimetrowych w filozofii SoC oraz SoP powoduje, że konieczne jest równoczesne uwzględnianie efektów nieliniowych elementów aktywnych, jak i efektów pasożytniczych powstałych w części pasywnej układu. Przykładowo, układy SoP integrują różne komponenty pasywne wykonane na wielowarstwowym podłożu jak LTCC [29]. Natomiast w przypadku SoC wykorzystuje się materiał SiGe na wysokorezystywnym podłożu krzemowym. W technologii tej możliwe jest wykonanie całego systemu (część pasywna i aktywna) w jednym chipie. Ważnym elementem jest zapewnienie krótkiego czasu analizy tak skomplikowanych układów, co jest szczególnie istotne w przypadku jego optymalizacji. Rozwiązaniem jest analiza układu wysokiej częstotliwości w dziedzinie czasu, np. korzystając z programu SPICE. W takim przypadku model matematyczny opisujący odpowiedź pasywnej części układu zastępowany jest przez schemat zastępczy, jednak wymagane jest aby powstały schemat

zastępczy był bezwzględnie pasywny. Konieczne jest zatem opracowanie uniwersalnej techniki konwersji odpowiedzi układu z dziedziny częstotliwości do pasywnego schematu zastępczego.

W ostanich latach silnie rozwijana jest koncepcja projektowania automatycznego, w chwili obecnej największy nacisk kładzie się na projektowanie układów z wykorzystaniem zaawansowanych algorytmów optymalizacyjnych [5, 10, 17]. Przy takim podejściu inżynier konstruuje odpowiednią funkcję celu i podaje zgrubnie strukturę układu, natomiast reszta procesu projektowania odbywa się automatycznie. W tym przypadku bardzo ważny jest czas obliczenia wartości funkcji celu, co znacznie ogranicza jego zastosowanie w momencie gdy do analizy układu wykorzystuje się symulator elektromagnetyczny.

1.1 Stan wiedzy w zakresie tematu pracy

Sparametryzowane modele zastępcze. Jedną z najstarszych i najprostszych technik modelowania jest zastosowanie tabeli przeglądowych (*lookup table*). Dziedzina modelu pokrywana jest gęstą siatką w której węzłach obliczana jest próbka odpowiedzi modelowanego układu. Podstawową wadą tego rozwiązania jest bardzo duża liczba próbek, szybko rosnąca ze wzrostem gęstości siatki i zmiennych.

Szeroko rozpowszechnione jest zastosowanie sieci neuronowych (*Artifcial Neural Networks, ANN*) w celu aproksymacji charakterystyk układu [9, 11, 39]. Zastosowanie sieci neuronowej ma jednak poważne wady: optymalna struktura sieci nie jest znana *a priori*, proces treningu jest trudny i nie gwarantuje sukcesu. Dodatkowo konieczne jest generowanie licznego zbioru próbek uczących i testujących.

Inną grupę stanowią techniki wykorzystujące schematy interpolacyjne, zwykle wielomianowe lub wymierne. Proste rozwiązanie problemu wykorzystujące równomierne próbkowanie dziedziny (stworzenie wielowymiarowej, równomiernej siatki) jest możliwe tylko w przypadku niewielu zmiennych. Ze wzrostem liczby parametrów modelu ilość punktów siatki w których należy przeprowadzić czasochłonną symulację rośnie potęgowo, co prowadzi do znacznego nadpróbkowania dziedziny i trudności w rozwiązaniu zagadnienia interpolacyjnego, a przede wszystkim może w ogóle uniemożliwić zbudowanie modelu ze względu na nieakceptowalnie długi łączny czas symulacji. Rozwiązaniem jest zastosowanie efektywnego algorytmu próbkowania adaptacyjnego. Dotychczas opublikowane rozwiązania [13, 30, 33] stosują próbkowanie adaptacyjne, w którym dziedzina funkcji nie jest przeszukiwana globalnie. Powoduje to zwiększenie liczby punktów koniecznych do zbudowania modelu z zadaną dokładnością. Dodatkowo maksymalna liczba zmiennych publikowanych modeli wynosi trzy, co poważnie ogranicza ich praktyczne zastosowanie.

Schematy zastępcze dedykowane analizie w dziedzinie czasu. Od czasu powstania, symulator SPICE (*Simulation Program with Integrated Circuit Emphasis*) stał się standardem przemysłowym w zastosowaniach do projektowania analogowych i analogowo-cyfrowych układów elektronicznych. SPICE jest symulatorem zorientowanym na analizę w dziedzinie czasu. Jego największe zalety to: posiadanie biblioteki elementów linowych i nieliniowych dostarczane od ich producentów, możliwość analizy stanu nieustalonego oraz możliwość jednoczesnej symulacji układów analogowych i cyfrowych.

Pomimo tych zalet zastosowanie symulatora SPICE do analizy układów wysokich częstotliwości jest mocno ograniczone z powodu braku wbudowanych modeli elementów o stałych rozłożonych. W celu rozszerzenia jego aplikacji konieczne jest dostarczenie skupionych schematów zastępczych układów o stałych rozłożonych, takich jak pasywne połączenia międzyukładowe. Kluczowe jest w tym przypadku zapewnienie pasywności schematu zastępczego w przypadku, gdy modelowany układ jest pasywny.

Istnieje wiele technik pozwalających na ekstrakcję układu zastępczego. Najbardziej wszechstronne podejście zakłada utworzenie modelu wymiernego funkcji przenoszenia układu w dziedzinie częstotliwości i jej realizację w postaci układu skupionego [3,4,35]. W celu zapewnienia pasywności utworzonego układu konieczne jest więc zapewnienie pasywności odpowiedniego modelu wymiernego. Jest to bardzo złożony problem. Pasywność można wymuszać na etapie tworzenia modelu wymiernego [12], jednak nie zapewnia to globalnej pasywności modelu. Inna technika pozwala na wymuszenie pasywności modelu w zadanych punktach częstotliwości [15], co także nie gwarantuje bezwzględnej pasywności.

Bezwzględna pasywność może zostać wymuszona korzystając z techniki wykorzystującej podejście optymalizacyjne [8] lub w sposób iteracyjny, przy jednoczesnej minimalizacji zniekształcenia odpowiedzi czasowej układu [14]. Pierwsze podejście jest ograniczone do układów niewielkiej złożoności, drugie natomiast powoduje duże zniekształcenie odpowiedzi w dziedzinie częstotliwości, gdy naruszenie pasywności układu jest duże.

1.2 Teza i zakres pracy

Głównym celem pracy jest zaproponowanie nowych narzędzi dedykowanych automatyzacji procesu projektowania. Co ważne, celem pracy nie jest prezentacja istniejących technik automatycznego projektowania. Praca pokazuje nowe techniki konstrukcji modeli i schematów zastępczych oraz możliwość ich wykorzystania do automatyzacji procesu projektowania. Tezy pracy zdefiniowane są następująco:

- Możliwe jest tworzenie sparametryzowanych modeli zastępczych pasywnych elementów mikrofalowych w sposób zautomatyzowany.
- Dla dowolnego układu liniowego i stacjonarnego możliwe jest utworzenie układu zastępczego bazując na jego odpowiedzi w dziedzinie częstotliwości.
- W przypadku gdy modelowany układ jest pasywny, możliwe jest wymuszenie pasywności odpowiedniego układu zastępczego.
- Sparametryzowane modele zastępcze umożliwiają znaczne przyspieszenie procesu projektowania oraz jego automatyzację.

W celu udowodnienia powyższych tez podjęte zostały następujące kroki:

- Opracowana została nowa metoda konstrukcji wieloparametrycznych modeli macierzy rozproszenia dowolnych, pasywnych układów mikrofalowych.
- Funkcja przenoszenia układu reprezentowana jest w formie wymiernej w dziedzinie częstotliwości.
- Opracowana została nowa technika wymuszenia pasywności modelu wymiernego
- Na podstawie modelu wymiernego tworzony jest schemat zastępczy układu.
- Pokazane zostały zaawansowane zastosowania opracowanych technik i ich wykorzystanie w celu przyspieszenia i automatyzacji procesu projektowego.

2 Sparametryzowane, matematyczne modele zastępcze

W pracy przedstawiona została nowa technika konstrukcji sparametryzowanych modeli elementów mikrofalowych, tworzonych na podstawie wyników symulacji elektromagnetycznych. Podstawowym założeniem opracowanej techniki jest reprezentacja parametrów rozproszenia modelowanego układu w postaci funkcji wymiernej N- zmiennych [23, 28]:

$$\widehat{S}(x_1,x_2,...,x_N) \approx S(x_1,x_2,...,x_N) = \frac{A(\underline{X})}{B(\underline{X})} = \frac{A(x_1,x_2,...,x_N)}{B(x_1,x_2,...,x_N)} \tag{1}$$

gdzie licznik A i mianownik B są to wielomiany wielu zmiennych [6], $\widehat{S}$ reprezentuje wzorcową odpowiedź modelowanego układu (rezultat symulacji elektromagnetycznej), natomiast $x_1,...,x_N$ to parametry modelu. Tak sformułowane zagadnienie interpolacyjne może zostać sprowadzone do rozwiązania problemu liniowego postaci:

$$A(\underline{X}) - \widehat{S}(\underline{X})B(\underline{X}) = 0 \tag{2}$$

Problem ten, zapisany dla M dyskretnych punktów dziedziny, może zostać rozwiązany za pomocą techniki uogólnionych najmniejszych kwadratów [2]. W tak postawionym problemie interpolacyjnym kluczowym zagadnieniem jest optymalny dobór punktów (węzłów) interpolacji oraz efektywna estymacja rzędu modelu.

2.1 Próbkowanie adaptacyjne

Zaproponowana technika bazuje na wynikach symulacji elektromagnetycznych, które są zwykle bardzo kosztowne numerycznie. Konieczna jest zatem minimalizacja liczby punktów (węzłów) interpolacji. W opracowanej metodzie zastosowano wydajną technikę próbkowania adaptacyjnego. Metoda ta polega na konstrukcji dwóch różnych modeli na rzadkiej wielowymiarowej siatce prostokątnej, następnie dokonywana jest estymacja położenia największego błędu między stworzonymi modelami i w tym miejscu dokładana jest nowa próbka. Procedura ta jest powtarzana do czasu uzyskania założonej dokładności.

2.2 Automatyczny wybór rzędu modelu

Kolejnym krokiem w stronę automatyzacji procesu tworzenia modelu jest efektywna procedura estymacji rzędu modelu, rozumianego jako maksymalne potęgi licznika i mianownika tworzących funkcję wymierną. Założono, że bazy licznika i mianownika są takie same. Opracowana procedura jest ściśle związana z procesem próbkowania adaptacyjnego. W pierwszej fazie modelowania tworzone są dwa modele wymierne różnych, niskich rzędów. Dla modeli tych uruchamiana jest procedura próbkowania adaptacyjnego i monitorowany jest poziom błędu pomiędzy nimi. Założono, że w przypadek wykrycia stagnacji błędu przy zwiększaniu liczby węzłów interpolacji jest wskazówką by zwiększyć rzędy obu modeli.

2.3 Automatyczny podział dziedziny

W przypadku, gdy modelowany układ ma złożoną (np. rezonansową) odpowiedź, stworzenie jednego modelu pokrywającego całą dziedzinę z wymaganą dokładnością może być niemożliwe, np. z powodu złego uwarunkowania problemu interpolacyjnego. Dlatego też przewidziana została możliwość automatycznego podziału dziedziny na mniejsze obszary i tworzenie niezależnych modeli w tych podobszarach.

3 Pasywne, skupione schematy zastępcze

Schematy zastępcze układów wysokiej częstotliwości można podzielić na dwie podstawowe kategorie: fizyczne układy zastępcze i skupione realizacje funkcji przenoszenia. Układy fizyczne konstruowane są na podstawie znajomości struktury układu i zjawisk fizycznych w nim występujących, dlatego też ich konstrukcja nie jest prosta, szczególnie dla skompilowanych układów o stałych rozłożonych. Realizacje funkcji przenoszenia są dużo bardziej wszechstronne, choć mogą wprowadzać pewną nadmiarowość elementów skupionych.

W ogólności, funkcje przenoszenia dla liniowego, stacjonarnego układu elektronicznego można przedstawić w postaci funkcji wymiernej w dziedzinie częstotliwości:

$$\boldsymbol{H}(s) = \begin{bmatrix} \sum_{i=1}^{M} \frac{k_i^{11}}{s+p_i} + c_{11} + s \cdot h_{11} & \sum_{i=1}^{M} \frac{k_i^{12}}{s+p_i} + c_{12} + s \cdot h_{12} & \cdots & \sum_{i=1}^{M} \frac{k_i^{1N}}{s+p_i} + c_{1N} + s \cdot h_{1N} \\ \sum_{i=1}^{M} \frac{k_i^{21}}{s+p_i} + c_{21} + s \cdot h_{21} & \sum_{i=1}^{M} \frac{k_i^{22}}{s+p_i} + c_{22} + s \cdot h_{22} & \cdots & \sum_{i=1}^{M} \frac{k_i^{2N}}{s+p_i} + c_{2N} + s \cdot h_{2N} \\ \vdots & \vdots & \ddots & \vdots \\ \sum_{i=1}^{M} \frac{k_i^{N1}}{s+p_i} + c_{N1} + s \cdot h_{N1} & \sum_{i=1}^{M} \frac{k_i^{N2}}{s+p_i} + c_{N2} + s \cdot h_{N2} & \cdots & \sum_{i=1}^{M} \frac{k_i^{NN}}{s+p_i} + c_{NN} + s \cdot h_{NN} \end{bmatrix} \tag{3}$$

W przypadku gdy modelowany jest układ pasywny konieczne jest zapewnienie pasywności $\boldsymbol{H}(s)$. Model wymierny może zostać przekształcony do równoważnego układu stanu:

$$\dot{\boldsymbol{x}} = \boldsymbol{A}\boldsymbol{x} + \boldsymbol{B}\boldsymbol{u} \tag{4}$$

$$\boldsymbol{y} = \boldsymbol{C}\boldsymbol{x} + \boldsymbol{D}\boldsymbol{u} \tag{5}$$

3.1 Kryterium pasywności

W celu ustalenia czy dana reprezentacja $\boldsymbol{H}(s)$ jest pasywna, możliwe jest skorzystanie z kryterium pasywności wykorzystującego macierz Hamiltonianu systemu [7, 14]. W przypadku, gdy $\boldsymbol{H}(s)$ reprezentuje parametry rozproszenia, otrzymujemy macierz Hamiltonianu postaci:

$$\boldsymbol{H}_m = \begin{bmatrix} \boldsymbol{A} - \boldsymbol{B}\boldsymbol{R}^{-1}\boldsymbol{D}^T\boldsymbol{C} & -\boldsymbol{B}\boldsymbol{R}^{-1}\boldsymbol{B}^T \\ \boldsymbol{C}^T\boldsymbol{Q}^{-1}\boldsymbol{C} & -\boldsymbol{A}^T + \boldsymbol{C}^T\boldsymbol{D}\boldsymbol{R}^{-1}\boldsymbol{B}^T \end{bmatrix} \tag{6}$$

gdzie $\boldsymbol{Q} = (\boldsymbol{D}^T\boldsymbol{D} - \boldsymbol{I})$ oraz $\boldsymbol{R} = (\boldsymbol{D}\boldsymbol{D}^T - \boldsymbol{I})$. System (5) jest pasywny jeżeli macierz Hamiltonianu (6) nie ma czysto urojonych wartości własnych. Na podstawie wartości własnych Hamiltonianu możliwa jest identyfikacja przedziałów częstotliwości $\Delta\omega_i$ ($i = 1 \ldots P$), w których warunek pasywności jest niespełniony. Przedziały te mogą zostać zapisane w postaci wektora:

$$\boldsymbol{\Delta\Omega} = \begin{bmatrix} \Delta\omega_1 \\ \Delta\omega_2 \\ \cdots \\ \Delta\omega_P \end{bmatrix} \tag{7}$$

3.2 Wymuszenie pasywności modelu wymiernego

W rozprawie przedstawiona została technika pozwalająca na korekcję parametrów modelu wymiernego w taki sposób, by przywrócona została jego pasywność, przy jednoczesnym zachowaniu odpowiedzi częstotliwościowej układu [25, 26]. Parametry modelu (bieguny) korygowane są w sposób

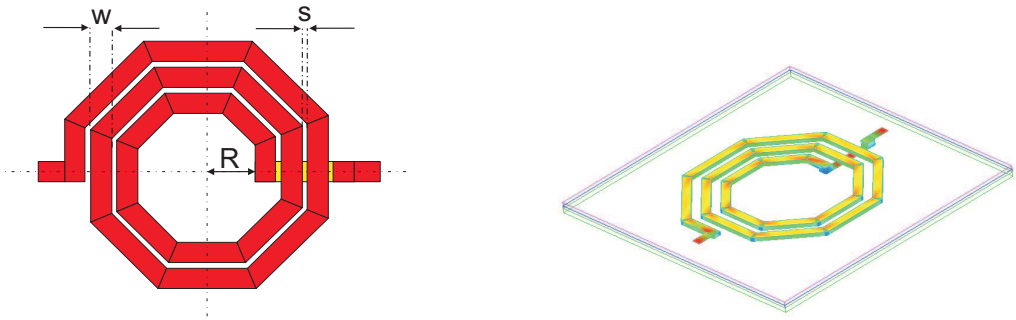

Rysunek 1: Struktura modelowanego układu induktora.

Tablica 1: Zakresy parametrów modelu induktora

Parametr	Zakres
częstotliwość (f)	0GHz - 10GHz
szerokość paska (w)	$10\mu m$ - $25\mu m$
szerokość szczeliny (s)	$5\mu m$ - $20\mu m$
wymiar wewnętrzny (R)	$30\mu m$ - $100\mu m$

optymalizacyjny, poprzez minimalizację wartości elementów wektora $\mathbf{\Delta\Omega}$. W szczególności, gdy $\mathbf{\Delta\Omega} = \mathbf{0}$, model jest pasywny. Co ważne zastosowanie rachunku zaburzonego problemu własnego pozwala na analityczne wyznaczenie gradientu funkcji celu. Aby w trakcie optymalizacji parametrów modelu zachować odpowiedź H(s), w pracy przedstawione zostały dodatkowe warunki nieliniowe optymalizacji umożliwiające kontrolę wprowadzanych zniekształceń.

3.3 Realizacja w postaci układu skupionego

Na podstawie reprezentacji wymiernej (3) możliwe jest konstrukcja skupionego układu zastępczego modelowanego układu w postaci Fostera lub Cauera [34]. W przypadku systemu stanu (5), jego realizacja bazuje na elementach skupionych R,C oraz prądowych i napięciowych źródłach sterowanych [1].

4 Przegląd zastosowań

4.1 Sparametryzowane modele matematyczne dedykowane dla automatycznego projektowania układów wysokiej częstotliwości

W pracy przedstawione zostały zaawansowane przykłady zastosowań opracowanych technik. Opracowane zostały sparametryzowane modele matematyczne o dużej złożoności (liczba parametrów modelu dochodzi do 7) i pokazane zostały możliwe zastosowania modeli do szybkiego projektowania układów mikrofalowych.

4.1.1 Sparametryzowany model induktora planarnego

Jednym z przykładów przedstawionych w pracy jest model zastępczy induktora planarnego wykonanego w technologii SiGe BiCMOS. Struktura modelowanego układu wraz z zakresem parametrów

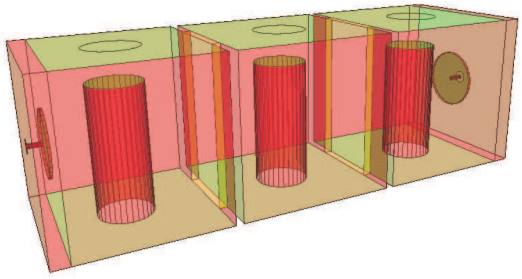

Rysunek 2: Układ trzech sprzężonych rezonatorów wykorzystany do ekstrakcji współczynników sprzężeń.

modelu pokazana jest na Rys.1. Utworzony model jest bardzo dokładny: błąd maksymalny bezwzględny modelu parametru S_{11} wynosi -55dB, błąd średni -67.3dB. Co ważne, symulacja elektromagnetyczna induktora na pojedynczej częstotliwości zabiera około 5 minut, a odpowiedź modelu uzyskujemy po 0.02s, co daje przyśpieszenie rzędu kilku tysięcy razy.

Zastosowanie modelu pozwala na szybkie, automatyczne projektowanie induktora dla zadanej specyfikacji (indukcyjność przy maksymalnej dobroci i minimalnych rozmiarach), co zostało pokazane w pracy. W pracy pokazana została także możliwość wykorzystania modelu matematycznego do konstrukcji fizycznego schematu zastępczego induktora, co prowadzi do uzyskania sparametryzowanego schematu zastępczego.

4.1.2 Modele współczynników sprzężeń dla szybkiej syntezy filtrów mikrofalowych

Zaproponowana technika zastosowana została także do stworzenia sparametryzowanego modelu współczynnika sprzężeń pomiędzy rezonatorami typu *combline* (Rys.2) [20, 21]. Współczynniki sprzężeń pomiędzy rezonatorami to wygodny sposób reprezentacji prototypów dolnoprzepustowych pasmowo-przepustowych i pasmowo-zaporowych układów filtrujących [16, 18, 24]. Wartości modelowanych elementów macierzy sprzeżeń ekstrachowane są bezpośrednio na podstawie wyników symulacji pełnofalowej trójki rezonatorów [28].

Model ma siedem parametrów kontrolujących wymiary rezonatorów i sondy zasilającej. Modelowane były nie tylko współczynniki sprzężeń, lecz także częstotliwości rezonansowe. Otrzymana reprezentacja układu pozwala na bardzo szybką i dokładną syntezę początkowych wymiarów filtrów typu *combline* o zadanej specyfikacji (rząd, straty odbiciowe, pasmo przenoszenia) [22, 27]. W odróżnieniu od syntezy klasycznej, ekstrachowany jest współczynnik sprzężenia rezonatorów obciążonych źródłem lub innym rezonatorem, co lepiej odzwierciedla faktyczne działanie układu. Dla przykładu na Rys.3 pokazany został wynik syntezy filtru na pasmo ISM 7-go rzędu (pasmo przenoszenia filtru 2,4-2,48GHz, straty odbiciowe 20dB). Co ważne, opracowany model został wykorzystany w komercyjnym oprogramowaniu wspomagającym automatyczne projektowanie tego typu filtrów.

4.1.3 Automatyzacja projektowania za pomocą modeli sparametryzowanych

W ostatnich latach rozpowszechniła się idea zastosowania technik optymalizacyjnych do projektowania układów elektronicznych [5, 10]. W podejściu tym konieczna jest wielokrotne obliczenie odpowiedzi struktury dla różnych jej parametrów. Bardzo istotny staje się zatem czas symulacji struktury, który może być bardzo długi w przypadku użycia metod pełnofalowych. Alternatywą jest użycie sparametryzowanych modeli zastępczych, które znacznie skracają czas obliczeń odpowiedzi układu.

Na Rys.4 przedstawiona jest struktura filtru falowodowego 5-go rzędu. Struktura ta podzielona

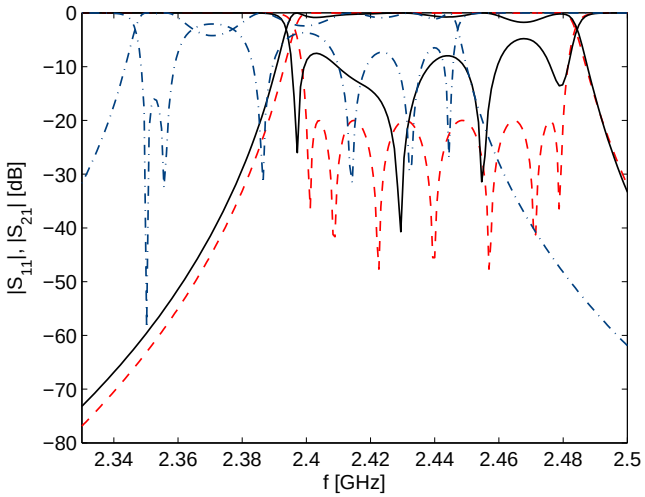

Rysunek 3: Rezultat syntezy filtru 7-go rzędu: (—) z zastosowaniem opracowanych modeli zastępczych, (-.-) klasyczna synteza, (- - -) odpowiedź filtru po optymalizacji

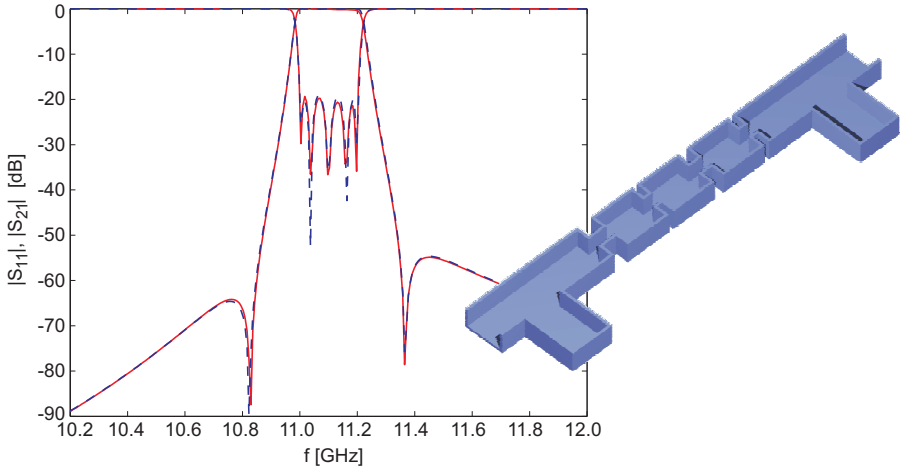

Rysunek 4: Struktura filtru falowodowego i porównanie odpowiedzi modeli zastępczych z wynikami analizy pełnofalowej.

została na pojedyncze nieciągłości, po czym stworzone zostały ich matematyczne modele zastępcze. Modele te wykorzystane zostały do zaprojektowania filtru o specyfikacji: pasmo przepustowe 11GHz-11,2GHz, straty odbiciowe w paśmie przepustowym 20dB, zera transmisyjne 10,88GHz i 11,32GHz. Do zaprojektowania układu wykorzystano podejście optymalizacyjne [19] umożliwiające automatyzację procesu projektowania filtrów mikrofalowych. Rezultat optymalizacji wymiarów struktury przedstawiony na Rys.4 pokazuje bardzo dobrą zgodność odpowiedzi modelu zastępczego i symulacji EM (metodą dopasowania rodzajów). Co ważne, czas optymalizacji struktury z użyciem modeli wyniósł tylko 500 sekund (1.6GHz PC). W przypadku zastosowania symulatora pełnofalowego cykl projektowy trwał około 8 godzin.

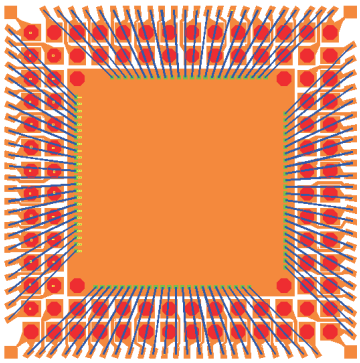

Rysunek 5: Rzut na wyprowadzenia modelowanej oprawy BGA.

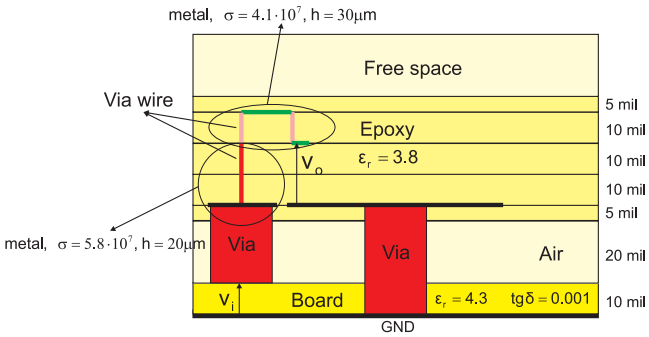

Rysunek 6: Przekrój poprzeczny oprawy BGA symulowanej w ADS Momentum.

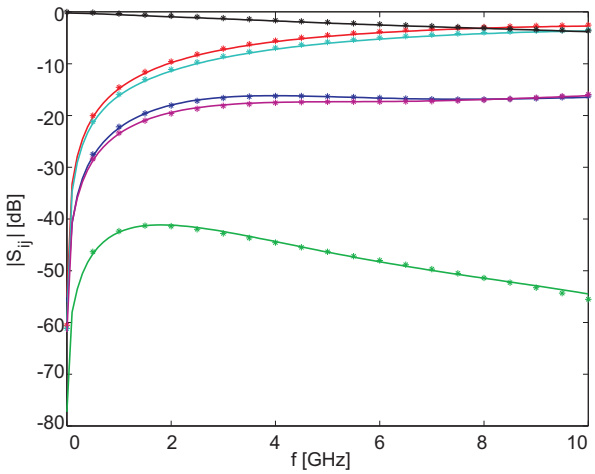

Rysunek 7: Porównanie parametrów rozproszenia układu pasywnego schematu zastępczego z wynikami symulacji elektromagnetycznej.

4.2 Pasywne schematy zastępcze

W pracy pokazano, że za pomocą opracowanej techniki wymuszania pasywności możliwe jest stworzenie schematów zastępczych dla bardzo złożonych struktur. Schemat zastępczy utworzyć można na podstawie wyników analizy elektromagnetycznej lub danych pomiarowych w dziedzinie częstotliwości.

4.2.1 Oprawa BGA96

Oprawy BGA (Ball Grid Array) zostały wprowadzone w celu ułatwienia montażu układów zintegrowanych z dużą ilością wyprowadzeń. Na Rys.5 pokazany został rzut wprowadzeń oprawy BGA z 96-ioma wyprowadzeniami. Struktura ta została przeanalizowana metodą momentów w symulatorze ADS Momentum (Rys.6) w zakresie częstotliwości DC-10GHz, a otrzymane parametry rozproszenia 1/4 struktury (96 wrót, jeden bok oprawy) wykorzystane zostały do stworzenia pasywnego układu zastępczego. Porównanie odpowiedzi elektromagnetycznej z otrzymanym schematem zastępczym pokazano na Rys. 7. Otrzymany schemat pasywny może zostać wykorzystany do estymacji przesłuchów pomiędzy wyprowadzeniami oprawy lub do symulacji czasowej w programie SPICE całego układu razem z oprawą.

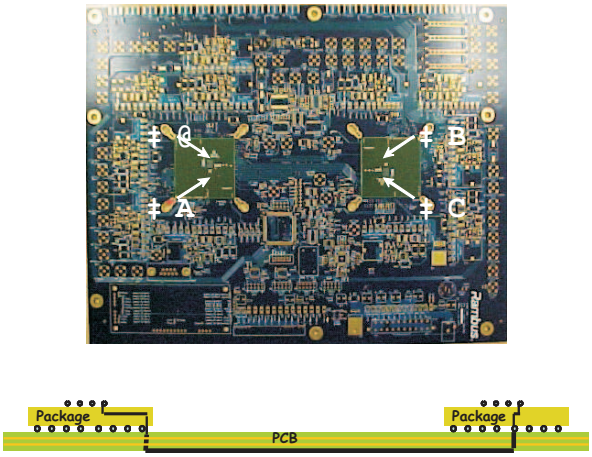

Rysunek 8: Ogólny widok struktury modelowanego kanału RAMBUS FlexIO.

4.2.2 Kanał RAMBUS FlexIO

Opracowana technika pozwala na konstrukcję modelu zastępczego układu na podstawie danych pomiarowych. Na Rys.8 pokazana została struktura pomierzonego kanału FlexIO firmy RAMBUS[1], którym przesyłane są sygnały o częstotliwościach dochodzących do 8GHz. Struktury tego typu używane są do połączeń między procesorami, procesorem i chipsetem w urządzeniach elektroniki użytkowej (konsole gier, urządzenia HDTV, PC). Kanał ten ma postać dwóch linii meandrowych długości 12 cali. Duży stopień komplikacji struktury powoduje trudności z dokładną symulacją układu, dlatego projekt musi zostać zweryfikowany poprzez pomiary.

Dane pomiarowe zostały użyte do konstrukcji schematu zastępczego układu. Reprezentacja wymierna funkcji przenoszenia ma wysoki rząd równy 100 i jest niepasywna w zakresach częstotliwości 58MHz-157MHz oraz 188MHz-237MHz. Pasywność modelu została przywrócona zaproponowaną techniką, co zajęło 5 minut (komputer osobisty z procesorem 1,5GHz). Porównanie danych pomiarowych z otrzymanym skupionym schematem zastępczym pokazane jest na Rys. 9. Wynikowy schemat zastępczy użyty może być w celu weryfikacji projektów wykorzystujących modelowany kanał, np. przy przeprowadzaniu analizy integralności sygnałowej (*signal itegrity*) urządzenia.

4.3 Pasywne, sparametryzowane schematy zastępcze

Połączenie dwóch technik: modeli sparametryzowanych oraz konstrukcji pasywnych schematów zastępczych, pozwala na uzyskanie sparametryzowanych, skupionych schematów zastępczych dedykowanych symulacjom w dziedzinie czasu.

4.3.1 Struktura filtrująca

Dla przykładu w pracy pokazany został model sparametryzowany układu filtrującego przedstawionego na Rys.10. Struktura została podzielona na pojedyncze nieciągłości, po czym stworzone zostały ich modele sparametryzowane. W rezultacie otrzymano sparametryzowany model całej struktury. Odpowiedź modelu została użyta do generacji pasywnego schematu zastępczego układu. Dokładność otrzymanych schematów zastępczych dla kilku zastawów wymiarów struktury pokazana jest w Tabeli 2. Dla porównania pokazano błąd odpowiedzi modeli zastępczych użytych w symulatorze

[1]Dane pomiarowe i zdjęcia struktury dzięki uprzejmości W.T. Beyene z RAMBUS Inc.

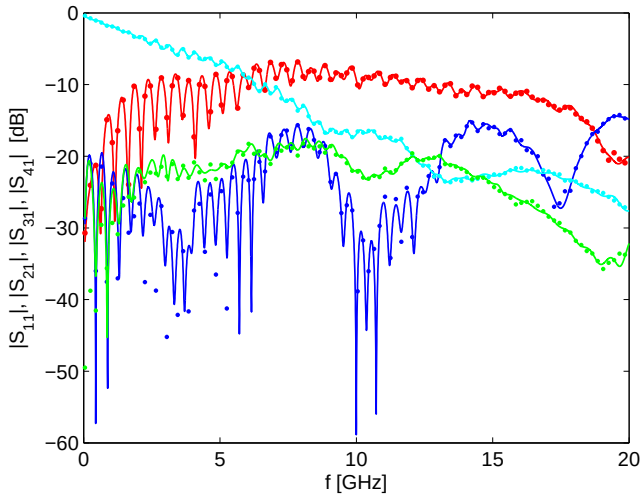

Rysunek 9: Dane pomiarowe (···)i odpowiedź pasywnego układu zastępczego (—) kanału FlexIO.

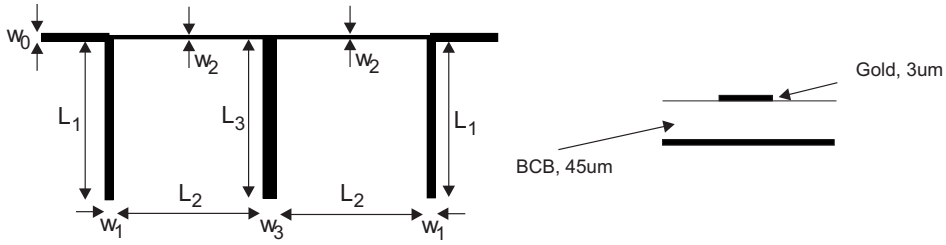

Rysunek 10: Modelowana struktura filtrująca.

obwodowym Agilent ADS. We wszystkich przypadkach opracowane modele zapewniają dużo lepszą dokładność.

Tablica 2: Dokładność (błąd średniokwadratowy) otrzymanego sparametryzowanego układu zastępczego struktury filtrującej w porównaniu do wyników symulacji elektromagnetycznej.

Wymiary struktury [mm]							Model niepasywny		Model pasywny		Modele ADS	
w_0	w_1	w_2	w_3	L_1	L_2	L_3	$E_{RMS}^{S_{11}}$	$E_{RMS}^{S_{21}}$	$E_{RMS}^{S_{11}}$	$E_{RMS}^{S_{21}}$	$E_{RMS}^{S_{11}}$	$E_{RMS}^{S_{21}}$
0.13	0.1	0.15	0.1	1.5	2	2	-55.7	-50.8	-53.0	-48.8	-40.8	-42.2
0.18	0.1	0.15	0.2	1.5	1.5	1.8	-52.9	-51.4	-52.7	-48.6	-37.3	-36.7
0.1	0.05	0.05	0.1	2.5	2	2	-47.6	-47.0	-46.7	-47.5	-35.8	-37.1
0.157	0.1	0.1	0.1	2	2	2	-53.1	-49.7	-53.0	-50.0	-37.3	-35.7
0.157	0.157	0.05	0.2	2.5	1.3	1	-53.1	-49.0	-51.8	-49.9	-37.1	-44.2

5 Podsumowanie

W pracy pokazane zostały techniki modelowania złożonych układów elektronicznych wysokiej częstotliwości. Modele zastępcze mają postać sparametryzowanych modeli matematycznych tworzonych za pomocą schematów interpolacyjnych lub skupionych, pasywnych układów zastępczych dedykowanych analizie w dziedzinie czasu. Do konstrukcji modeli wykorzystywane są wyniki symulacji elektromagnetycznych, co pozwala na osiągnięcie lepszej dokładności niż w przypadku modeli dotychczas używanych. Zaproponowane techniki pozwalają na istotne rozszerzenie funkcjonalności istniejących narzędzi projektowych.

Rozprawa rozszerzyła dotychczasową wiedzę w zakresie modelowania układów mikrofalowych o następujące elementy:

- Opracowana została nowa technika wymuszania pasywności modelu wymiernego funkcji przenoszenia układu. Technika modyfikuje parametry modelu (bieguny lub zera) aby uzyskać pasywność przy jednoczesnym zachowaniu odpowiedzi częstotliwościowej. Technika pozwala na tworzenie pasywnych schematów zastępczych skomplikowanych układów, w przypadkach gdy inne techniki zawodzą.

- Zaproponowana została nowa technika konstrukcji sparametryzowanych modeli zastępczych układów wysokiej częstotliwości, bazujące na wynikach symulacji elektromagnetycznych. Pokazane zostało, że technika pozwala na tworzenie modeli aż siedmiu zmiennych. Przeprowadzone zostały testy efektywności pokazujące, że w porównaniu do dotychczasowych technik zaproponowane podejście potrzebuje dużo mniej symulacji pełnofalowych do konstrukcji modelu przy zachowaniu podobnej dokładności.

- Tworzone modele zastępcze znacznie przyspieszają czas analizy złożonych układów, przy zachowaniu wysokiej dokładności obliczeń.

- Pokazane zostały zastosowania modeli zastępczych przy automatyzacji projektowania złożonych układów mikrofalowych. Praktyczne znaczenie modeli potwierdzone zostało opracowaniem komercyjnego narzędzia dedykowanego automatycznemu projektowaniu filtrów typu *combline* [22, 27], opracowanego przy współpracy z firmą Mician GmbH.

- Pokazane zostało, że oba podejścia mogą zostać połączone, w wyniku czego otrzymuje się sparametryzowane, pasywne schematy zastępcze dla analizy w dziedzinie czasu układów wysokiej częstotliwości (liniowych, nieliniowych, aktywnych i pasywnych), połączonych z szybką optymalizacją geometrii.

Podsumowując, techniki opracowane w ramach rozprawy mają szerokie zastosowanie przy projektowaniu układów wysokiej częstotliwości. Wyniki badań mają duży potencjał komercyjny. Tworzone modele sparametryzowane mogą łatwo zostać dołączone do podstawowych narzędzi projektowych, takich jak oprogramowanie Advanced Design System czy Microwave Office. W chwili obecnej w Centrum Doskonałości Wicomm działającym na Politechnice Gdańskiej tworzone są kolejne narzędzia komercyjne wykorzystujące opracowane modele zastępcze, umożliwiające szybkie, automatyczne projektowanie multiplekserów oraz filtrów dwu-rodzajowych o uogólnionej charakterystyce Czebyszewa. Dodatkowo, matematyczne modele zastępcze mogą znaleźć zastosowanie w innych obszarach, takich jak elektrodynamika obliczeniowa. Dla przykładu, jednym z możliwych rozwiązań umożliwiających przyspieszenie analizy struktur planarnych metoda momentów jest tworzenie modeli zastępczych macierzy impedancyjnej [32]. Opracowane techniki umożliwiają istotne skrócenie czasu projektowania, co jest bardzo ważne przy obserwowanym wzroście wymagań przemysłu na redukcję całkowitego czasu cyklu produkcyjnego.

Literatura

[1] R. Achar and M. S. Nakhla, "Simulation of High-Speed Interconnects," *Proceedings of the IEEE*, vol. 89, pp. 693–728, May 2001.

[2] R. S. Adve, T. K. Sarkar, S. M. Rao, E. K. Miller, and D. R. Pflug, "Application of the Cauchy Method for Extrapolating/Interpolating Narrow-Band System Responses," *IEEE Transactions on Microwave Theory and Techniques*, vol. 45, pp. 837–845, May 1997.

[3] G. Antonini, "SPICE Equivalent Circuits of Frequency-Domain Responses," *IEEE Transactions on Electromagnetic Compatibility*, vol. 45, pp. 502–512, Aug. 2003.

[4] R. Araneo, "Extraction of Broad-Band Passive Lumped Equivalent Circuits of Microwave Discontinuities," *IEEE Transactions on Microwave Theory and Techniques*, vol. 54, pp. 393–401, Jan. 2006.

[5] J. W. Bandler and S. Chen, "Circuit Optimization: The State of the Art," *IEEE Transactions on Microwave Theory and Techniques*, vol. 36, pp. 424–443, Feb. 1988.

[6] R. H. Bartels and J. J. Jezioranski, "Least-Squares Fitting Using Orthogonal Multinomials," *ACM Transactions on Mathematical Software*, vol. 11, pp. 201–217, Sept. 1985.

[7] S. Boyd, V. Balakrishnan, and P. Kabamba, "A Bisection Method for Computing the H_∞ Norm of a Transfer Matrix and Related Problems," *Math. Control Signals Syst.*, vol. 2, pp. 207—219, 1989.

[8] C. P. Coelho, J. Phillips, and L. M. Silveira, "A Convex Programming Approach for Generating Guaranteed Passive Approximations to Tabulated Frequency-Data," *IEEE Transactions on Computer-Aided Design of Integrated Cicruits and Systems*, vol. 23, pp. 293–301, Feb. 2004.

[9] G. L. Creech, B. J. Paul, C. D. Lesniak, T. J. Jenkins, and M. C. Calcatera, "Artificial Neural Networks for Fast and Accurate EM-CAD of Microwave Circuits," *IEEE Transactions on Microwave Theory and Techniques*, vol. 45, pp. 794–801, May 1997.

[10] D. De Zutter, J. Sercu, T. Dhaene, J. D. Geest, F. J. Demuynck, S. Hammadi, and C.-W. P. Huang, "Recent Trends in the Integration of Circuit Optimization and Full-Wave Electromagnetic Analysis," *IEEE Transactions on Microwave Theory and Techniques*, vol. 52, no. 1, pp. 245–256, Jan. 2004.

[11] V. K. Devabhaktuni, M. C. E. Yagoub, and Q.-J. Zhang, "A Robust Algorithm for Automatic Development of Neural-Network Models for Microwave Applications," *IEEE Transactions on Microwave Theory and Techniques*, vol. 49, pp. 2282–2291, Dec. 2001.

[12] R. Gao, Y. S. Mekonnen, W. T. Beyene, and J. E. Schutt-Ainé, "Black-Box Modeling of Passive Systems by Rational Function Approximation," *IEEE Transactions on Advanced Packaging*, vol. 28, pp. 209–215, May 2005.

[13] J. D. Geest, T. Dhaene, N. Fache, and D. D. Zutter, "Adaptive CAD-model Building Algorithm for General Planar Microwave Structures," *IEEE Transactions on Microwave Theory and Techniques*, vol. 47, pp. 1801–1809, Sept. 1999.

[14] S. Grivet-Talocia, "Passivity Enforcement via Perturbation of Hamiltonian Matrices," *IEEE Transactions on Circuits and Systems*, vol. 51, pp. 1755–1769, Sept. 2004.

[15] B. Gustavsena and A. Semlyen, "Enforcing Passivity for Admittance Matrices Approximated by Rational Functions," *IEEE Transaction on Power Systems*, vol. 16, pp. 97–104, Feb. 2001.

[16] J. S. Hong and M. J. Lancaster, *Microstrip Filters for RF/Microwave Application*. New York: Wiley, 2001.

[17] N. Jain and P. Onno, "Methods of Using Commercial Electromagnetic Simulators for Microwave and Millimeter-Wave Circuit Design and Optimization," *IEEE Transactions Microwave Theory and Techniques*, vol. 45, pp. 724–746, May 1997.

[18] P. Kozakowski, A. Lamecki, P. Sypek, and M. Mrozowski, "Eigenvalue Approach to Synthesis of Prototype Filters with Source/Load Coupling," *IEEE Microwave and Wireless Components Letters*, vol. 15, pp. 98–100, Feb. 2005.

[19] P. Kozakowski and M. Mrozowski, "Automated CAD of Coupled Resonator Filters," *IEEE Microwave and Wireless Components Letters*, vol. 12, no. 12, pp. 470–472, Dec. 2002.

[20] A. Lamecki, L. Balewski, P. Kozakowski, and M. Mrozowski, "Multivariate models of inter-resonator couplings and their application in filter design," in *XXVIII-th General Assembly of International Union of Radio Science Proceedings*, New Delhi, India, Oct. 2005.

[21] A. Lamecki, L. Balewski, and M. Mrozowski, "Multivariate Models of Inter-Resonator Couplings for Microwave Filter Synthesis," in *International Conference on Adaptive Modeling and Simulation ADMOS*, Barcelona, Spain, 2005.

[22] A. Lamecki, Ł. Balewski, and M. Mrozowski, "Synthesis of combline filters with application of surrogate model of inter-resonator and source-resonator coupling (Synteza filtru *combline* z wykorzystaniem modelu sprzężeń miedzyrezonatorowych i źródło-rezonator," *Zgłoszenie innowacyjne, Politechnika Gdańska*, no. 4/07, Feb. 2007.

[23] A. Lamecki, P. Kozakowski, and M. Mrozowski, "Efficient Implementation of the Cauchy Method for Automated CAD-model Construction," *IEEE Microwave and Wireless Components Letters*, vol. 13, pp. 268–270, July 2003.

[24] ——, "Fast Synthesis of Coupled-Resonator Filters," *IEEE Microwave and Wireless Components Letters*, vol. 14, pp. 174–176, Apr. 2004.

[25] A. Lamecki and M. Mrozowski, "Passive SPICE Networks from Non-Passive Data," in *16-th International Conference on Microwaves, Radar and Wireless Communications Mikon*, Krakow, May 2006.

[26] ——, "Equivalent SPICE Circuits With Guaranteed Passivity From Nonpassive Models," *IEEE Transaction on Microwave Theory and Techniques*, vol. 55, pp. 526–532, Mar. 2007.

[27] ——, "Parameterized surrogate models of combline resonators (Sparametryzowane modele zastępcze dla trójki rezonatorów typu combline)," *Zgłoszenie innowacyjne, Politechnika Gdańska*, no. 1/07, Feb. 2007.

[28] A. Lamecki, P.Kozakowski, and M. Mrozowski, "Multimode, Multiparametric Surrogate Models for Fast Design of Waveguide Components," in *European Microwave Conference Proceedings*, Munich, Germany, Oct. 2003.

[29] J.-H. Lee, G. DeJean, S. Sarkar, S. Pinel, K. Lim, J. Papapolymerou, J. Laskar, and M. M. Tentzeris, "Highly Integrated Millimeter-Wave Passive Components Using 3-D LTCC System-on-Package (SOP) Technology," *IEEE Transactions on Microwave Theory and Techniques*, vol. 53, no. 6, pp. 2220–2229, June 2005.

[30] R. Lehmensiek and P. Meyer, "Creating Accurate Multivariate Rational Interpolation Models of Microwave Circuits by Using Efficient Adaptive Sampling to Minimize the Number of Computational Electromagnetic Analyses," *IEEE Transactions on Microwave Theory and Techniques*, vol. 49, pp. 1419–1430, Aug. 2001.

[31] A. Matsuzawa, "RF-SoC—Expectations and Required Conditions," *IEEE Transactions on Microwave Theory and Techniques*, vol. 50, no. 1, pp. 245–253, Jan. 2002.

[32] M. Mongiardo, R. Sorrentino, and C. Tomassoni, "Efficient Planar Electromagnetic Analysis by Impedance Matrix Interpolation," in *IEEE MTT-S Internatial Microwave Symposium Digest*, USA, 2005.

[33] S. F. Peik, R. R. Mansour, and Y. L. Chow, "Multidimensional Cauchy Method and Adaptive Sampling for an Accurate Microwave Circuit Modeling," *IEEE Transactions on Microwave Theory and Techniques*, vol. 46, pp. 2364–2371, Dec. 1998.

[34] G. C. Temes and J. Lapatra, *Introduction to Circuit Synthesis and Design*. McGraw-Hill, 1977.

[35] I. Timmins and K.-L. Wu, "An Efficient Systematic Approach to Model Extraction for Passive Microwave Circuits," *IEEE Transactions on Microwave Theory and Techniques*, vol. 48, pp. 1565–1573, Sept. 2000.

[36] R. R. Tummala, "SOP: What Is It and Why? A New Microsystem-Integration Technology Paradigm-Moore's Law for System Integration of Miniaturized Convergent Systems of the Next Decade," *IEEE Transactions on Advanced Packaging*, vol. 27, pp. 241–249, May 2004.

[37] www.agilent.com.

[38] www.mwoffice.com.

[39] A. H. Zaabab, Q. J. Zhang, and M. Nakhla, "A Neural Network Modeling Approach to Circuit Optimization and Statistical Design," *IEEE Transactions on Microwave Theory and Techniques*, vol. 43, pp. 1349–1558, June 1995.